Multipoint Video Distribution System (MVDS) in the 28 GHz and the 42 GHz frequency bands

Vugts, J.A.G.

Award date:
1995

Eindhoven University of Technology
Faculty of Electrical Engineering
Telecommunications division

Multipoint Video Distribution System (MVDS) in the 28 GHz and the 42 GHz frequency bands

by

John J.A.G. Vugts.

Concerns : Graduation project
Period of work : November 1994 - June 1995

Supervisors: ir. P.G.M. de Bot (Philips)
prof. dr. ir. G. Brussaard (TUE)
ir. J. Dijk (TUE)

Eindhoven, June 1995

Author John J.A.G. Vugts

Title Multipoint Video Distribution System (MVDS) in the 28 GHz and the 42 GHz frequency bands

Abstract

Multipoint Video Distribution System (MVDS) is a terrestrial point-to-multipoint radio system for distributing TV signals to the homes of end users as an alternative to the conventional cable networks. Such a system is to be operated at high RF frequencies (40.5-42.5 GHz) because of the relatively large bandwidth required which is not available at lower frequencies. The objective of the work is to examine the possibilities of MVDS in a Single-Frequency Network (SFN) and to see if a Line Of Sight (LOS) is always required. This work results in a system proposal.

The propagation aspects such as refraction, diffraction, fading, attenuation etc. of the 42 GHz electromagnetic waves have been examined. Furthermore the possibilities and effects of reflection on building materials is examined. There has been analytically shown that the increase in coverage due to diffraction is negligible.

Measurements have been performed which showed that the link-budget calculations were accurate. They also gave an indication of the loss due to foliage (20-30 dB), reflection coefficients (10 dB) and the negligible possibilities of using diffraction and reflection. They also showed that multipath reception can be prevented largely by using narrow beam reception antennas.

A program has been written which predicts the percentage of coverage within a specific area and a model of Eindhoven has been created. With these tools it is shown that the increase in the percentage of coverage due to reflections is negligible for a typical Dutch city. This is due to the lack of appropriate reflection surfaces in such an environment and the small reflection coefficients of rough surfaces. The percentage of the cell surface which is covered depends very much on the heights of the buildings and the antennas.

Research on networks has been done to assess the feasibility of SFNs. Both omni-directional antennas and directional antennas have been used to find a good solution of the SFN problem. Using directional antennas resulted in an SFN using two polarizations (C/I of 11 dB). The performance degradation due to the interference is calculated and simulated. The CIR found in the proposed network can be dealt with using the built in error correction capabilities. Three different schemes are given to feed the cellular SFN network.

It is found that an example system with typical parameters has a cell diameter of 4.69 km and can support in the band 40.5 42.5 GHz up to 48 channels (41.6 MHz spacing), corresponding to 336 different programs.

Contents

List of Symbols and Acronyms

a	earth radius	$[km]$
a_e	effective earth radius	$[km]$
B	bandwidth	$[Hz]$
B_c	transponder bandwidth	$[MHz]$
B_n	Nyquist bandwidth	$[MHz]$
BER	bit error rate	$[s^{-1}]$
c	carrier power	$[W]$
c	velocity of an electromagnetic wave in a vacuum	$[m/s]$
C	carrier power	$[dBW]$
$CATV$	cable television system	[]
CNR	carrier to noise ratio	$[dB]$
CIR	carrier to interference ratio	$[dB]$
cl	fresnel zone clearance	$[m]$
d	path length (distance)	$[m]$
d	Hamming distance	[]
D	antenna diameter	$[m]$
e	water vapour pressure	$[mbar]$
E	received field strength	$[V/m]$
$\overline{E}$	average electric field	$[V/m]$
E_t	transversal electric field	$[V/m]$
$eirp$	effective isotropic radiated power	$[W]$
$EIRP$	effective isotropic radiated power	$[dBW]$
E_0	direct wave field strength	$[V/m]$
E_s	symbol energy	$[Ws]$
f	frequency	$[Hz]$
FEC	forward error correction	[]
F	noise figure	$[dB]$
G	gain	$[dB]$
$G(f)$	power spectral density function	$[dB]$
$G_n(f)$	power spectral density function	$[W/Hz]$
g_r	receiver antenna gain	[]
G_r	receiver antenna gain	$[dB]$
g_t	transmitter antenna gain	[]
G_t	transmitter antenna gain	$[dB]$

$H(f)$	channel transfer function	[]
h_r	receiver antenna height	$[m]$
$H_r(f)$	receive filter (amplitude response)	[]
h_t	transmitter antenna height	$[m]$
H_t	transversal magnetic field	$[A/m]$
$H_t(f)$	transmit filter (amplitude response)	[]
I	interference power	$[dBW]$
k	k-factor	[]
k	Boltzmann's constant	$[J/K]$
k	propagation constant	$[1/m]$
l_a	rain attenuation	[]
L_a	rain attenuation	$[dB]$
l_{bf}	free space loss	[]
L_{bf}	free space loss	$[dB]$
l_c	antenna feed loss	[]
L_{df}	diffraction loss	$[dB]$
L_f	fade margin	$[dB]$
L_{feed}	feeding loss of the antennas	$[dB]$
L_m	medium loss	$[dB]$
l_m	medium loss	[]
$LFSR$	linear feedback shift register	[]
LOS	line of sight	[]
$LMDS$	local multipoint distribution system	[]
l_p	pointing loss	[]
L_p	pointing loss	$[dB]$
$MMDS$	multipoint microwave distribution system	[]
$MPEG$	motion picture experts group	[]
$MVDS$	multipoint video distribution system	[]
n	noise power	$[W]$
n	refractivity index	[]
$n_c(t)$	narrow band noise power spectrum (cosine)	[]
$n_s(t)$	narrow band noise power spectrum (sine)	[]
N	noise power	$[dBW]$
N	refractivity	[]
p	outage time percentage over a whole year	[]
P_b	probability of a bit error	[]
P_e	probability of an error	[]
p_t	transmitted power	$[W]$
p_w	outage worst month time percentage	[]
P	atmospheric pressure	$[mbar]$
$P(W)$	time fraction of W power received	[]
QEF	quasi error free operation	[]
$QPSK$	quadrature phase shift keying	[]
r	path length reduction factor	[]

r	radius of a cell	$[m]$
$r(t)$	noise signal in time domain	[V]
R	rain rate	$[mm/hr]$
R	convolutional coding rate	[]
R	reflectivity	[]
R_n	n^{th} Fresnel zone radius	$[m]$
RP	radiated power	$[dBM]$
R_{rs}	Reed Solomon coding rate	[]
$R_{0.01}$	rain rate exceeded 0.01 % of the year	$[mm/hr]$
s	signal power	$[W]$
S	signal power	$[dBW]$
S_{av}	power flux density	$[W/m^2]$
SFN	single frequency network	[]
SNR	signal to noise ratio	$[dB]$
$S_y(f)$	voltage^2 spectral density function	$[V^2/Hz]$
T	temperature	$[K]$
T	transmission coefficient	[]
T_a	ambient temperature	$[K]$
T_{ant}	antenna noise temperature	$[K]$
T_r	receiver noise temperature	$[K]$
T_{rain}	rain temperature	$[K]$
T_{sys}	system noise temperature	$[K]$
T_{sky}	sky noise temperature	$[K]$
v	velocity	$[m/s]$
v_{medium}	velocity of an electromagnetic wave in a medium	$[m/s]$
$Y(f)$	signal in frequency domain	$[V]$
XPD	cross-polar discrimination	$[dB]$
$y(t)$	signal in time domain	$[V]$
α	roll-off factor	[]
β	effective aperture	$[m^2]$
γ_r	rain attenuation (CCIR model)	$[dB/km]$
ϵ_r	relative electric permittivity	[]
η	power spectrum density white noise	$[W/Hz]$
λ	wave length	$[m]$
μ_r	relative magnetic permeability	[]
ρ	reflection coefficient	$[kg/m^3]$
$\rho\|\|$	parallel reflection coefficient	[]
$\rho\perp$	orthogonal reflection coefficient	[]
ρ_s	specular reflection coefficient	[]
σ	electrical conductivity	$[\Omega m]$
τ	time difference	$[s]$
ϕ	power flux	$[W/m^2]$
ψ	phase difference due to path length difference	[]

Chapter 1

Introduction

This report describes the graduation work for the department of Electrical Engineering of the Eindhoven University of Technology. The research is in the field of communications engineering. The research is carried out at Philips Research in Eindhoven during the period November 1994 - June 1995.

The work is related to a Multipoint Video Distribution System (MVDS). Multipoint Video Distribution System (MVDS) is a terrestrial point-to-multipoint radio system for distributing TV signals to the homes of end users as an alternative to the conventional cable networks. Therefore it is also referred to as "Wireless cable". Such a system is to be operated at high RF frequencies because of the large amount of spectrum required which is not available at lower frequencies. For research purposes, an experimental 28 GHz single channel link has been installed at Philips.

With this link the propagation aspects which are of concern for a MVDS are investigated. The objective of the work is to examine the possibilities of MVDS in a Single-Frequency Network (SFN), to see if a Line Of Sight (LOS) is always required for good reception, the planning of the cellular network and to see if it is possible to have a Single frequency network (SFN). Therefore it is important to investigate the coverage area, signal attenuation, shielding of buildings within the covered area, reuse distances and acceptable interference levels. For research on interference from different cells, a second transmitter is available. Theoretical models will predict the allowable carrier to interference ratio C/I. Using the trial results of the analog link it can be verified if this criteria can be met.

In Chapter 2 a general discussion of an MVDS system is given. In Chapter 3 the propagation aspects will be discussed. In the following Chapter the different topologies of the networks are discussed. The influence of the interference is discussed in Chapter 5; from there the link-budgets can be calculated. If the cell sizes are known, one is interested in the percentage of coverage in a cell, this is discussed in Chapter 6. To confirm the theories measurements are performed which are discussed in Chapter 7. In the final Chapter some conclusions and suggestions for further work are given.

Chapter 2

Multipoint Video Distribution System (MVDS)

2.1 Introduction

Multipoint Video Distribution Systems (MVDS)[1] are systems to provide a means for wireless local distribution of television services. They may be employed as an alternative or a supplement to the cable TV distribution systems (CATV). The system described here is a microwave multipoint video distribution system operating in the 27.5-29.5 GHz range and a future system operating in the 40.5 GHz-42.5 GHz range.

The first trial used a single 28 GHz link which enabled us to acquire practical propagation information. In the next step a second transmitter is involved to acquire information on single frequency network behaviour and to investigate the tolerance of the link to interference.

The future MVDS system will be a digital system based on the Digital Video Broadcasting (DVB) satellite standard. This is because of the availability of the system components. This results in a relatively inexpensive solution for digital MVDS.

2.2 Cellular system

To cover a large area with limited power, it is necessary to use multiple cells. The total area to be covered is then divided in a number of subsections. Every subsection has its own transmitter. Since simple reuse of frequency in the adjacent cell would result in strong interference near the edge of the cell, it is necessary to use a more sophisticated system. The most simple of course is to use different frequencies in different cells, although this is very inefficient. The reuse distance depends on

[1] In the USA, the systems are known as Multipoint Microwave Distribution Systems (MMDS)

e.g. antenna gain patterns and on natural attenuation. The reuse distance can be shortened by using frequency offset, orthogonal-polarization and very narrow-beam reception antennas. The frequency offset is of no use in our system because of the overlapping of the channels as discussed in Section 5.1.

The ultimate situation will obvious be a single frequency network where in all the adjacent cells the same frequency can be reused with acceptable interference. The possibilities for a single frequency network will be described in Section 4.

2.3 System description of the current analog system

In Appendix A there will be a short overview of the available system presented. In Figure 2.1 a global overview of the total link is given.

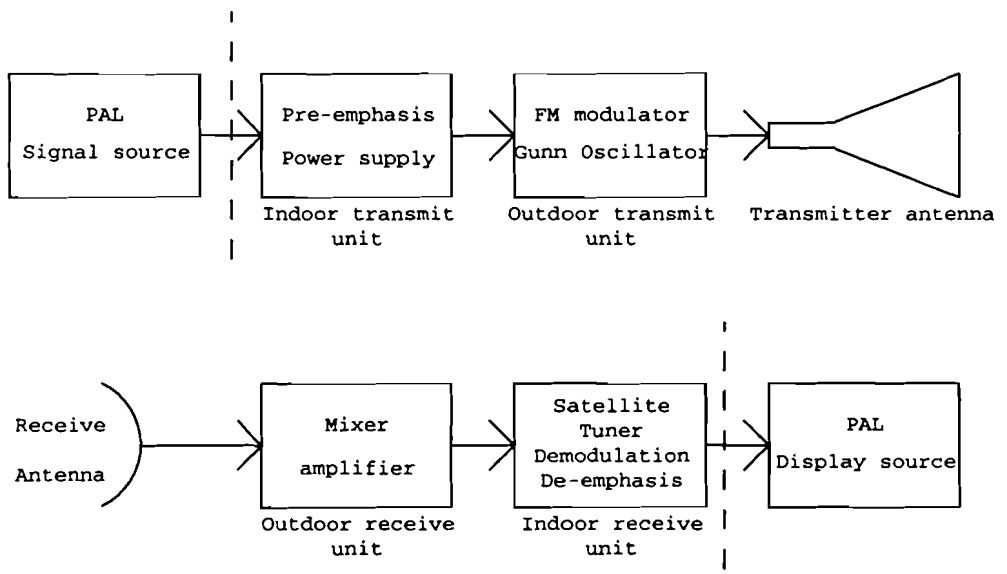

Figure 2.1: Global overview of the link

All the blocks except the PAL source and the PAL TV in Figure 2.1 will be individually described in Appendix A. The system description is a copy of the description in [39]. Although the system is an analog FM modulated system propagation effects etc. with this link can be studied. This information can then be extrapolated to a digital 42 GHz system which will be used in the future.

2.4 Description of the digital system

The future digital system used for MVDS will use the channel coding and modulation of the digital satellite system defined by Digital Video Broadcasting (DVB)[13, 14]. This ensures that there will be very little additional costs involved in developing a digital MVDS receiver system. In principle a standard digital satellite receiver with a special designed down converter can be used. The low noise block converter shifts the 42 GHz frequency range in one or two steps down to L-band, the desired frequency range for the standard satellite receiver. From that point onwards the standard digital satellite demodulation equipment can be used. In Figure 2.2 the transmitter and receiver setup is shown.

The only differences between the digital satellite scheme and the MVDS scheme are the transmitter front-end and the receiver LNB which convert the signal to and from 42 GHz respectively. The individual blocks in the link will be briefly described below [38].

The satellite system (digital MVDS system) uses QPSK-modulation. The forward error correction (FEC) of the satellite system consists of concatenated coding with Reed-Solomon outer coding and convolutional inner coding.

2.4.1 Transmitter description

The bit stream to be transmitted is build up of MPEG-2 packets that contain 187 data bytes and one synchronization byte. The MPEG-2 data structure is beyond the scope of this report.

Energy dispersal scrambling

In order to comply with radio regulations and to ensure adequate binary transitions, the data will be scrambled. The scrambling method is based on a pseudo-random bit sequence. This sequence has a flat power spectrum, so the energy will be equally dispersed over the whole spectrum [5]. The pseudo-random sequence is generated by a shift register with linear feedback (LFSR). The polynomial of the LFSR is given by

$$1 + X^{14} + X^{15}. \tag{2.1}$$

In Figure 2.3 the implementation is shown [13].

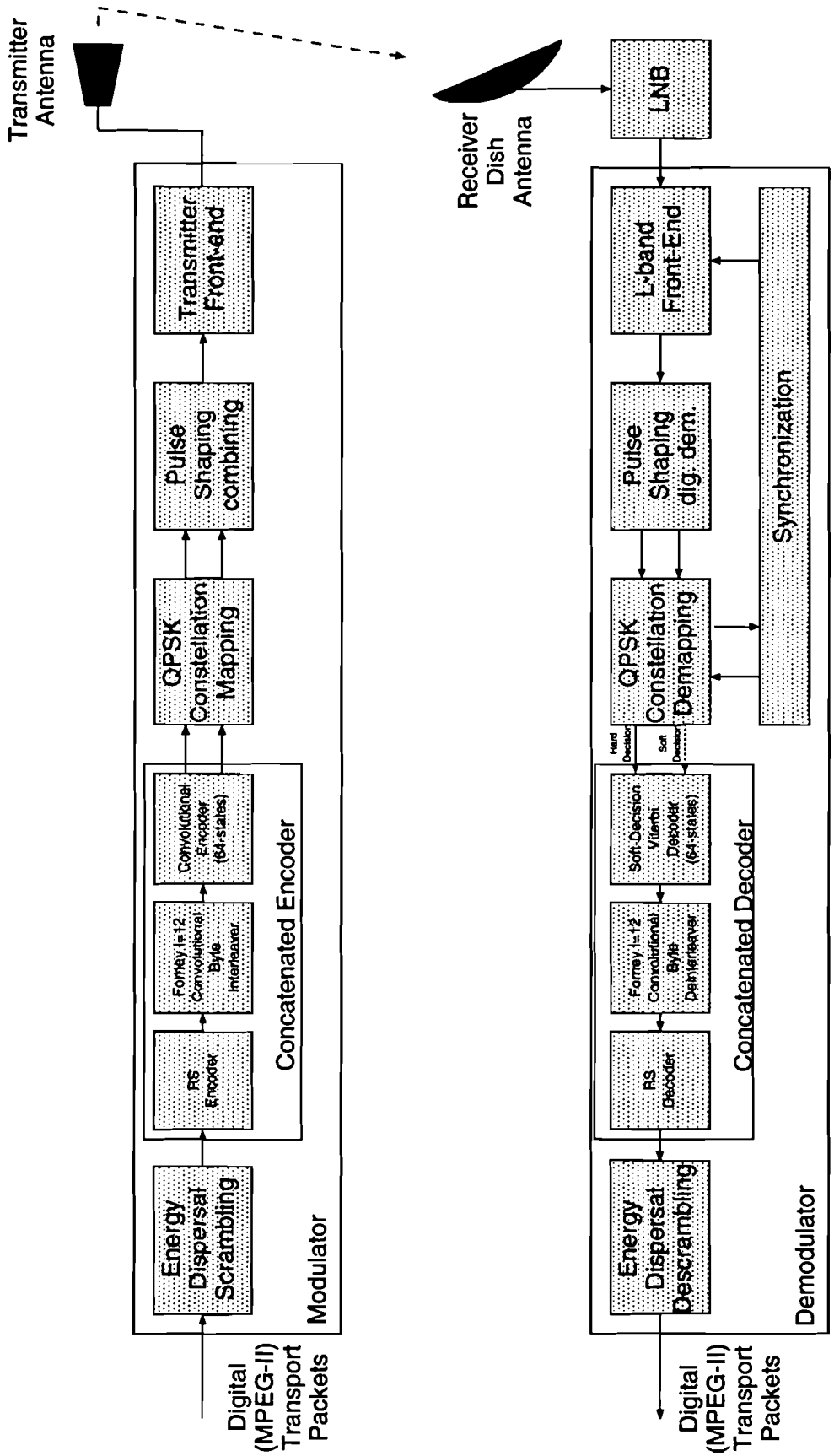

Figure 2.2: Digital MVDS transmitter and receiver setup

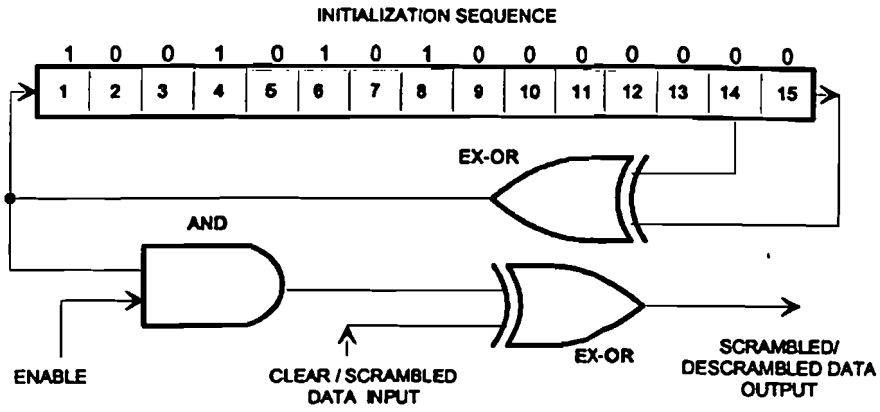

Figure 2.3: Scrambler de-scrambler schematic diagram

Reed-Solomon coding

Reed-Solomon codes are first constructed by Reed and Solomon [25]. The mathematical fundamentals of the codes are beyond the scope of this report. The practical results and the classification of this code will be discussed.

Reed-Solomon codes are non-binary linear block-codes. A linear block code consists of a set of fixed length code words in which the elements of the code words are selected from an alphabet of q symbols. Usually $q = 2^p$ so that p information bits are mapped onto a symbol. A codeword has length n, dimension k and $n - k$ redundant symbols.

The minimum Hamming distance between two code words is denoted as d. The number of errors that can be corrected by the Reed-Solomon codes is denoted by the letter t and given by [25]

$$t = \frac{d-1}{2}. \tag{2.2}$$

Hence, a code can be characterized by three parameters; the code word length n, the symbols per code word k and Hamming-distance d. These three parameters are normally given as $RS[n, k, d]$ to indicate the type of Reed-Solomon code. Since Reed-Solomon codes are maximum distance separable (MDS) [25],

$$d = n - k + 1. \tag{2.3}$$

The $RS[204, 188, t = 8]$, shortened code from the original $RS[255, 239, t = 8]$ code, is in this system applied to each randomized transport packet of $k = 188$ bytes. Substituting the parameters $n = 204$ and $k = 188$ in (2.3) yields $d = 17$. Substituting this value in (2.2) gives $t = 8$, this is the number of bytes that can be corrected.

The code can also be presented by $RS[204, 188, 17]$ which is a more common notation. The redundancy $(n - k) = 2t$, which is required to achieve an error correcting capability of up to t errors, yields a code rate

$$R_{RS} = \frac{k}{n}. \tag{2.4}$$

Convolutional interleaving

The convolutional byte interleaver is used to interleave the bytes [13]. The inner Viterbi decoder produces burst errors at its output. Most of the codes are effective when the errors caused by the channel are statistically independent. A sequence of t errors is defined as a burst of errors of length t-bytes. The Reed-Solomon coding of Section 2.4.1 can correct burst of errors of length $t = 8$. To improve the performance, the coded data will be interleaved. This interleaving is done in such a way that the burst channel has random errors. Hence, a code for random errors can be used. In the satellite system a convolutional interleaver based on the Forney approach is used. Figure 2.4 shows the conceptual diagram of the convolutional interleaver.

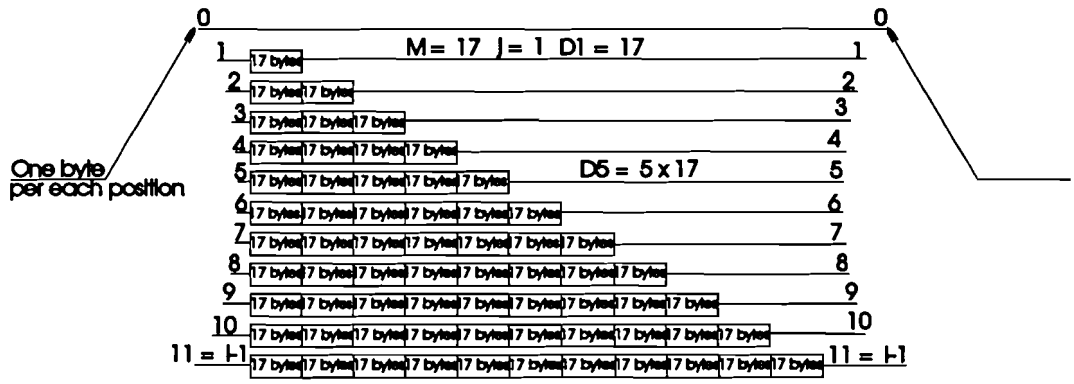

Figure 2.4: conceptual diagram of the convolutional interleaver

The interleaving depth $I = 12$ is the total number of branches of the interleaver. Each branch, except the first one, contains a shift-register (FIFO). The length D_j of the FIFO in branch j is given by

$$D_j = M \cdot j, \tag{2.5}$$

where $M = 17$ and j = 0 to I-1.

The total number n of bytes per error protected packet has to be divided over the I branches because the first byte (synchronization byte) of each MPEG-packet will be routed through branch $j = 0$. This is needed to provide a good synchronization of the MPEG-2 data stream. This division determines the depth of one block of a branch and thus the value of M

$$M = \frac{n}{I}. \tag{2.6}$$

For the satellite system with $n = 204$ bytes and $I = 12$, M equals 17. The advantage of a convolutional interleaver with respect to a block structured interleaver is that it better matches for use with the class of convolutional codes [30]. The satellite system uses a convolutional coder.

Convolutional code

The principle of the convolutional encoder is shown by Figure 2.5 , [31].

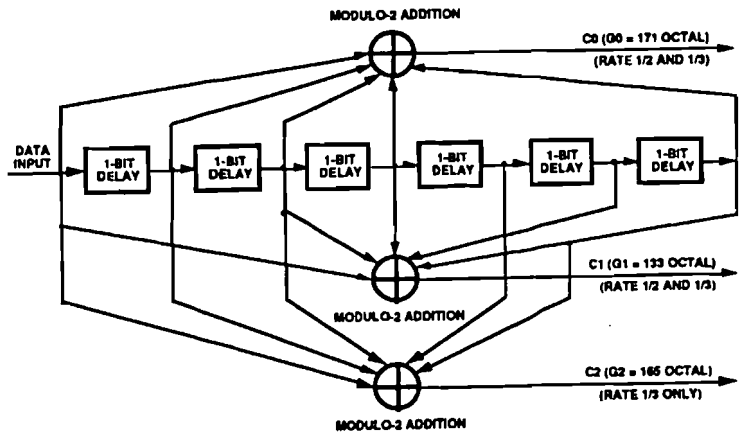

Figure 2.5: The principle of the convolutional encoder, [31]

From Figure 2.5 it is seen that the output of the encoder is determined by six previous bits plus the current input bit. This is known as a constraint length 7 code, denoted as $K = 7$, [31]. From Figure 2.5 it is also seen that there is one input bit and there are two or three output bits, so the coding rates of $R = 1/2$ and $R = 1/3$ are possible. In addition to these fundamental codes other higher code rates are achieved through a punctured coding technique [7].

Punctured coding techniques allow a lower bit rate to be used on the communication channel in comparison with the situation without puncturing and still the same data rate can be used. This is possible because some bits of the data rate are punctured or deleted in a repeating pattern and they are not transmitted. Figure 2.6 shows the principle for $R = 1/2$ to $R = 3/4$, [31].

The mathematical details of this coding scheme are beyond the scope of this report.

QPSK Constellation mapping

The encoded bits are mapped onto QPSK symbols as shown in Figure 2.7. If an error is made in receiving a QPSK signal the symbol received is most probable the symbol adjacent to the transmitted symbol. Therefore it is interesting to use a gray mapping such that a symbol error introduces most probably one bit error instead of two.

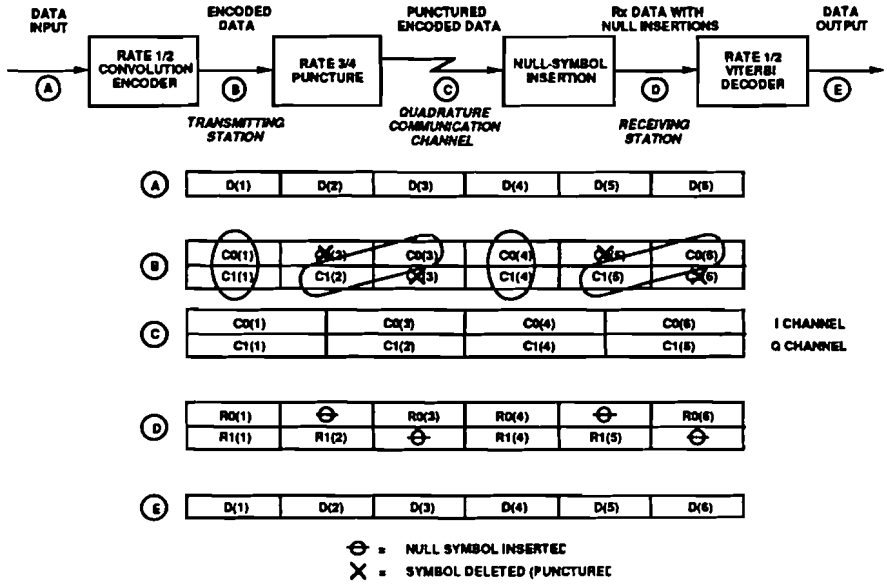

Figure 2.6: The principle of puncturing [31]

The axes of this constellation are represented by the in phase modulation carrier component I and the Quadrature modulation carrier component Q. Figure 2.7 shows a QPSK constellation.

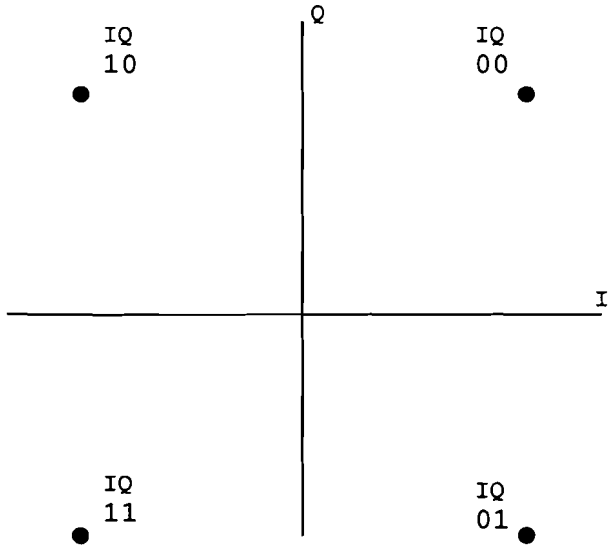

Figure 2.7: A QPSK constellation diagram

In a QPSK there is always the $\pi/2$ phase ambiguity. The demodulator does not know which symbol is received. It is possible however to detect the phase difference between the previous received symbol and the current received symbol. One way to use a QPSK link is thus to differentially encode the bits.

Differential encoding however decreases the performance of the link. If one symbol is received incorrect the result of the differential decoding is that two adjacent symbols are decoded incorrect. This is because the information is in the phase difference rather than in the phase itself.

The probability of a symbol error versus the carrier to noise ratio is shown in Figure 2.8. The exact derivation of this figure will be given in Section 5.1.2.

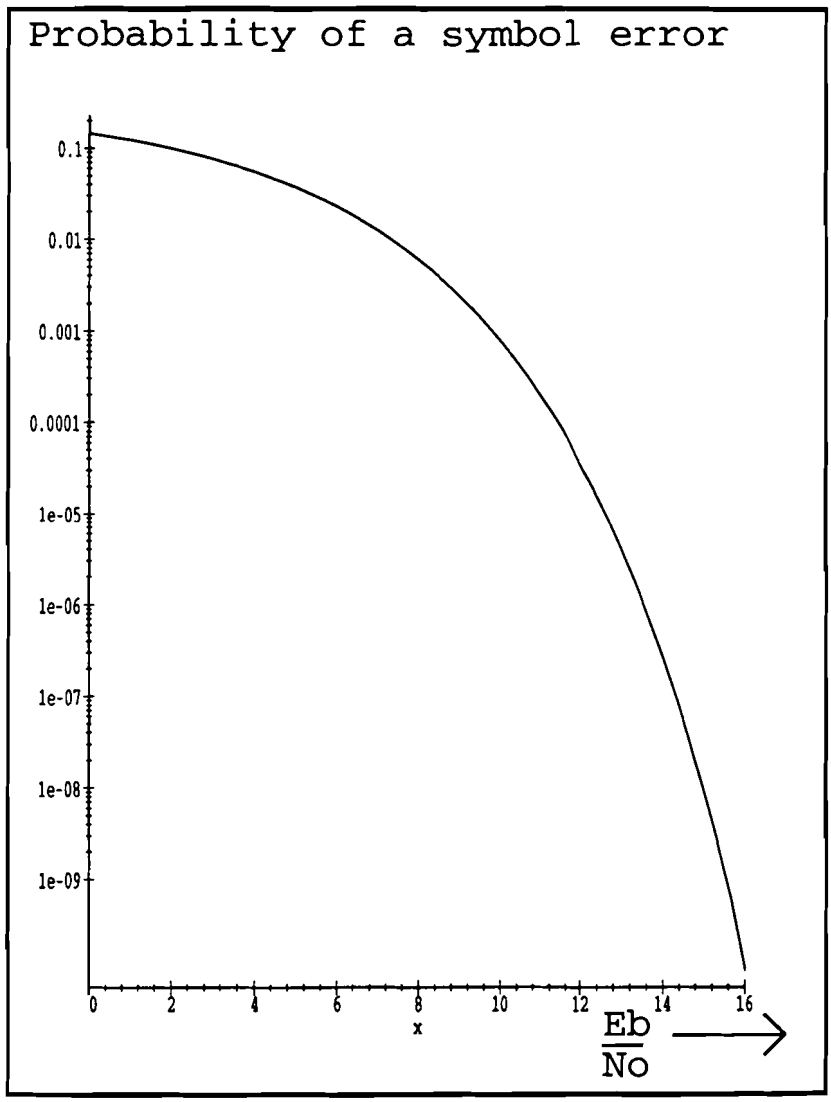

Figure 2.8: Probability of error versus carrier to noise ratio

From this Figure one can see that for links using high power, large carrier to noise ratios, the fact that the errors come in pairs and thus the probability of an error is

increased is no problem. The extra power required is negligible. For power restricted systems, low carrier to noise ratio, this effect is more severe as can be seen from Figure 2.8. The required increase in the carrier to noise ratio due to the differential encoding is then considerable. The exact relation between the probability of error and the carrier to noise ratio will be discussed in Section 5.1.2.

The MVDS system is to be operated at 42 GHz. Since it is difficult to build an power amplifier at these high frequencies the MVDS system is a power restricted system. The differential coding is thus not very interesting for an MVDS system.

The phase ambiguity has thus to be solved in a different way for instance using a unique pattern in the transmitted sequence. The correct phase can be selected on the reception of this pattern [18]. Another simple method is to look at the performance of the different decoding algorithms (Viterbi, Reed Solomon). If the performance with the current phase assumption isn't adequate a different phase can be assumed. The total synchronization time will increase with this method of synchronization. It is therefore very interesting to detect an erroneous phase assumption in the very first parts of the decoding e.g. the Viterbi decoder. There are of course numerous other techniques of solving the phase problem. A more detailed discussion is not in the scope of this report.

Pulse shaping

The I and Q signal will be square-root raised-cosine filtered to minimize ISI. The roll off factor is 35%, also denoted as $\alpha = 0.35$. The amplitude response of such a filter is given by

$$H(f) = \begin{cases} 1 & 0 \leq |f - f_o| \leq (1-\alpha)\frac{1}{2T} \\ \sqrt{\frac{1}{2} + \frac{1}{2}\sin\left[\pi \cdot T\left(\frac{\frac{1}{2T} - |f-f_o|}{\alpha}\right)\right]} & (1-\alpha)\frac{1}{2T} \leq |f - f_o| \leq (1+\alpha)\frac{1}{2T} \\ 0 & |f - f_o| > (1+\alpha)\frac{1}{2T} \end{cases} \tag{2.7}$$

where α represents the roll off factor, f_o is the central frequency of the filter and $1/T$ is the (Nyquist) symbol frequency.

The roll off factor $\alpha = 0.35$ used for minimizing ISI is an important parameter in a communication system. A large roll off factor can make the system more robust for timing jitter and reduces the inter symbol interference in the demodulator at the cost of some bandwidth.

After pulse shaping the I and Q signals are digital combined. This combining means multiplying the I component with a cosine and the Q component with a sine and adding up these signals. In the digital domain this is very simple. Each sample of the component (I) is multiplied by 1 and -1 and oversampled by a factor of two. This means that it is multiplied by a cosine sampled at 0 + k $\pi/2$ (1,0,-1,0 ....).

If the other component (Q) is treated the same but the result is shifted over one sample it is in fact multiplied with a sine sampled at 0 + k $\pi/2$ (1,0,-1,0 ....). If these samples are added up the result is a QPSK modulated carrier in the digital domain.

Transmitter front end

The input of the transmitter front-end is the digital signal from the pulse shaper/combiner. First the fundamental interval is filtered out from the digital information and the signal is converted to an analog signal. The next step is to transpose the signal to the L-band frequency. From the L-band the signal must be up-converted to the RF frequency of 42 GHz in one or more steps. In the last step the signal is amplified and fed to the transmitter antenna.

This description is of course a simplified and a theoretical description of the real situation (direct up conversion). The practical method of up conversion is more complex and technology dependent. A main problem of direct up conversion is the linear amplification at 42 GHz. It is very difficult to generate power at these high frequencies using linear amplifiers.

Another method is using a non-linear device to double or triple the frequency after it has been amplified at a lower frequencies. This is a very common method when analog FM modulation is used. For QPSK modulation this method is not ideal since it introduces ISI even without noise and with perfect Nyquist filters. The amount of ISI depends on the nyquist filters used. Since the MVDS must comply to the satellite standard the Nyquist filters can not be changed. This means that this method is not usable. A third method is to mix the L-band source signal to an intermediate frequency of 14.5 GHz. At this frequency linear power amplifiers can be used. An oscillator generates a frequency of 13 GHz. This can be amplified and doubled by a not linear device since it is only a carrier. Then it is possible to mix the 26 GHz power signal and the 14.5 GHz power signal by means of a power mixer to the 40.5 GHz. The last step involves filtering and feeding it to the transmitter antenna. On all the schemes a back-off in the transmitter amplifier must be used of course to guarantee linearity.

There are other scenarios possible. The best practical solution has to be further examined and is not in the scope of this report.

2.4.2 Receiver description

Low noise block converter (LNB)

The low noise block converter LNB converts the 42 GHz RF signal to the L-band signal. From that point the standard digital satellite receiver can be used. The LNB consists in principle of a band pass filter, low noise amplifier, local oscillator, mixer

and a L-band amplifier as shown in Figure 2.9.

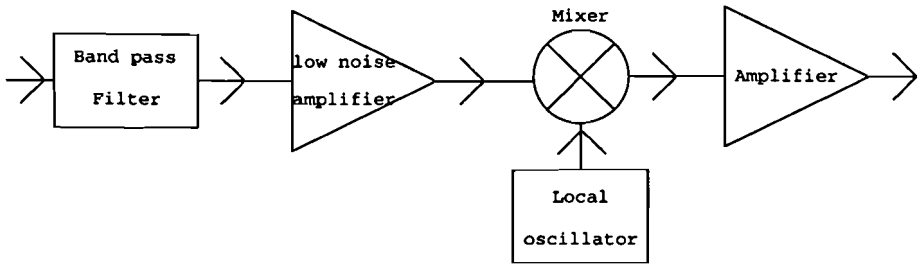

Figure 2.9: A low noise block setup

To reduce the noise factor of the total system it is of course interesting to amplify the signal as soon as possible. The noise influence of the succeeding parts of the receiver will have little influence on the noise figure in this case. In this situation however again a linear amplifier at 42 GHz is required. This amplifier must be a low noise amplifier. If this is too expensive the first amplifier can be left out. In this situation the received signal is immediately mixed after filtering and amplified. The result is of course a very high noise figure F. This will have influence on the link budget and hence the maximum path length will decrease.

Front end

The L-band front-end selects one channel out of the spectrum. The tuner must be tunable e.g. between 950 MHz and 2050 MHz. In this case only one GHz of the MVDS spectrum can be tuned. This could be solved by using a switchable local oscillator in the LNB. In this way one could select the upper or lower 1 GHz.

Matched filter

The in phase signal I and the quadrature signal Q are recovered by means of digital demodulation.

Complementary pulse shaping filters of square-root raised-cosine type with roll off $\alpha = 0.35$ are used as described in Section 2.4.1.

QPSK constellation demapping

The symbol to bits mapping mechanism is the inverse operation of the bits to symbol mapping mechanism described in Section 2.4.1.

Convolutional de interleaver

The convolutional de interleaver performs the inverse operation of the convolutional interleaver described in Section 2.4.1. The convolutional interleaver is shown in Figure 2.4 and the convolutional de interleaver is shown by Figure 2.10.

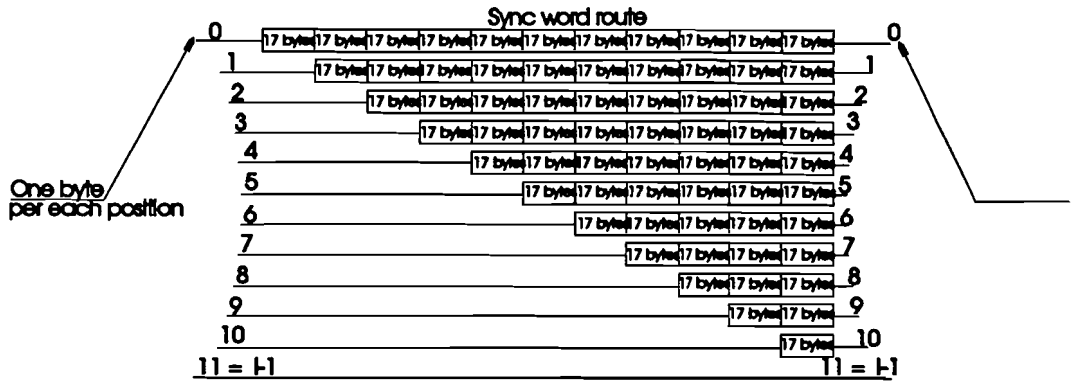

Figure 2.10: conceptual diagram of the convolutional de interleaver

Reed-Solomon decoder

For decoding Reed-Solomon codes, a standard decoding mechanism developed by Berlekamp & Massey can be used. The mathematical fundamentals of the decoding mechanism are beyond the scope of this report.

Energy dispersal de scrambling

The Energy dispersal de scrambling is the inverse operation of the energy dispersal scrambling described in Section 2.4.1.

2.5 Discussion

The future MVDS system will be a digital system based on the Digital Video Broadcasting (DVB) satellite standard. This results in a relatively inexpensive solution for digital MVDS.

Because of the power limitations (linear amplification) and the large losses it is necessary to use multiple cells to cover a large area. This results in interference between the different cells.

The modulation used is non differential QPSK-modulation with forward error correction (FEC) consisting of concatenated coding of Reed-Solomon outer coding and convolutional inner coding. Raised-cosine filtering is used with a roll-off factor of 0.35.

Chapter 3

Propagation aspects

In this Chapter we shall consider different propagation aspects, as discussed by Freeman [15], relevant for calculating the link budget in Chapter 5. This Chapter is based on [39] with some modifications.

3.1 Free space

The first step in looking at propagation is to calculate the free space loss L_{bf} which occurs in an idealized situation, this means an infinite empty space where the medium is assumed to be a vacuum.

We start with defining the transmitting antenna as an isotropic source in vacuum. We consider the envelope surrounding the antenna to be a sphere and the total power is p_t. The net power flux density s_{av} through a part of the surface of 1 square meter of the sphere with radius d equals

$$s_{av} = \frac{p_t}{4\pi d^2} \tag{3.1}$$

where d is the distance.

An isotropic receiver antenna at distance d from the transmitting antenna will absorb power which is equal to $\beta \cdot s_{av}$ where β is the effective aperture. The effective aperture for an isotropic antenna is given by $\lambda^2/(4\pi)$ where λ is the wavelength [2]. The total received power becomes

$$p_r = p_t(\frac{\lambda}{4\pi d})^2 \tag{3.2}$$

The loss is defined as

$$l_{bf} = \frac{p_t}{p_r} = \left(\frac{4\pi d}{\lambda}\right)^2 \tag{3.3}$$

or

$$L_{bf,\mathrm{dB}} = 10\log(\frac{p_t}{p_r}) = 10\log\left(\frac{4\pi d}{\lambda}\right)^2 \tag{3.4}$$

3.2 Refractivity

In this section it is assumed that the radio beam is an infinite thin line in order to simplify calculations. However in section 3.3 it will be shown that the actual radio path is not a thin line.

In free space the path of a radio beam follows a straight line. In the earths atmosphere however this is not always the case. This is due to the variation in the refractivity index n in the atmosphere. The refractivity index is defined as follows [15]

$$n = \frac{c}{v_{medium}} = \sqrt{\epsilon_r \cdot \mu_r} \tag{3.5}$$

where the relative magnetic permeability $\mu_r = 1$ in the atmosphere, ϵ_r is the relative electric permittivity, c is the velocity of light in vacuum and v_{medium} is the velocity of the electromagnetic waves in the medium.

The refractivity index $n \approx 1.003$. The refractivity N is defined as

$$N = (n-1) \cdot 10^6 \tag{3.6}$$

For radio frequencies the following relation holds (CCIR recommendation 453-2 [22]):

$$N = \frac{77.6}{T}\left(P + 4810 \cdot \frac{e}{T}\right) \tag{3.7}$$

where

P = atmospheric pressure in millibar
T = temperature in Kelvin
e = water vapor pressure in millibar
77.6 = constant with dimension K/millibar
4810 = constant with dimension K.

The error in this relation is less than 0.5% for frequencies up to 100 GHz. For a small temperature deviation ΔT, a small pressure deviation ΔP and a small water vapour pressure deviation Δe we obtain the refractivity deviation. [2]

$$\Delta N = -1.12\Delta T + 0.268\Delta P + 4.44\Delta e \tag{3.8}$$

where the ground level values for the Netherlands are

$T_0 = 290$
$P_0 = 1026$ mbar
$e_0 = 11.4$ mbar
$N_0 = 325$.

From the definition of the refractivity index and the fact that it decreases with altitude it follows that the travelling speed of the waves increases with increasing altitude [2]. This results in a curved ray path through the atmosphere. Measurements have shown that the refractivity index doesn't change too much in the horizontal direction. It is therefore allowed to look at the problem as if the atmosphere is divided into spherical layers.

In Appendix C a relation is derived for the effective curvature of the earth and a relation to calculate the related k-factor. The k-factor is the ratio of the effective radius of the earth, if it is assumed that a ray beam follows a straight line, and the true earth radius. In Figure 3.1 the relation between the two earth radii is shown.

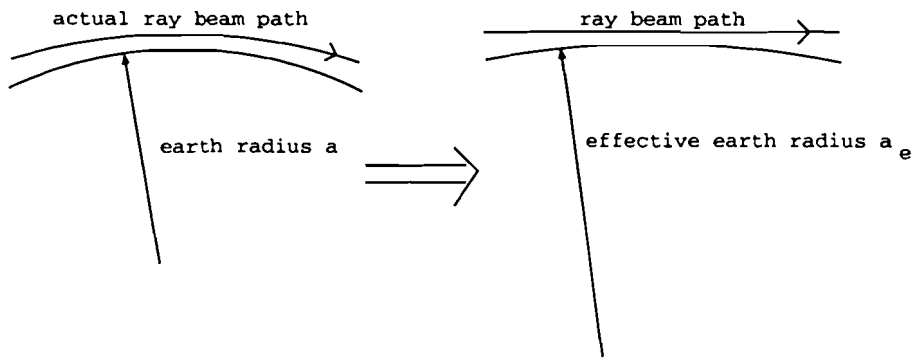

Figure 3.1: Earth radius and the effective earth radius

The k-factor can be calculated with

$$k = \frac{1}{1 + a \cdot \frac{dN}{dh} \cdot 10^{-6}} \tag{3.9}$$

where

$k = a_e/a$
a = earth radius (6378.155 km)
a_e = effective earth radius (km)
N = refractivity (/km)
h = height (km).

Since the refractivity N is depending on temperature, atmospheric pressure and the water vapour pressure the k-factor is also related to these quantities. This results in a varying k-factor, in time as well as in space. The median value however is often taken as $k = 4/3$ [16]. To predict the k-factor there are standard atmospheres defined by the CCIR [16] for different global areas. From these it is possible to estimate e.g. a k-factor which is not exceeded e.g. for 99.9% or 99% of the time.

Due to the water vapour, temperature and pressure changes in the vertical extend in the lower part of the troposphere ducting can occur. If $dN/dh \leq -157$ /km the

k-factor becomes negative. This means that the electromagnetic rays transmitted parallel to the earths surface are bended towards the earths surface. If they are then reflected on the earths surface we have a surface duct. The wave is no longer a spherical wave and the formula for the free space loss can't be used. If such a duct exists more power than expected can be received. If in the lowest part $dN/dh \geq -157$ /km an elevated ducting layer can exist.

If this phenomena occurs in a network much more interference than expected may be the result.

3.3 Diffraction

Diffraction of a radio wave occurs when there is an obstacle in the radio path which is relatively large compared to the wavelength. The amount of loss due to obstruction is proportional to the area of the beam which is obstructed.

To calculate the obstructed area the principles of Huygens-Fresnel are used. The Fresnel zones are defined as the areas perpendicular to the ray beam where the waves have the same phase [15]. The phase between the n^{th} and the $n + 1^{th}$ equals π. It can be derived that the power of the wave travels approximately within half of the first Fresnel zone. In Figure 3.2 the attenuation due to refraction can be seen [15]. In this figure the attenuation as a function of the clearance related to the first Fresnel zone is plotted.

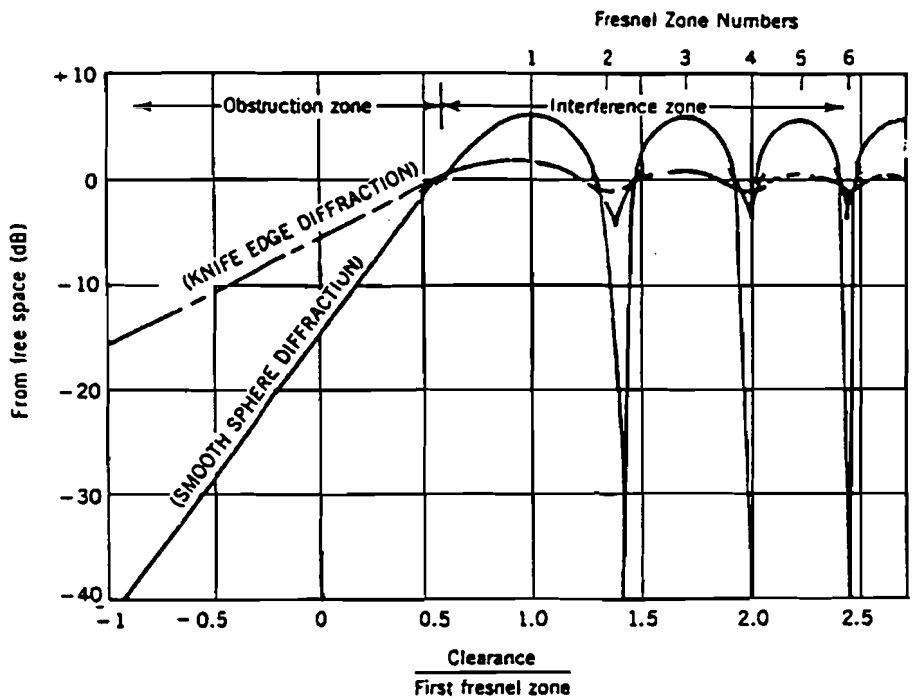

Figure 3.2: Path attenuation versus path clearance[2]

It is stated [15] that in the far field situation 0.6 times the first Fresnel zone clearance from obstruction of the beam edge is required to obtain an attenuation due to the obstacle of less than 3 dB.

The radius R_n of the n^{th} Fresnel zone can be approximated with

$$R_n = 547 \cdot 10^3 \sqrt{\frac{n}{f} \cdot \left(\frac{d_1 d_2}{d_1 + d_2} \right)} \tag{3.10}$$

where

R_n = the radius of the n^{th} Fresnel zone (m)
d_1 and d_2 are the distances from a point in the radio path to the antennas (km)
f = the used frequency (Hz).

Providing a Fresnel zone clearance $cl = 0.6$ is sufficient to ensure that attenuation due to an obstacle in or near the beam path is negligible [15]. It is however a very common use in microwave communications to use the following clearance criteria (high reliability system):

$cl \geq 0.3 \cdot R_1$ at $k = \frac{2}{3}$
$cl \geq 1.0 \cdot R_1$ at $k = \frac{4}{3}$.

If we take a look at the system at trial where the transmitter antenna height h_t is approximately 65 m and receiver antenna height h_r is assumed to be 10 m we can draw the path of the ray beam (Figure 3.3). In this curve a coverage distance of 5 km is assumed (the worst case will be at the edge of a cell). It is now possible to calculate the minimum height of the first Fresnel zone along the path.

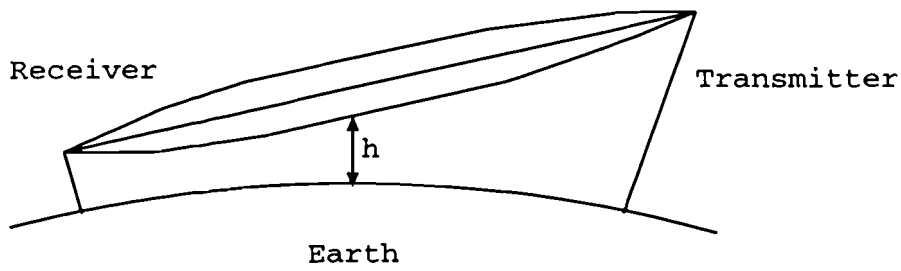

Figure 3.3: Ray beam path and the first Fresnel zone

In figure 3.4 the height of the first Fresnel zone is plotted. In this figure a k-factor of -0.3, $4/3$ and 0.3 is assumed. This height is given by

$$h(d_1) = \frac{(h_t - h_r)}{d_1 + d_2} \cdot d_1 + h_r - R_1(d_1) - \frac{d_1 d_2}{12.75 \cdot k} \tag{3.11}$$

where

h is the height of the first Fresnel zone
h_r is the height of the receiver antenna
h_t is the height of the transmitter antenna
d_1 is the distance of the specific point to the receiver
d_2 is the distance of the specific point to the transmitter
R_1 is the radius of the first Fresnel zone
$(d_1 d_2)/(12.75 \cdot k)$ is a correction for the earth curvature [15].

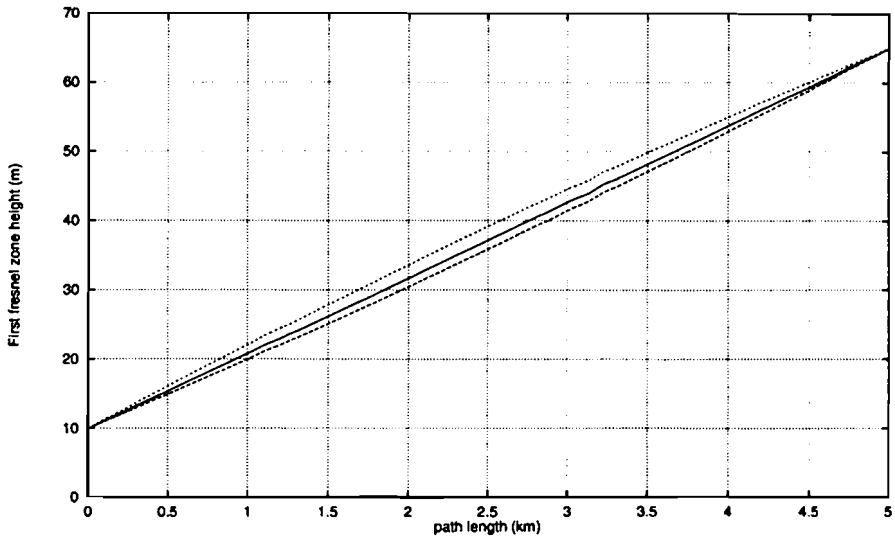

Figure 3.4: The height of the first Fresnel zone (k=-0.3, 4/3 and 0.3)

From Figure 3.4 we can see that the extra clearance required for the fresnel zone for this link is negligible. A line-of-sight between the transmitter and receiver will be sufficient.

With this figure we can predict whether obstruction is a problem and if so what antenna height will be necessary to overcome this problem. It obvious that for a city with high buildings a line-of-sight (LOS) with antennas on lower buildings is not always possible. The number of possible reception sites will vary with different cities and will be examined in Chapter 6.

3.4 Diffraction around obstacles

As we have seen in the previous section the bending of the waves due to the gradient in the refractivity index is negligible for the distances of concern. It is thus assumed that the waves travel in a straight line.

This means that if the surface is flat the total coverage area is illuminated with the microwaves, no shadows. In an urban environment however there may be tall

buildings blocking the Line Of Sight (LOS). As can be seen from Figure 3.2 the received energy in a shadow area is not zero. Therefore it may be possible to have a good reception behind a tall building. This is very interesting because it will increase the percentage of the coverage area where reception is possible in an urban environment.

Since we are interested in the percentage of the coverage area where reception is possible we are interested in the maximum angle of usable diffraction. In Figure 3.5 the coverage gain due to diffraction is illustrated.

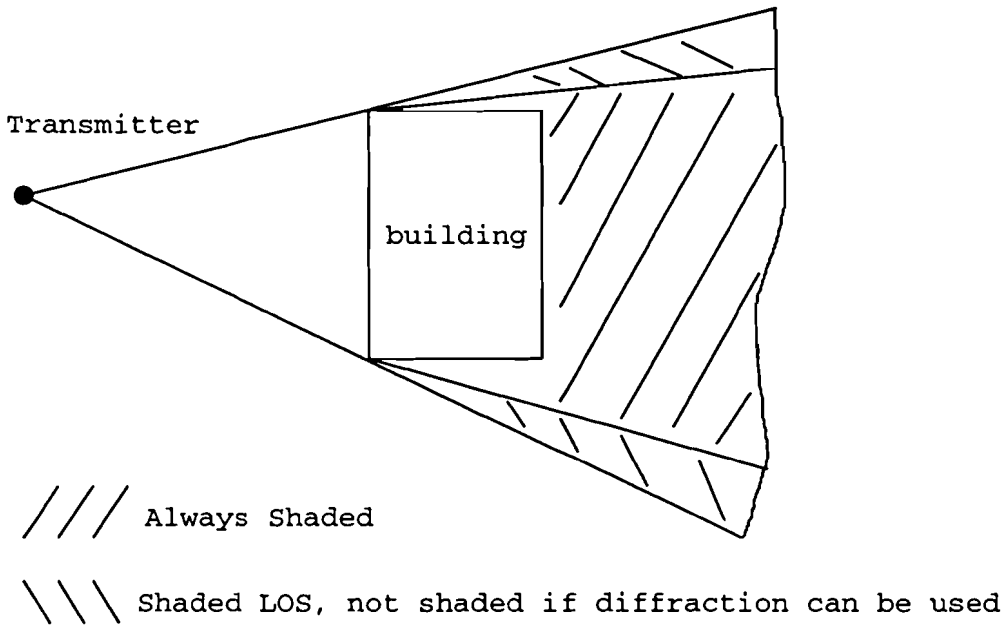

Figure 3.5: Coverage gain due to diffraction

It is thus necessary to have a close look at the diffraction problem. In Appendix D a simple analysis of a single knife edge diffraction is performed. The analysis assumed a infinitely long knife edge and line sources. The results from a single knife edge can be very well used on real situations however. This is if we take the source to be a point source and the knife edge to be longer than the width of the first Fresnel zone if there where no obstruction. The radius of the First Fresnel zone is in our case always smaller than 3.7 m and 3.0 m assuming a maximum distance to be covered of 5 km and a frequency of respectively 28 and 42 GHz [39]. This theory can thus be very well used on diffraction by large buildings.

The loss L_{df} due to diffraction can be high for high frequencies however. As shown in Appendix D the attenuation L_{df} of a single knife edge L_{df} is given by

$$L_{df} = 20 * \log\left(\left|\frac{1}{2}\sqrt{2} \cdot \left[\frac{1}{2}(1+j) - (C(\Delta) + j \cdot S(\Delta))\right]\right|\right) \tag{3.12}$$

where $C(\Delta)$ and $S(\Delta)$ are the Fresnel integrals defined as

$$C(\Delta) = \int_0^{\Delta} \cos(\frac{\pi}{2} \cdot \nu^2)\, d\nu \tag{3.13}$$

and

$$S(\Delta) = \int_0^{\Delta} \sin(\frac{\pi}{2} \cdot \nu^2)\, d\nu \tag{3.14}$$

The parameter Δ is defined as

$$\Delta = h \cdot \sqrt{\frac{2}{\lambda} \cdot (\frac{1}{d_1} + \frac{1}{d_2})} \tag{3.15}$$

where λ is the wave length, h is the height of the obstruction as defined in Figure 3.7. d_1 and d_2 are the distances from the receiver and transmitter to the obstruction.

Now let us model a building as a rectangular shield as shown in Figure 3.6

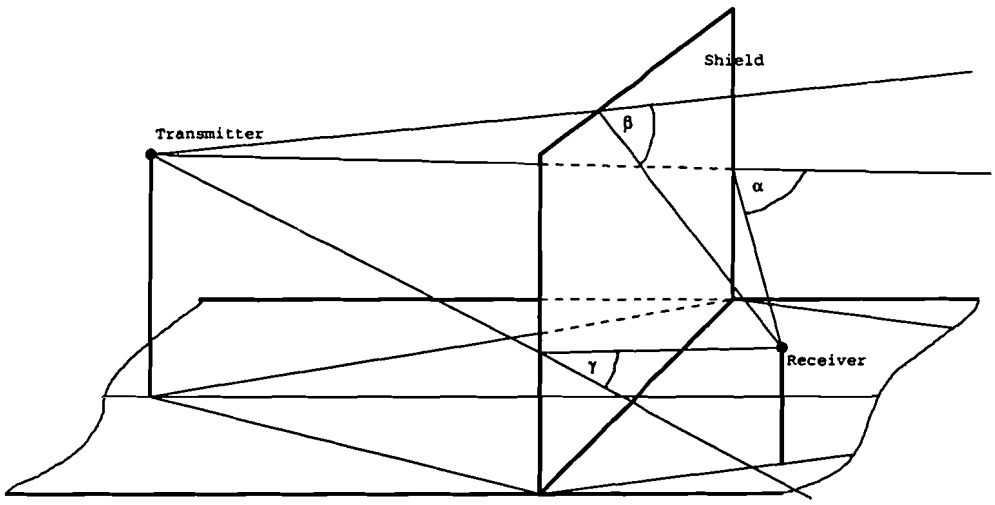

Figure 3.6: Model of a building

In this model we leave out the corner diffraction for simplicity. In the model the reception antenna is positioned in the area where reception via diffraction might be possible. In such a case it assumed that the diffraction angles α and β are much larger than the diffraction angle γ. If this is the case it is enough to take only that dominant diffraction ray with diffraction angle γ into account. The difference in the attenuation between these rays is huge. The model can thus be simplified to only one diffraction ray as shown in Figure 3.7.

The difference between the obstructed received field strength and the un obstructed received field strength can than be estimated with formula 3.12.

With the model above the angle at which diffraction is still possible can simply be estimated if the allowed loss is known. For very small Δ the Fresnel integrals can

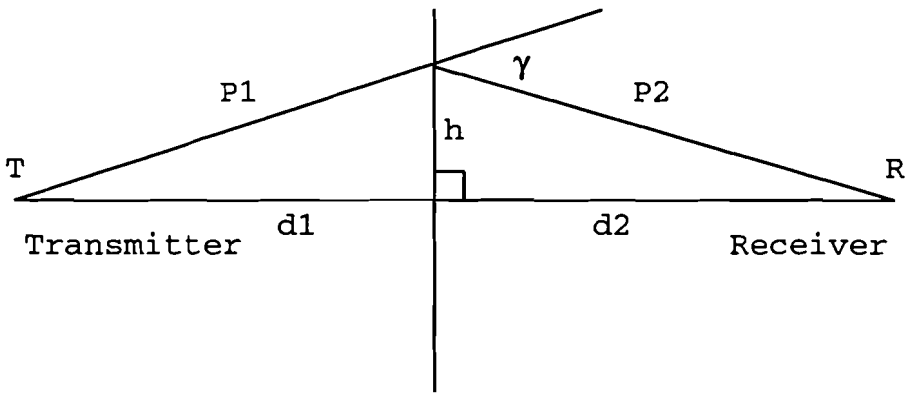

Figure 3.7: Diffraction simplified to one ray

be replaced by its series expansion.

$$C(\Delta) = \Delta + \Delta^5 + \Delta^9 + ... \tag{3.16}$$

$$S(\Delta) = 0 + \Delta^3 + \Delta^7 + ... \tag{3.17}$$

Using the series expansion of the Fresnel integrals the attenuation due to diffraction can be approximated for very small angles by [3]

$$L_{df} = -6 - 8.7 \cdot \Delta \tag{3.18}$$

Formula 3.12 for estimating the attenuation can be approximated with the following formulae

$$\begin{array}{rcccl} & \Delta & \leq & -0.78 & L_{df} = 0dB \\ -0.78 & < \Delta & \leq & 0.8 & L_{df} = -6 - 8.7 \cdot \Delta dB \\ 0.8 & < \Delta & \leq & 2.0 & L_{df} = -14 - 16 \cdot \log(\Delta) \\ 2.0 & < \Delta & & & L_{df} = -13 - 20 \cdot \log(\Delta) \end{array} \tag{3.19}$$

These formulae are simply fitted on the curve predicted by formula 3.12. These formulae can be very well used for computing the attenuation. In Figure 3.8 the loss due to diffraction is given.

With the aid of these formulae the coverage gain due to diffraction can be calculated if the dimensions of the buildings are known. As an example a the diffraction around a large building will be calculated. Assume a building with the dimensions as shown in Figure 3.9

With the formulae above it is possible to predict the received field strength. In this example we assume the use of 28 GHz. The diffraction loss L_{fd} over the top of the building equals more than 40 dB, it is thus concluded that its contribution is negligible as stated before. To estimate the received field the diffraction around the sides of the building is calculated. In Figure 3.10 the received field strength is shown as a function of x, where x is the distance to the optical shadow line in m.

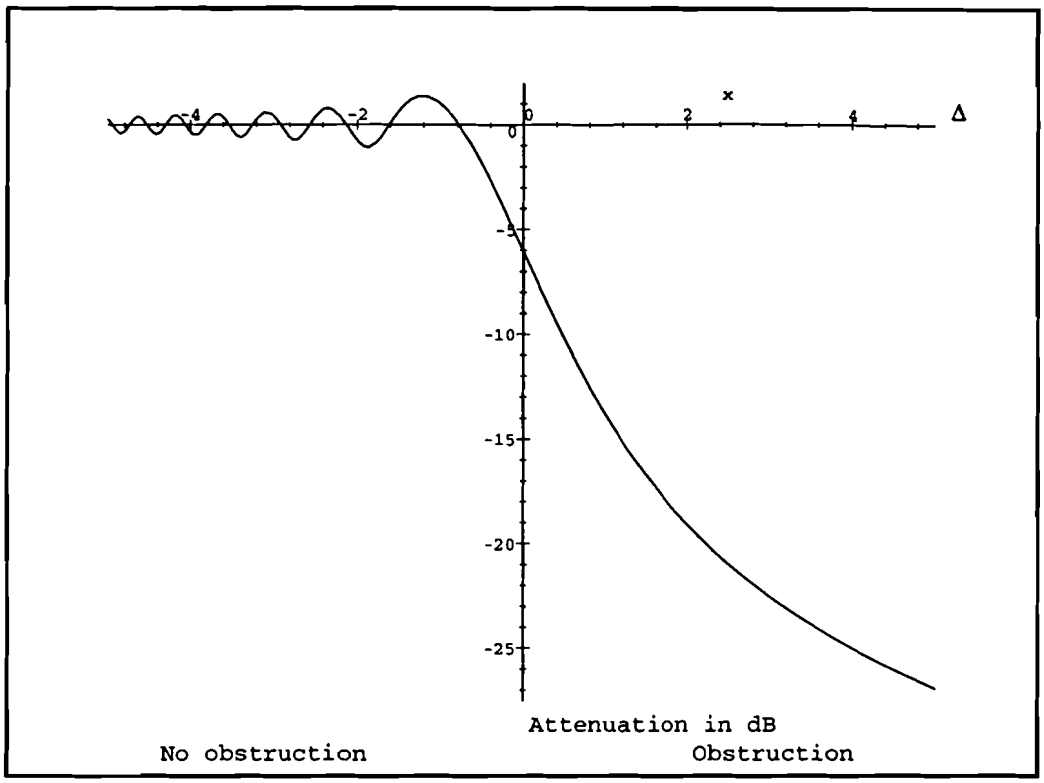

Figure 3.8: Attenuation due to diffraction

From this figure it can be seen that reception by diffraction is not very useful for MVDS at high frequencies. The attenuation at 42 GHz is even larger. For comparison the curves for 1 GHz, 28 GHz and 42 GHz are plotted in Figure 3.10

In the 1 GHz example the diffraction loss over the top of the building equals 26 dB.

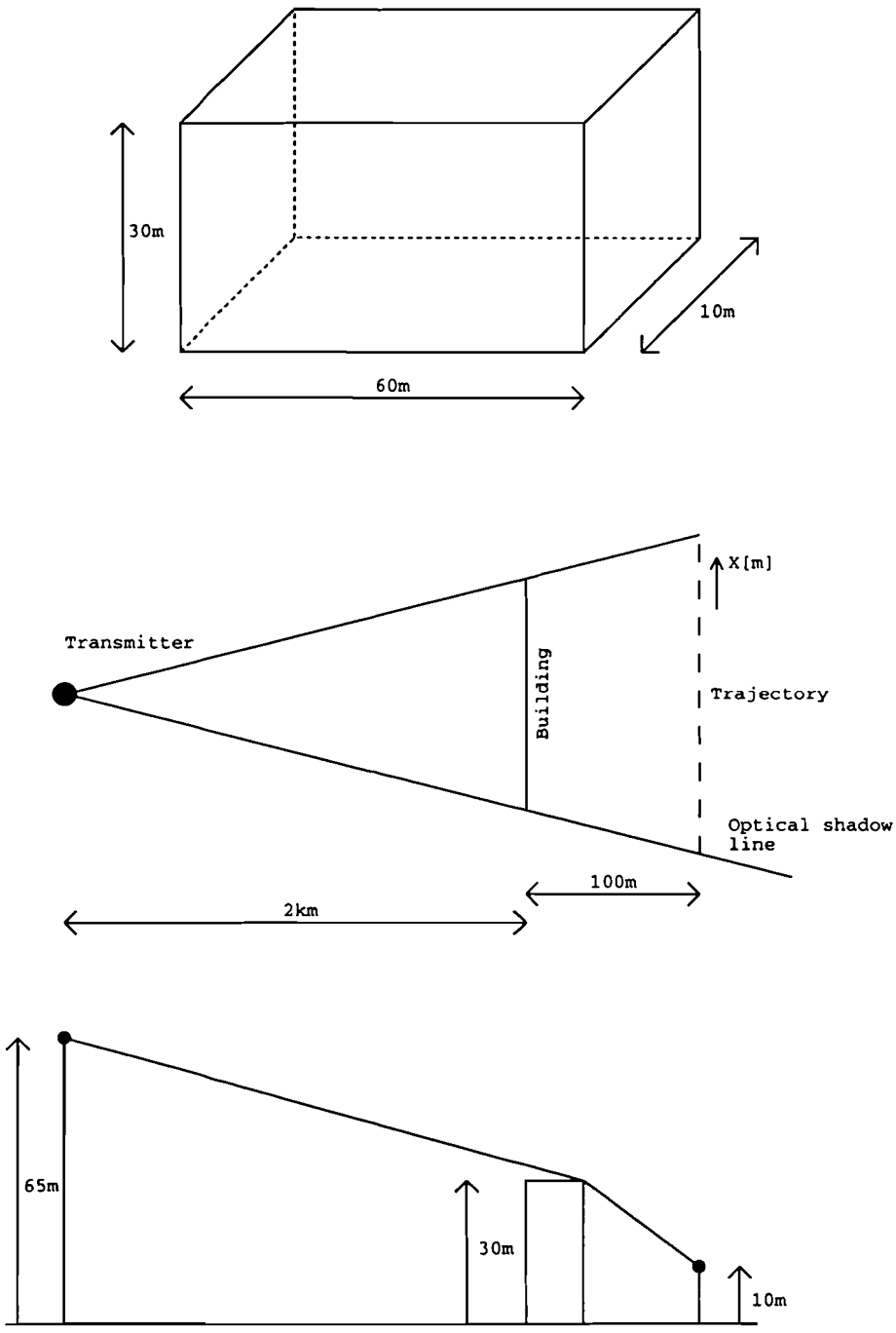

Figure 3.9: An example of diffraction

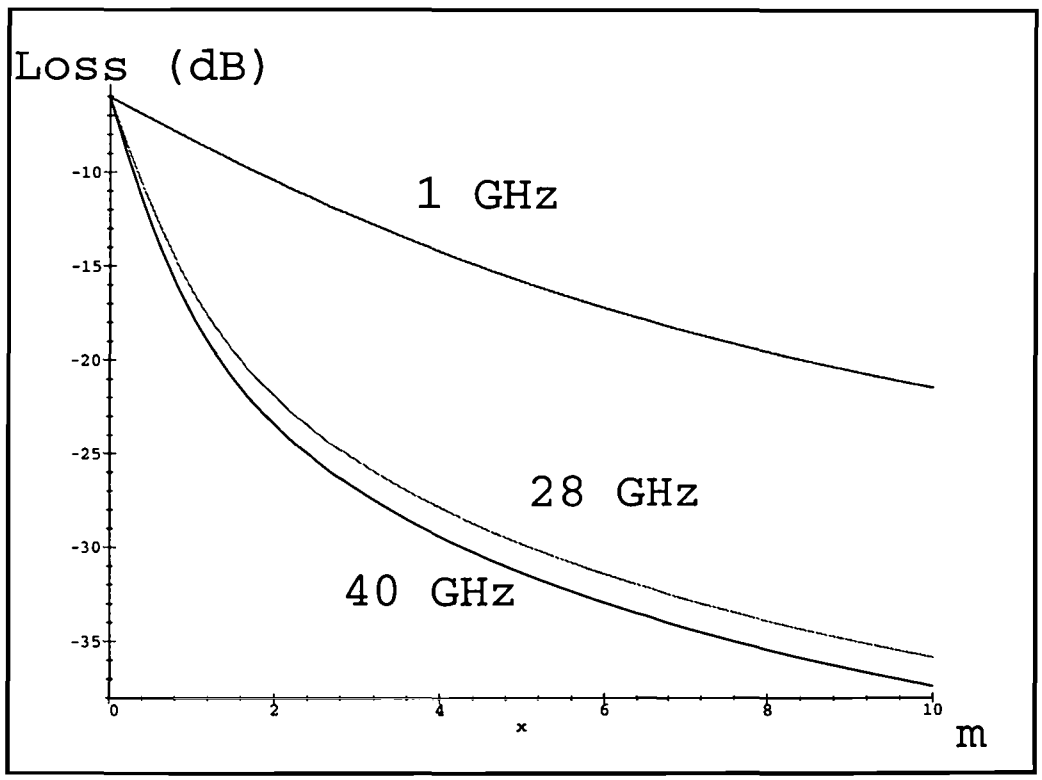

Figure 3.10: Diffraction loss around a building

3.5 Reflections

In this section the reflection of incident waves on a surface is discussed. If electromagnetic waves can be reflected on a surface, then such a reflection might be usable for an MVDS system to increase the percentage of coverage. In Figure 3.11 a configuration is shown how the percentage of possible coverage can be increased due to a reflection.

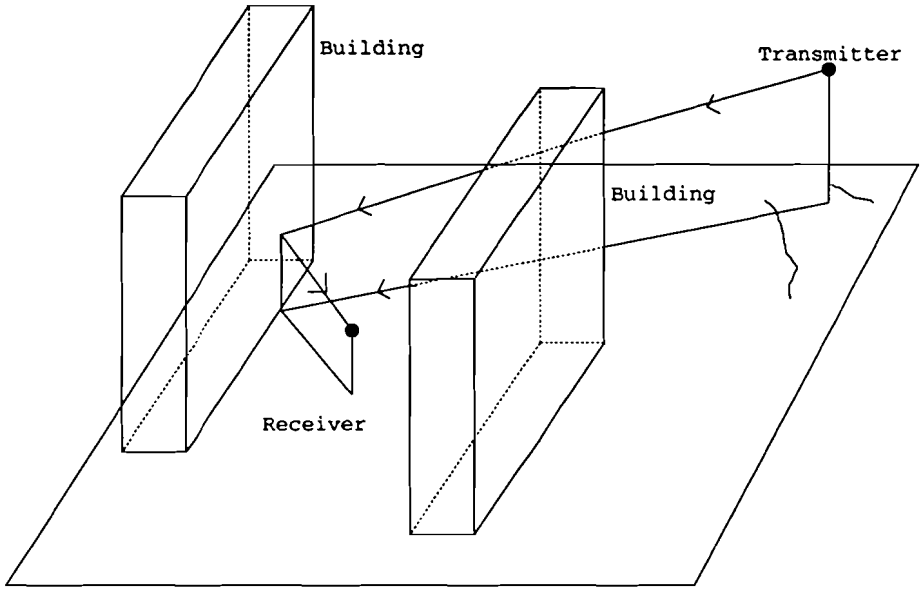

Figure 3.11: Increase in coverage due to one single reflection

If reception by means of a reflection is an interesting feature for MVDS depends on the nature of the reflection and the nature of the environment, urban suburban etc. In the following sections a surface reflection is further examined.

In the first approach it is assumed that the ray beams obey the rules of optical reflection e.g. no refraction.

In Figure 3.12 there is a model which uses two rays. In this figure h_t is the transmitter antenna height, h_r is the receiver antenna height and d is the distance between transmitter and receiver.

The field strength E at the receiver antenna consists of a contribution of the direct wave and the reflected wave.

$$E = E_o \cdot |(1 + \rho e^{j\psi})| \tag{3.20}$$

where

E_o = direct wave field strength
ρ = reflection coefficient
ψ = phase difference due to path length difference.

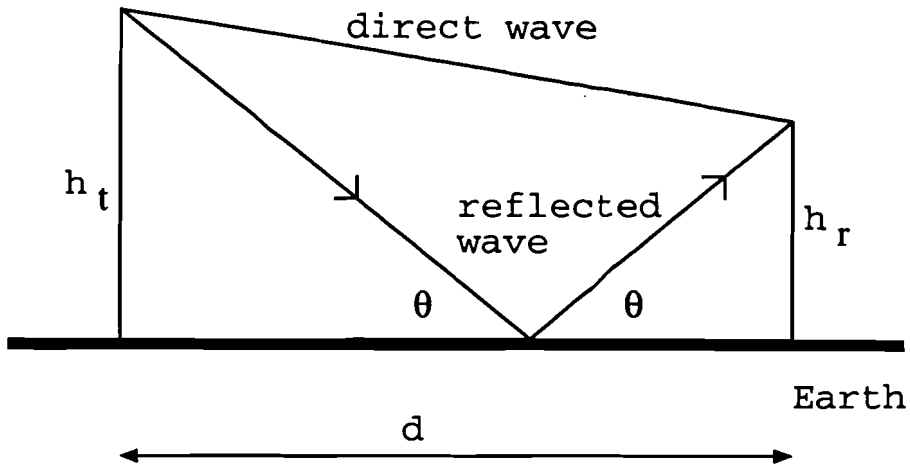

Figure 3.12: Two ray model ($k = \infty$)

The reflection coefficient ρ equals -1 for very small angles θ and a perfectly smooth infinite surface. If the distance $d \gg h_t$ and $d \gg h_r$ and thus h_t and h_r are very small in comparison with the path length b of the reflected wave and the path length a of the direct wave a, the path length difference $b - a$ can be approximated with $(2h_r h_t)/d$. The phase difference ψ equals $(4\pi h_r h_t)/(\lambda d)$. This results in a position dependent relative field strength:

$$\frac{E}{E_o} = |2 \cdot \sin(\frac{2\pi h_r h_t}{\lambda \cdot d})| \tag{3.21}$$

The height-gain function is depending on the antenna heights h_t and h_r, the distance d and the used wavelength λ. Now it is possible to obtain the antenna height-gain pattern and the distance gain pattern as shown in Figure 3.13 and Figure 3.14 respectively. From these figures it is possible to define heights in an area where the antenna should be mounted. In these figures the amplitude a of the reflected signal equals 1.

The notches in the height-gain pattern are a distance of $(\lambda d)/(2h_t)$ apart. For the used 28 GHz link with an antenna height $h_t = 65$ m, $\lambda = 10.7$ mm and a distance d of 5 km this is a distance of 0.41 m. For the 42 GHz range this even becomes smaller. This means that at every location there is a usable height available. The notches in the distance gain pattern are a problem since the attenuation is infinite according to this theory at the distances $d = (2h_t h_r)/(n\lambda)$ where n is an integer.

The parameters in these figures are of course related to the used wavelength. Therefore when a modulated signal will be transmitted, signal distortion may occur. This distortion will be amplitude distortion in the modulated signal. Suppose the received signal $y(t, \tau)$ looks like

$$y(t, \tau) = x(t) + a \cdot x(t - \tau) \tag{3.22}$$

where $x(t)$ is the transmitted signal, a is the relative echo amplitude and τ is the

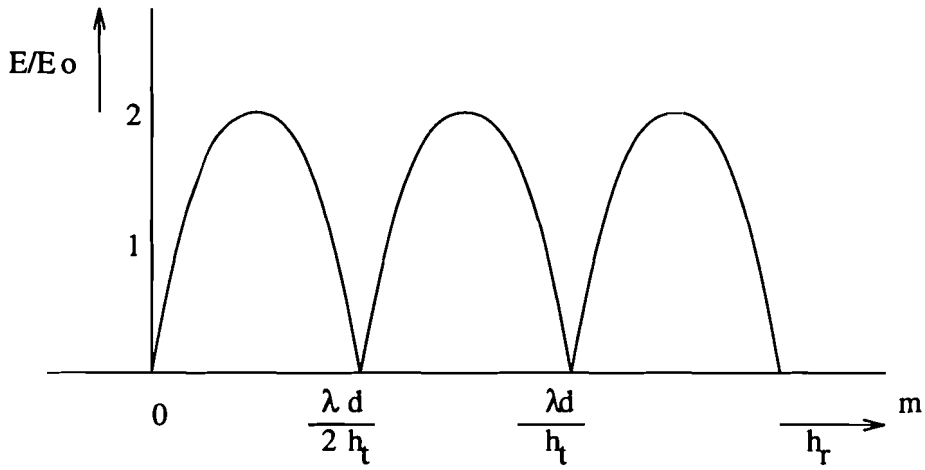

Figure 3.13: The height gain pattern with a single echo

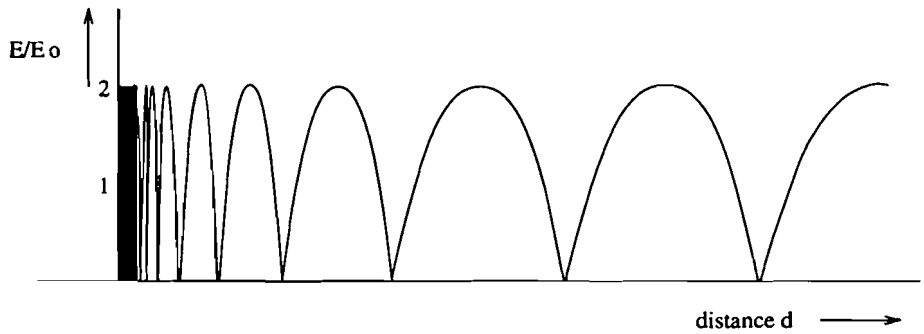

Figure 3.14: The distance gain pattern with a single echo

echo delay.

In the frequency domain this becomes

$$Y(f) = (1 + a \cdot e^{-j2\pi f\tau})X(f) \tag{3.23}$$

From here we obtain the power spectrum as $S_y(f) = |Y(f)|^2 = Y(f)Y(f)^*$ This results in the following equation

$$|Y(f)|^2 = (1 + a^2 + 2a \cdot \cos(2\pi f\tau))|X(f)|^2 \tag{3.24}$$

where $(1+a^2+2a\cos(2\pi f\tau)) = |H(f)|^2$ gives the frequency selectivity of the channel. In Figure 3.15 an example of frequency selectivity is shown. The minima (notches) in the channel transfer function $|H(f)|^2$ occur at distances $\Delta f = 1/\tau$.

Measurements, discussed in Chapter 7, have shown that due to the directivity of the antenna it was always possible to receive only one signal and thus acquire a flat spectrum.

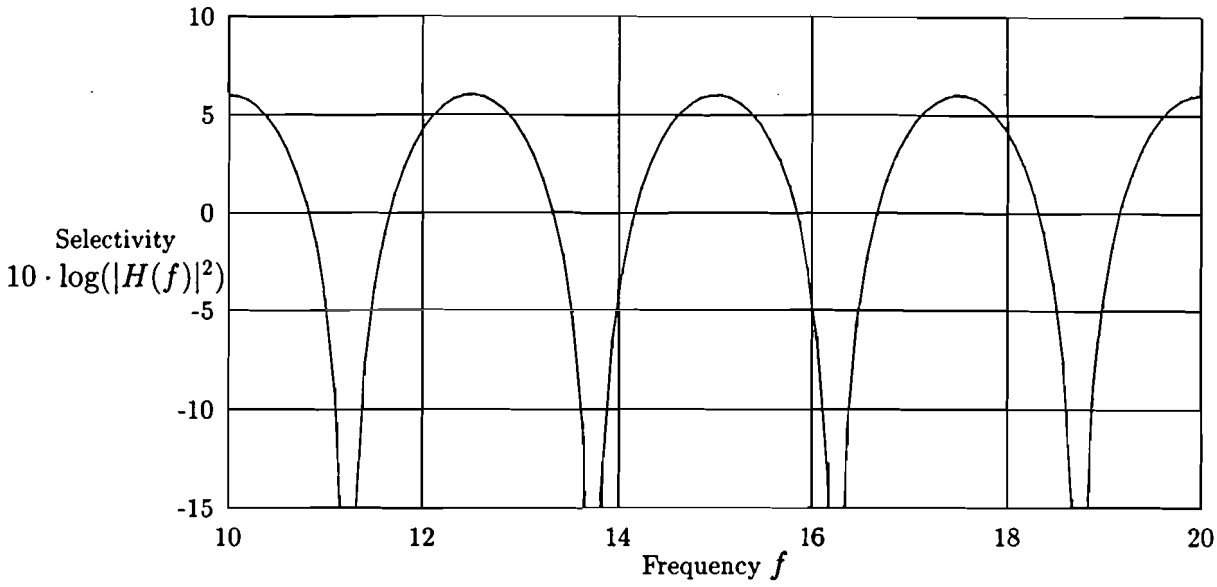

Figure 3.15: Frequency selectivity $10 \cdot \log(|H(f)|^2)$ (a=1)

3.5.1 Fresnel reflection coefficients

If electromagnetic waves reflect on a surface the waves can be decomposed into a parallel reflection and a orthogonal reflection. Orthogonal reflection means that the polarization of the incident wave is orthogonal to the surface of incidence, parallel reflection obviously means the opposite where the polarization of the wave is parallel to the surface of incidence. In Figure 3.16 and Figure 3.17 the angle of arrival θ_i is defined and parallel and orthogonal reflection is depicted.

The Fresnel reflection coefficients for orthogonal and parallel reflection can be found in numerous text books and are defined as

$$\rho_{\perp} = \frac{\cos(\theta_i) - \sqrt{\left(\frac{n_2}{n_1}\right)^2 - \sin^2(\theta_i)}}{\cos(\theta_i) + \sqrt{\left(\frac{n_2}{n_1}\right)^2 - \sin^2(\theta_i)}} \tag{3.25}$$

and

$$\rho_{\parallel} = \frac{\left(\frac{n_2}{n_1}\right)^2 \cos(\theta_i) - \sqrt{\left(\frac{n_2}{n_1}\right)^2 - \sin^2(\theta_i)}}{\left(\frac{n_2}{n_1}\right)^2 \cos(\theta_i) + \sqrt{\left(\frac{n_2}{n_1}\right)^2 - \sin^2(\theta_i)}} \tag{3.26}$$

where the angle of incidence θ_i is defined as shown in Figure 3.16 and n_1 and n_2 are the refractivity indexes in the two media. The refractivity index n is defined as

$$n = \frac{c}{v_{medium}} = \sqrt{\epsilon_r \cdot \mu_r} \tag{3.27}$$

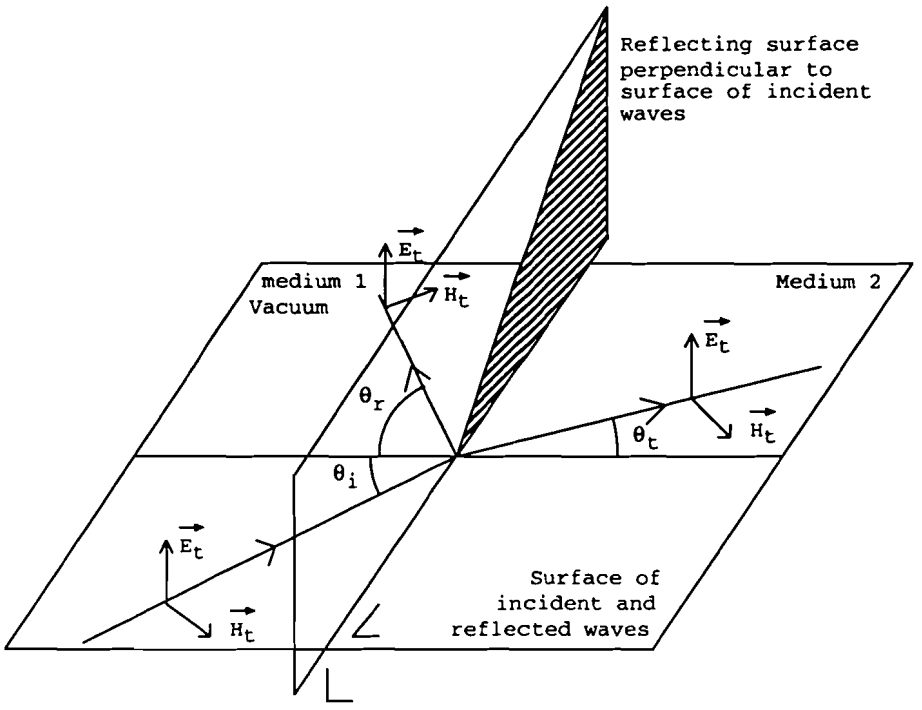

Figure 3.16: Orthogonal polarization reflection

where c is the speed of a wave in a vacuum, v_{medium} is the speed of the wave in the specified medium. ϵ_r is the permittivity of the material and μ_r is the permeability of the material.

For non magnetic materials the permeability μ_r is 1. The refractivity index is thus only depending on the permittivity ϵ_r. The permittivity ϵ consisting of two parts is defined as [17]

$$\epsilon_r = \epsilon'_r - j\epsilon''_r \tag{3.28}$$

where ϵ''_r represents losses in the material and ϵ'_r represents the polarization effects in the material.

If medium two is conducting and thus lossy the refractivity index n_2 becomes thus complex. The refractivity index can be written as

$$n_2^2 = \epsilon'_{r2} - j \cdot \frac{\sigma_2}{\omega\epsilon_0} \tag{3.29}$$

where σ_2 is the conductivity in $1/(\Omega \cdot m)$ in medium two, ω is the angular frequency and ϵ_0 is the permittivity in vacuum.

Using the definition of the velocity of light the refractivity index can be written as

$$n_2^2 = \epsilon'_{r2} - j \cdot 60\sigma_2\lambda \tag{3.30}$$

where λ is the wave length in m.

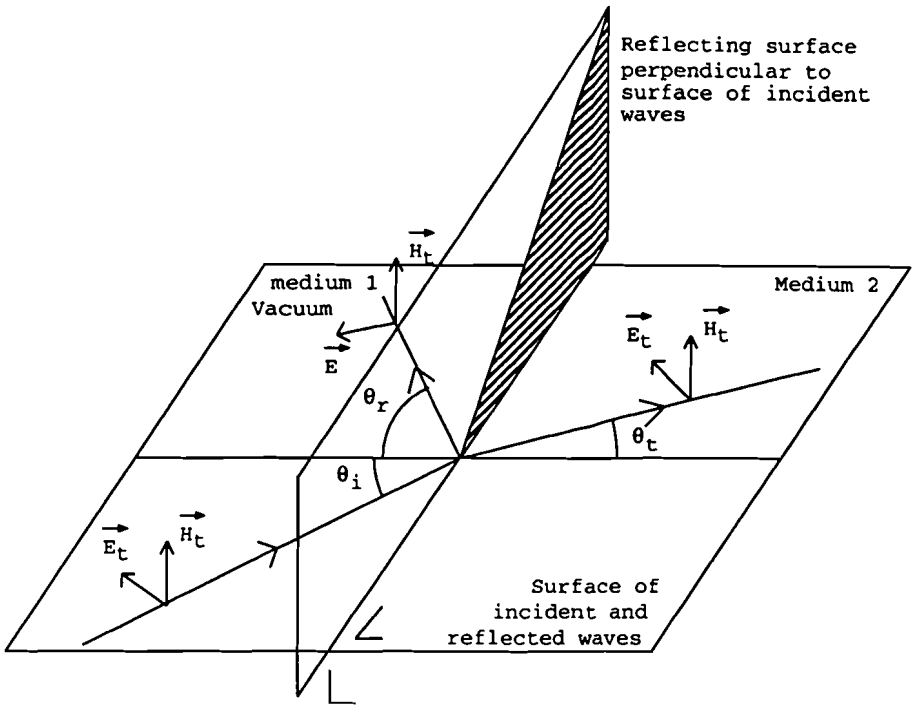

Figure 3.17: Parallel polarization reflection

In literature the material parameters are often given as ϵ_r and the loss tangent $\tan(\delta)$ with δ the loss angle. These parameters can be converted with

$$\epsilon_r \equiv \epsilon_r' \tag{3.31}$$

and

$$\tan(\delta) = \frac{\epsilon_r''}{\epsilon_r'} = \frac{60 \cdot \lambda\sigma}{\epsilon_r'} \tag{3.32}$$

Thus the refractivity index can also be written as

$$n_2 = \epsilon_r - j \cdot \epsilon_r \cdot \tan(\delta) \tag{3.33}$$

In table 3.1 some material parameters at 60 GHz are given [10].

Since the refractivity index becomes complex if the media is lossy the Fresnel reflection coefficients also become complex. This results in a phase difference between the incident wave and the reflected wave. At this time the only interest is in the ratio of the amplitudes of the incident and the reflected signal. Therefore the amplitude of the reflection coefficients $\rho_\perp$ and $\rho_\parallel$ is of interest and not its argument. With the given material parameters the reflection coefficient of the material can be calculated.

This simple model may result in errors if the material is only slightly lossy or relatively thin[24]. In such a case the attenuation within the material is very small and thus a different model must be used.

Material	ϵ_r	$\tan(\delta)$	$\alpha\ [dB/cm]$
Stone	6.81	0.0401	5.73
Marble	11.56	0.0067	1.25
Aerated concrete	2.26	0.0449	3.70
Concrete	6.14	0.0491	6.67
Tiles	6.30	0.0568	7.81
Glass	5.29	0.0480	6.05
Acrylic glass	2.53	0.0119	1.03
Plaster board	2.81	0.0164	1.51
Wood	1.57	0.0614	4.22
Wood (chipboard)	2.86	0.0556	5.15

Table 3.1: Estimated material characteristics [10]

3.5.2 Reflection model of thin layers

A better model for reflection on thin layers is shown in Figure 3.18

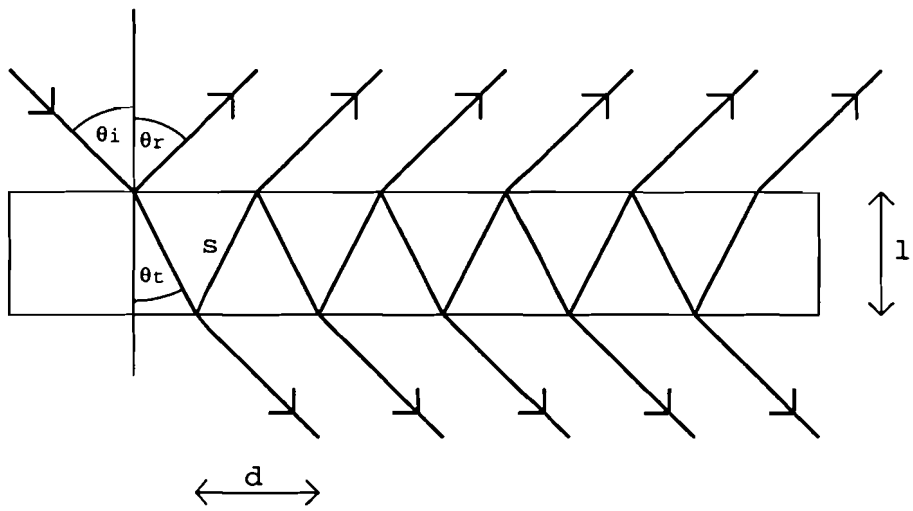

Figure 3.18: A reflection model of thin layers[10]

This model uses an infinite series of reflections inside the material. If we assume the building material thickness of approximately 5 cm to 10 cm the attenuation within the building material will be that large at the frequencies of concern that this complex model is overdone for this application. If however the reflection material is e.g. un coated glass which is thin and has very little attenuation this model is preferred.

The generalized reflection ρ_g coefficient is then given by [10]

$$\rho_g = \rho - (1-\rho^2) \cdot \frac{\rho e^{-j2k\sqrt{\epsilon_r}s} \cdot e^{-2\alpha s} \cdot e^{-jkd\sin(\theta_i)}}{1-\rho^2 \cdot e^{-j2k\sqrt{\epsilon_r}s} \cdot e^{-2\alpha s} \cdot e^{-jkd\sin(\theta_i)}} \tag{3.34}$$

where the propagation constant k is defined as

$$k = \frac{2\pi}{\lambda} \tag{3.35}$$

α is the attenuation coefficient defined as

$$\alpha = \frac{\omega \tan(\delta)}{2} \cdot \sqrt{(\mu_0 \epsilon_0 \cdot \epsilon_r)} \tag{3.36}$$

s is the path length inside the slab between the two surfaces given by

$$s = \frac{l}{\sqrt{1 - \frac{\sin^2(\theta_i)}{\epsilon_r}}} \tag{3.37}$$

and d is the path length difference on the slab of two consecutive departing reflections given by

$$d = \frac{2l}{\sqrt{\frac{\epsilon_r}{\sin^2(\theta_i)} - 1}} \tag{3.38}$$

In Figure 3.19 and Figure 3.20 the absolute values of the reflection coefficients of aerated concrete are given.

3.5.3 Reflection at rough surfaces

The measured reflection coefficients do not match these Fresnel reflection coefficients. This difference is assumed to be due to the roughness of the building material at high frequencies. The reflection coefficients defined above assume coherent reflection. If electromagnetic waves reflect on buildings this is not the case due to the very short wavelengths and the roughness of the reflection surface. To illustrate the effect of a rough surface on the amplitude of the reflection coefficient a simple model is used. This model is based on the assumption that the reflection surface can be modeled with a large number of small squares which have a uniform height distribution between $-h$ and h as depicted in Figure 3.21. This figure shows a reflection in detail.

The Fresnel zones are defined as the areas perpendicular to the ray beam where the waves have the same average phase [15]. The phase between the n^{th} and the $n+1^{th}$ equals π. It can be derived that the power of the wave travels approximately within half of the first Fresnel zone [3]. If the reflection surface is very large so it encompasses the first Fresnel zone completely it can be assumed that the reflection

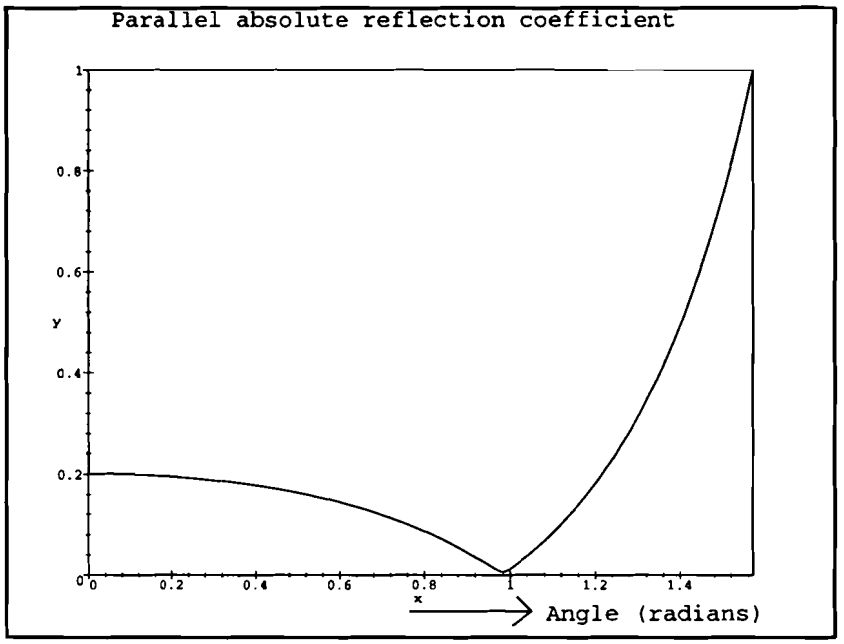

Figure 3.19: Parallel reflection (aerated concrete)

surface is infinite. To find the received field at the receiver the field distribution on the surface must be integrated.

Since only the half of the first Fresnel zone contributes to the received field the integration limits are set to half of the first Fresnel zone. For simplicity the reflection surface is reduced to a reflection line (one dimension). Now using the kirchoff relation and the assumption that the distance from the transmitter and the receiver to the reflection point is long the received field on a perfectly smooth surface can then be expressed as

$$\overline{E} = \int_{-\frac{\pi}{2}}^{\frac{\pi}{2}} A \cdot e^{j\psi}\, d\psi \tag{3.39}$$

where $\overline{E}$ equals the received field, ψ equals the phase of the electromagnetic field on the surface and A is un arbitrary constant. The field strength on the surface is thus for simplicity assumed homogeneous. The total received power can then be found as

$$2A \cdot \sin(\frac{\pi}{2}) = 2A \tag{3.40}$$

If now a rough surface is taken into account a random phase is introduced. Since it is assumed that the surface is uniformly distributed in height h the phase ψ is also uniformly distributed. In Figure 3.21 the relation between the difference in surface height h and the resulting phase difference $\Delta\psi$ is shown. The phase difference $\Delta\psi$

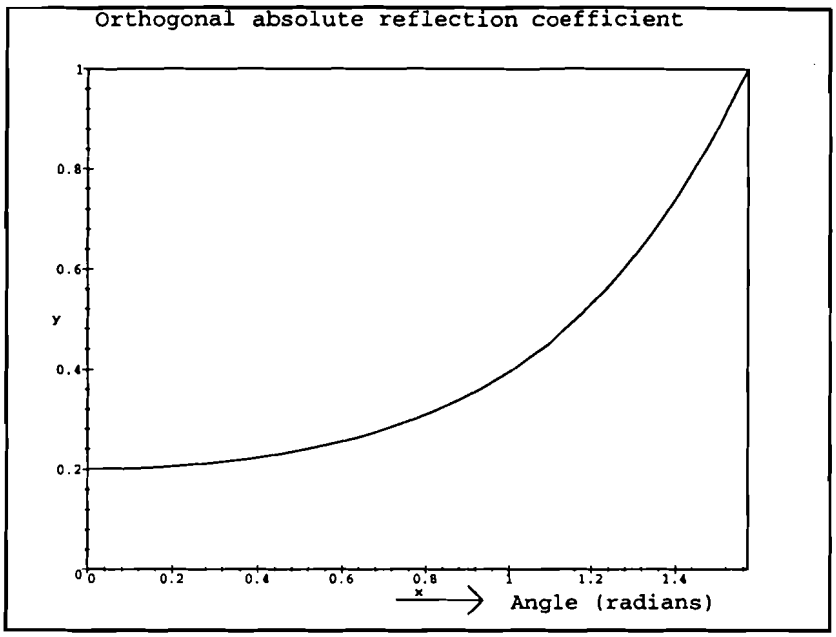

Figure 3.20: Orthogonal reflection (aerated concrete)

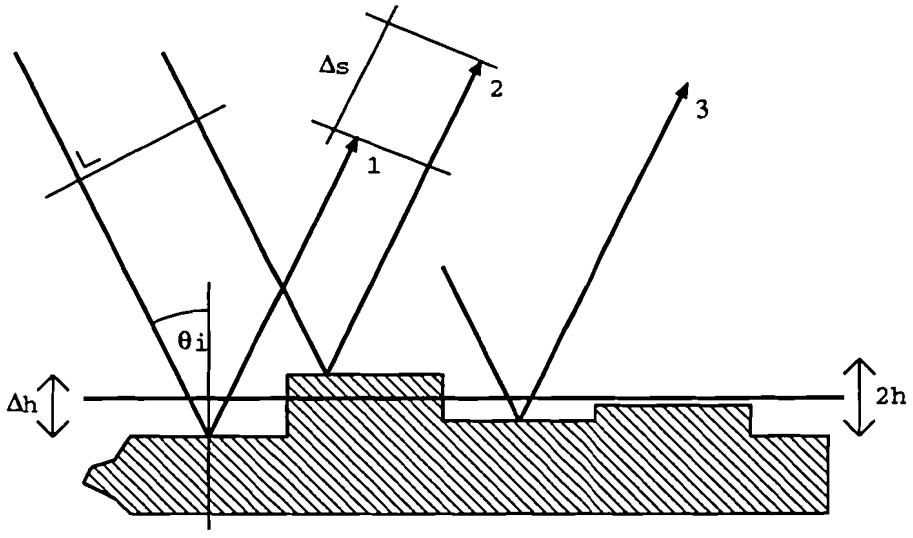

Figure 3.21: Non-coherent reflection detail

is given by

$$\Delta\psi = \frac{2\pi}{\lambda} \cdot \Delta s = \frac{8\pi \cdot h}{\lambda} \cdot \cos(\theta_i) \tag{3.41}$$

The phase ψ thus fluctuates between $\psi + \delta$ and $\psi - \delta$ where δ is defined as

$$\delta = \frac{4\pi \cdot h}{\lambda} \cdot \cos(\theta_i) \tag{3.42}$$

Assuming the above calculated homogeneous phase variation of $[-\delta, \delta]$ the expectation of the electromagnetic field $< \overline{E} >$ can be calculated as

$$< \overline{E} >=< A \int_{\frac{-\pi}{2}}^{\frac{\pi}{2}} e^{j\psi} \cdot e^{jx} > \tag{3.43}$$

where x is the random variable uniformly distributed from $-\delta$ to δ.

The result from this integration is

$$< \overline{E} >= 2A \cdot < e^{jx} > \tag{3.44}$$

Now taking the expectation assuming that there is no dependence between adjacent squares

$$< \overline{E} >= 2A \cdot \int_{-\delta}^{\delta} e^{jx} \cdot \frac{1}{2\delta}\, dx \tag{3.45}$$

this results in

$$2A \cdot \frac{\sin(\delta)}{\delta} \tag{3.46}$$

It can now be concluded that if the Fresnel reflection coefficient on a perfectly smooth surface is given by ρ_0, the specular reflection coefficient on a rough surface ρ_s is given by

$$\rho_s = \rho_0 \cdot \frac{\sin(\delta)}{\delta} \tag{3.47}$$

From the formula above it can be seen that the reflection coefficient is reduced dramatically if the surface is rough. According to definition by Rayleigh a surface is smooth as

$$2h < \frac{\lambda}{8\sin(\theta_i)} \tag{3.48}$$

and rough as

$$2h > \frac{\lambda}{8\sin(\theta_i)} \tag{3.49}$$

According to our simple model this means if the specular reflection coefficient ρ_s is smaller than 0.9 the surface is defined as rough. In the simple model this means that δ equals $\pi/4$ and $2h$ equals 1.34 mm if 28GHz is used and the angle of incidence θ_i equals 0.

A much more thorough and sophisticated analysis is done by P. Beckmann [4]. In this book a lot of models are used, a good model covered by P. Beckmann is based on the assumption that the distribution is Gaussian. This leads to the following result for the specular reflection coefficient

$$\rho_s = \rho_0 \cdot \exp\left\{-\frac{1}{2}\left(\frac{4\pi \cdot \sigma \cdot \cos(\theta_i)}{\lambda}\right)^2\right\} \tag{3.50}$$

where θ_i is the angle of incidence on the surface, λ is the wave length and σ is the variance of the Gaussian distribution of the reflection surface height.

It is concluded that the reflection coefficients can only be found if the roughness of the building material is known. The roughness of the building materials used is not negligible. If the frequency of 42 GHz is used the influence of the surface of the building material increases and the reflection coefficient further reduces. In Figure 3.22 the specular reflection coefficient is shown for different surfaces. From this figure one can see the effect of the surface roughness using a specific frequency.

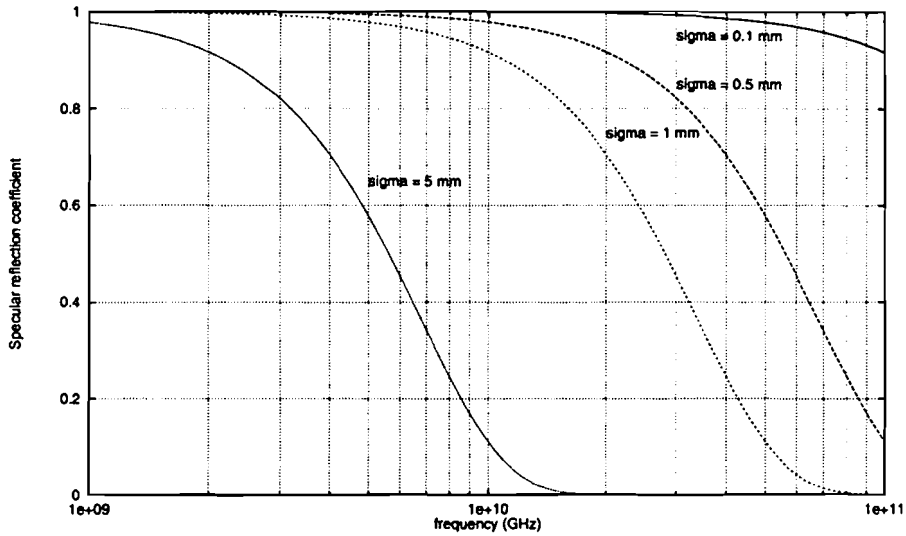

Figure 3.22: The specular reflection coefficient of rough surfaces

In Chapter 7 measurement results are shown and compared with this theory.

In theory the reflection coefficient becomes 1 if the angle of incidence θ_i becomes $\pi/2$, this is in a practical situation however not the case since the reflection surface doesn't encompass the first Fresnel zone anymore because it becomes infinite at such an angle. The size of the Fresnel zone at grazing angle of incidence can be calculated with [4]

$$x_n = \frac{d}{2}\frac{\sqrt{\left(1+\frac{4h_t h_r}{n\lambda d}\right)}}{1+\frac{(h_t+h_r)^2}{n\lambda d}} \tag{3.51}$$

where x_n is the semi-major axis of the n_{th} ellipsoid, h_t is the transmitter antenna height, h_r is the receiver antenna height and d is the path length.

The semi-minor axis y_n can be calculated with

$$y_n = \frac{\sqrt{n\lambda d}}{2}\sqrt{\frac{\left(1+\frac{4h_t h_r}{n\lambda d}\right)}{1+\frac{(h_t+h_r)^2}{n\lambda d}}} \tag{3.52}$$

In table 3.2 some values of roughness [24], material parameters and reflection coefficients are given. These values were measured however at 60 GHz. The value R in this table is the value (down in dB) of the reflected field from the specific material in comparison with a metal sheet.

Perpendicular polarization	R (10°) -dB	R (50°) -dB	R (70°) -dB
Material (thickness d [cm]; estimated roughness σ [mm]			
Aerated concrete (5; 0.2)	14.1	9.6	5.1
Concrete (5; 0.1)	7.5	5.3	2.0
Brick (11; micro 0.3; macro 2)	14.8	12.3	4.8
Glass rough (0.4; 0.3)	6.7	2.9	0.8
Glass smooth (0.4; 0.0)	17.6	5.3	2.9
Glass smooth (0.6; 0.0)	10.7	7.6	3.4
Glass smooth (0.8; 0.0)	8.8	5.5	2.6

Table 3.2: Material reflection properties[24]

3.6 Power fading (flat fading)

Fading is defined as the time variation of the level, phase or polarization of the received signal. Power fading is a wide band or frequency non-selective form of fading which can be a result of one of the following:

- obstruction of the propagation path (variation of k-factor)
- antenna decoupling (variation of k-factor) (narrow-beam antennas)
- partial refraction of elevated layers in the propagation path
- the receiver or transmitter antenna in a ducting layer
- precipitation in the propagation path (rain, snow, fog, clouds etc.)

The fading due to obstruction of the propagation path, variation of the k-factor, can be predicted with the statistics of the standard atmospheres. The solution is to adjust the antenna heights to make sure that the first Fresnel zone clearance is met in the worst case.

Antenna decoupling is the result of the bending of the ray beam in the troposphere. This can result in an incorrect angle of arrival of the transmitted power at the antenna as shown in Figure 3.23.

The amount of antenna decoupling depends on the antenna beam width. With high gain receiver antennas, narrow beam width, this can become a problem. The angle

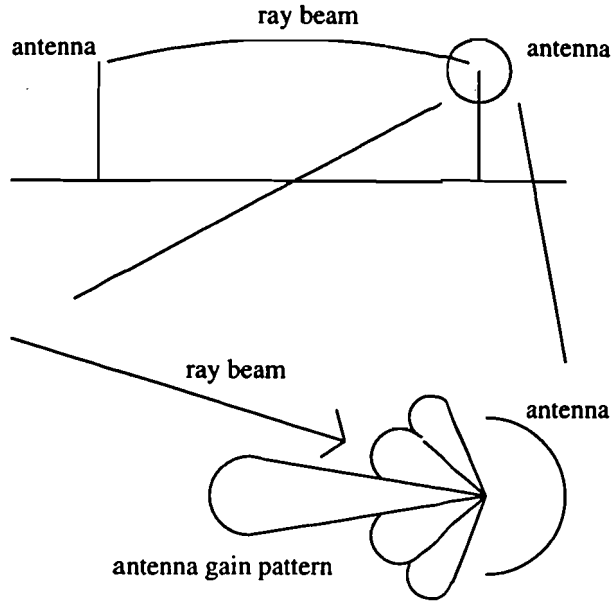

Figure 3.23: Decoupling of the antenna

of arrival or launch of the ray beam depends on the gradient of the refractive index along the path. The deviation is primarily in the vertical plane of the antennas, CCIR report 338-6 [22]. The variations in the launch or arrive angles are in the order of 10^{-3}deg./km. Since the distances of interest are very short (high attenuation at 28 or 42 GHz) the decoupling should be no problem to this type of links.

Power fading can be caused by defocussing or partial reflection. This depends on the gradient of the refractive index.

Protection against fading caused by ducting can be based on the fact that only ray beams with very little inclination with respect to the horizon are subject to ducting (e.g. less than 0.5 deg.) as stated in the CCIR report 338-6 and 718-3 [22]. This means that multipath fading caused by ducting can be reduced if sites can be chosen such that the LOS has an inclination of more than 0.5 deg. In the case discussed the transmitter antenna is mounted at a height of 65 m and the receivers on the roofs of single houses will be mounted at approximately 10 m. The lowest inclination will of course be at the receivers at the edge of the cell. With an estimated cell diameter of approximately 5 km this angle will be 0.63 deg. In this situation the multipath effects due to ducting are expected to be negligible. In the case where the receiver antennas are on top of high buildings this technique obvious can't be used. This solution thus depends the building structures in the coverage area.

Fading due to precipitation is discussed in section 3.8.

3.7 Fading due to multipath propagation (frequency selective fading)

We have seen in Section 3.5 that in theory multipath propagation can be very dramatic in the case of a strong single reflection. The multipath fading is frequency selective as shown in Section 3.5. The reception of a secondary ray beam can be reduced if not eliminated with a very narrow beam width of the receiver antenna. This is of course depending on the attenuation by a reflection and the number of reflections a ray beam makes before it reaches the receiver antenna and the path length difference. A disadvantage of this technique is that the antenna decoupling can become a problem with very narrow-beam antennas. On this subject there has to be thoroughly research done to make a good prediction. For such a prediction model very much data is required.

The statistics of fading caused by weak surface reflections are different from those caused by strong surface reflections. On a line-of-sight link there is no deep fading expected [16]. On these paths scintillation, slow non selective fading and more rapid frequency selective fading is expected. Except for scintillation the fading is due to the atmosphere forming ducts which is most likely to occur at night and early in the morning in overland paths. Scintillation is less severe as the attenuation due to precipitation using 42 GHz as will discussed in Section 3.5. Since scintillation is based on stratified conditions which most probable do not exist if it is raining it is of no problem. The margin required in the link budget for the rain attenuation will provide protection against scintillation.

If there is multipath reception the received signal consists of the direct line of sight signal and a number of attenuated echoes. Such a channel is modeled by a Rice-Nagakami fading channel.

For large fade depths the average worst time fading time fraction can be approximated with the following formula (CCIR report 338-6) [22, 16]

$$P(W) = K \cdot Q \cdot \frac{W}{W_0} \cdot f^B \cdot d^C \tag{3.53}$$

where

d = distance (km)
f = frequency (GHz)
W = the received power (W)
W_0 = the unfaded received power (W)
$K \cdot Q$ is a factor for different climate and terrain effects.

This formula is considered valid for attenuations of more than 15 dB or the value exceeded for 0.1% of the worst month for distances from 15 to 100 km. The constants for various circumstances can be found in table 3.7

Proposed for	Japan	N.W. Europe	United kingdom	United states	USSR	Northern Europe
B:	1.2	1.0	0.85	1.0	1.5	1.0
C:	3.5	3.5	3.5	3.0	2.0	3.0
$K \cdot Q$ for maritime temperate, mediterranean, coastal, or high humidity and temperature climatic regions:	-	-	-	$\frac{4.1 \cdot 10^{-6}}{S_1^{1.3}}$	$2 \cdot 10^{-5}$	-
$K \cdot Q$ for maritime sub-tropical climatic regions:	-	-	-	$\frac{3.1 \cdot 10^{-5}}{S_1^{1.3}}$	-	-
$K \cdot Q$ for continental temperate climates or mid latitude inland climatic regions with average rolling terrain:	10^{-9}	$1.4 \cdot 10^{-8}$	$\frac{8.1 \cdot 10^{-7}}{S_2^{1.4}}$ to $\frac{4.0 \cdot 10^{-6}}{S_2^{1.4}}$	$\frac{2.1 \cdot 10^{-5}}{S_1^{1.3}}$	$4.1 \cdot 10^{-6}$	$\frac{2.3 \cdot 10^{-5}}{S_1^{1.3}}$
$K \cdot Q$ for high dry mountainous climatic regions:	$3.9 \cdot 10^{-10}$	-	-	$\frac{10^{-5}}{S_1^{1.3}}$	-	10^{-8}
$K \cdot Q$ for temperate climates, coastal regions with fairly flat terrain:	$\frac{9.9 \cdot 10^{-8}}{\sqrt{h_1 + h_2}}$	-	-	-	$4.9 \cdot 10^{-5}$	$\frac{6.5 \cdot 10^{-5}}{S_1^{1.3}}$
$K \cdot Q$ for temperate climates, inland regions with fairly flat terrain	-	-	-	-	$7.6 \cdot 10^{-6}$ to $2 \cdot 10^{-5}$	$\frac{3.3 \cdot 10^{-5}}{S_1^{1.3}}$

Table 3.3: Empirical values for formula 3.53[16]

Note: h_1 and h_2 are the antenna heights in meters.
S_1 is the terrain roughness measured in meters by the standard deviation of terrain elevations at 1 km intervals (6 m $\leq S_1 \leq$ 42 m).
S_2 is defined as the RMS value of the slopes (mrad) measured between points separated by 1 km along the path, but excluding the first and the last complete km interval (1 $l S_2 l$ 80).
Source: CCIR report 338-6 [22].

With this formula it is possible to predict the attenuation due to multipath fading. In the link discussed however the distance is much shorter, the attenuation will therefore be less, the formula is thus not applicable for our calculation. If in future there will longer links (larger cell radii) this formula is preferable.

Another prediction method is based on the results of fitting a Rice-Nagakami distribution to data measured over average rolling terrain in northwest of Europe [16] (Figure 3.24). This method was developed for 4 GHz but it can be used for other frequencies if the path length d is replaced by an equivalent path length d_{eq} calculated with the following formula [16]

$$d_{eq} = d \cdot \left(\frac{f}{4}\right)^{0.25} \tag{3.54}$$

where

d = distance (km)
d_{eq} = equivalent distance (km)
f = frequency (GHz).

This method also predicts the attenuation in the worst month of the year. Using formula 3.55 [22] the outage time over a whole year can be calculated.

$$p = 0.3 \cdot p_w^{1.15} \tag{3.55}$$

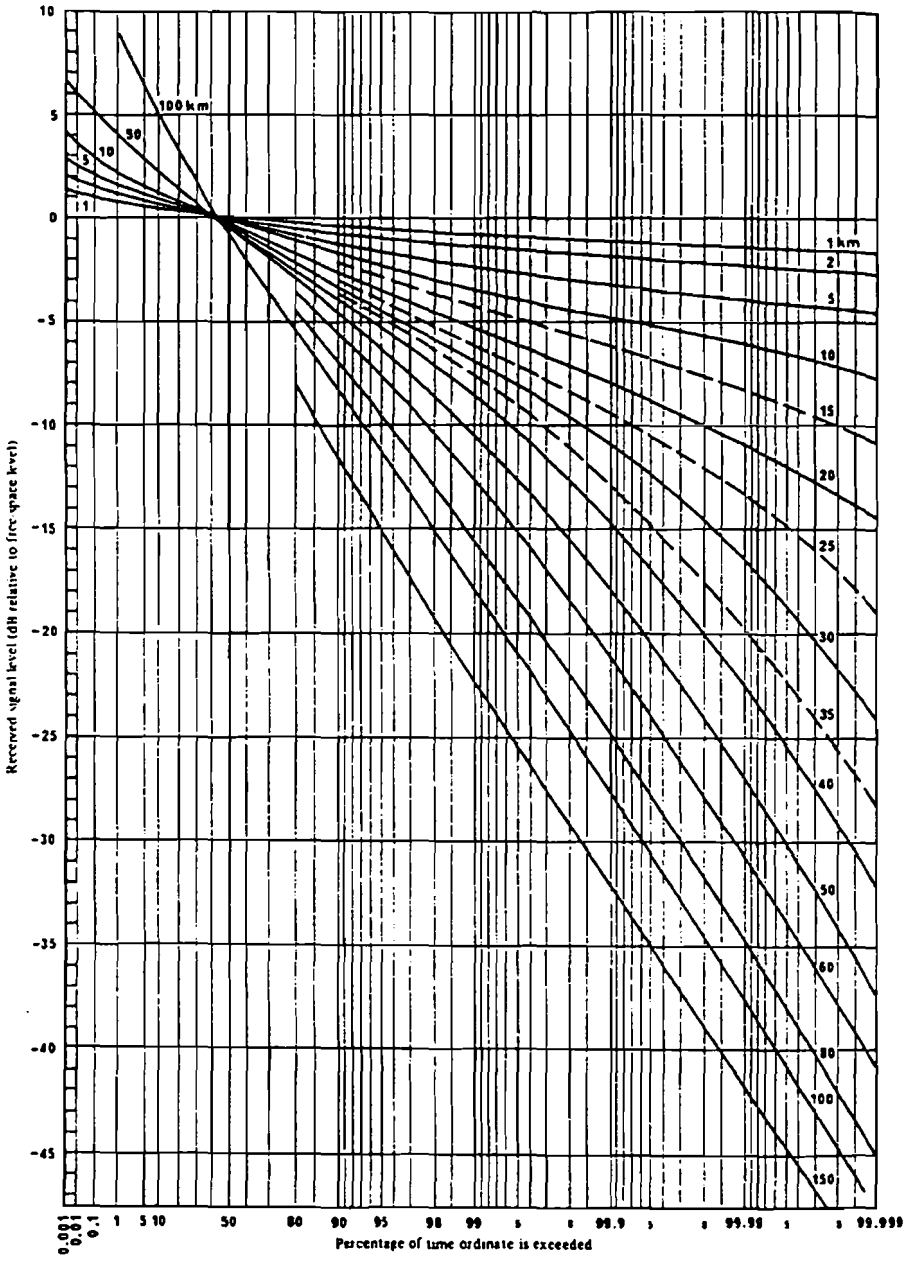

Figure 3.24: Worst month multipath fading (f = 4 GHz) report 718-3 CCIR[22]

where

p = outage time percentage over the whole year
p_w = outage worst month time percentage.

If the last method is used the fading level not exceeded for 99.9% and 99% of the time over a year is given in table 3.4. The fading levels are given for different path lengths.

Path length (km)	fading depth 28 GHz 99 % (dB)	fading depth 42 GHz 99.9% (dB)	fading depth 28 GHz 99.9 % (dB)	fading depth 42 GHz 99% (dB)
3	2.5	2.8	1.8	2.1
4	3.1	3.3	2.1	2.3
5	3.5	3.7	2.3	2.5
6	4.0	4.3	2.5	2.8
7	4.3	4.7	2.8	3.0

Table 3.4: Fading depth as a function of path length for 28 GHz and 42 GHz

The last method is based on smooth rolling terrain, therefore the prediction of the fading level for cities may be incorrect. For now this value is used but the statistics of attenuation of a 28 GHz or 42 GHz signal due to multipath fading within cities has to be reviewed thoroughly. Measurements as described in Chapter 7 did not show any fast or slow fading using the narrow-beam antenna.

3.8 Rain attenuation

Attenuation caused by rain plays a very important role in millimeter wave transmission. It has been recognized as one of the principal causes of attenuation in the millimeter wave propagation [11]. Rain is not the only cause however, clouds will also cause attenuation in the lower part of the atmosphere. In the case of the MVDS the signal loss due to the clouds is of less importance since we rely on a line of sight transmission at 28 and 42 GHz and therefore the clouds do not intersect the path. With the exceptions of the frequency bands about the 22 GHz water vapour absorption line and the 60 GHz complex of oxygen lines, the attenuation exceeded less than 2 percent of the year is caused by rain or clouds [11]. At the smaller percentages rain is the only cause of increased attenuation.

A reliable estimation of the attenuation by rain is therefore necessary to realistically determine the link availability. If this signal loss is taken account for in the link margin the rain should not be a real problem. There are numerous models which predict the statistical behaviour of rain attenuation,

Very well known models are those of Rice-Holmberg [32], Lin [28], Crane [11] and the CCIR model. The model used will be the CCIR model.

On terrestrial paths the CCIR model is one of the most accepted methods of estimating the rain attenuation. The attenuation is specified for both horizontal and vertical polarization. This is important for a cellular network since this will probably make use of the cross-polar discrimination of antennas. Such a system must then cope with the different cell sizes when the different polarizations are used.

The CCIR model has very small regions where the predicted attenuation would be constant and thus has a very fine rain rate variations. The CCIR model is based both on physics and on mathematical curve fitting on the attenuation measurements.

3.9 ITU-R rain model

The CCIR model to predict the attenuation by rain is based on the empirical approximate relation between the specific attenuation γ_r and the rain rate R [20].

$$\gamma_r = kR^a \tag{3.56}$$

where

γ_r = the specific attenuation (dB/km)
R = rain rate (mm/hr)
k and a are functions of frequency and rain temperature.

The values of k and a can be found in Table 3.5 [21]. Due to the shape of the rain drops (oblate spheroids) the attenuation in horizontal and vertical polarized waves differ (Figure 3.25) [16, 12]. The horizontal polarized waves encounters the highest attenuation because in this plane there is relatively more water.

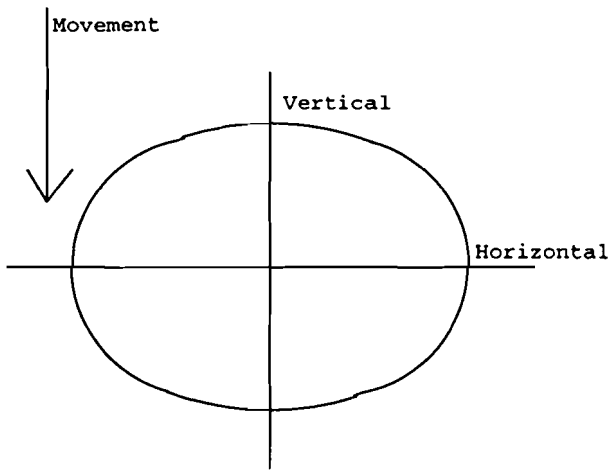

Figure 3.25: Model of a falling rain drop without a vertical wind gradient [12]

To estimate the long term statistics of rain attenuation the following steps must be taken. First (3.56) is applied with the rain rate $R_{0.01}$ taken from Table 3.6 with help of Figure 3.28, where $R_{0.01}$ is the rain rate exceeded 0.01 % of the time. The next step is to calculate the effective path length using the reduction factor r [20].

$$r = \frac{1}{1 + \frac{d}{d_0}} \tag{3.57}$$

where

r = the reduction factor
d = the path length (km)
$d_0 = 35 \cdot \exp(-0.015 \cdot R_{0.01})$.

Frequency (Ghz)	k_h	k_v	a_h	a_v
1	0.0000387	0.0000352	0.912	0.880
2	0.000154	0.000138	0.963	0.923
4	0.000650	0.000591	1.121	1.075
6	0.00175	0.00155	1.308	1.265
7	0.00301	0.00265	1.332	1.312
8	0.00454	0.00395	1.327	1.310
10	0.0101	0.00887	1.276	1.264
12	0.0188	0.0168	1.217	1.200
15	0.0367	0.0335	1.154	1.128
20	0.0751	0.0691	1.099	1.065
25	0.124	0.113	1.061	1.030
30	0.187	0.167	1.021	1.000
35	0.263	0.233	0.979	0.963
40	0.350	0.310	0.939	0.929
45	0.442	0.393	0.903	0.897
50	0.536	0.479	0.873	0.868
60	0.707	0.642	0.826	0.824
70	0.851	0.784	0.793	0.793
80	0.975	0.906	0.769	0.769
90	1.06	0.999	0.753	0.754
100	1.12	1.06	0.743	0.744
120	1.18	1.13	0.731	0.732
150	1.31	1.27	0.710	0.711
200	1.45	1.42	0.689	0.690
300	1.36	1.35	0.688	0.689
400	1.32	1.31	0.683	0.684

Table 3.5: Coefficients for estimating specific attenuation [21]

In calculating the effective path length with help of the reduction factor r a homogeneous rain rate throughout the path is assumed. This is however unlikely to happen. To compensate for this assumption the factor d_0 is included. The higher the rain rate $R_{0.01}$ the more local this will be and thus the effective path length is reduced.

In the last step the actual attenuation $A_{0.01}$ along the path is calculated.

$$A_{0.01} = \gamma_r \cdot d \cdot r \tag{3.58}$$

where d is the path length in km.

If one is interested in other time percentages p in the range 0.001% to 1% the value can be corrected with formula 3.59 [20].

$$\frac{A_p}{A_{0.01}} = 0.12 \cdot p^{-[0.546+0.043 \cdot \log(p)]} \tag{3.59}$$

where A_p = the corrected attenuation.

In Figure 3.26 some attenuation curves are given to show the relation between the attenuation and the time percentage and in Figure 3.27 the attenuation is shown as a function of the distance for vertical and horizontal polarization in rainfall region E.

The average annual percentage of time P exceeding a given attenuation level may be derived from the worst month percentage of time P_w by use of the following formula

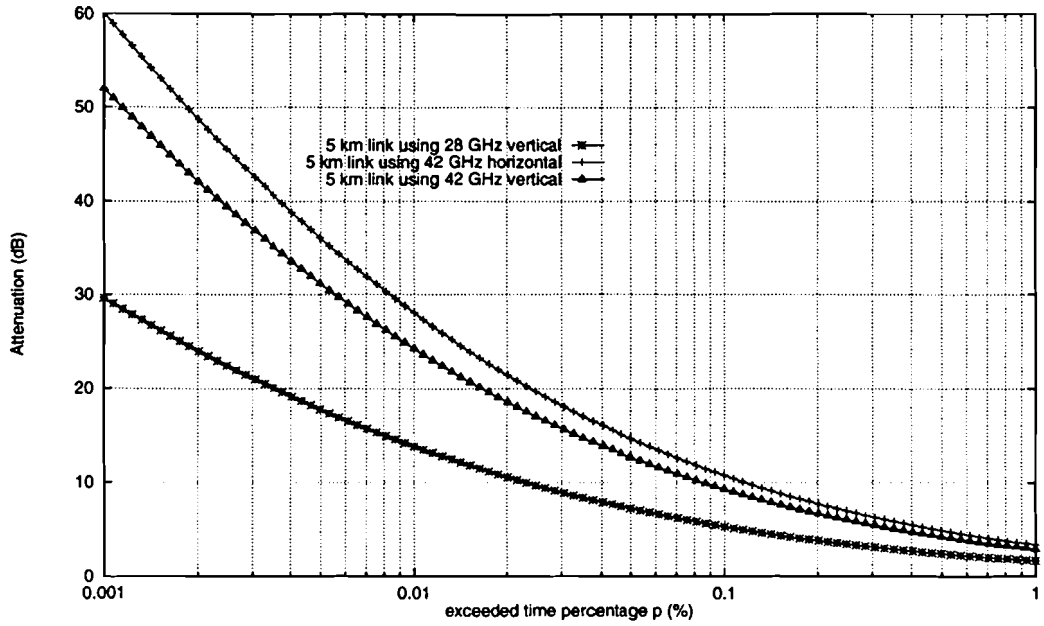

Figure 3.26: Attenuation curves versus time percentage p %

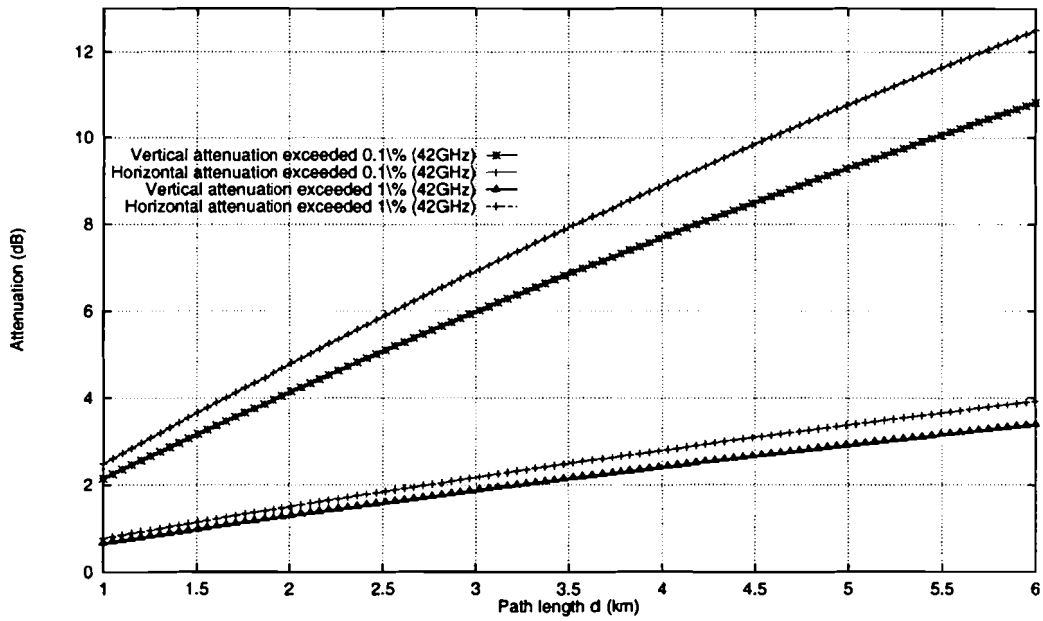

Figure 3.27: Attenuation curves versus distance d in km

[20]

$$P = 0.3 \cdot P_w^{1.15} \tag{3.60}$$

Percentage of time (%)	A	B	C	D	E	F	G	H	J	K	L	M	N	P
1.0	–	1	–	3	1	2	–	–	–	2	–	4	5	12
0.3	1	2	3	5	3	4	7	4	13	6	7	11	15	34
0.1	2	3	5	8	6	8	12	10	20	12	15	22	35	65
0.03	5	6	9	13	12	15	20	18	28	23	33	40	65	105
0.01	8	12	15	19	22	28	30	32	35	42	60	63	95	145
0.003	14	21	26	29	41	54	45	55	45	70	1O5	95	140	200
0.001	22	32	42	42	70	78	65	83	55	100	150	120	180	250

Table 3.6: Rain rate (mm/hr) (CCIR)[21]

3.10 Cross-polar discrimination

To make effective use of the available spectrum frequency reuse by means of orthogonal polarizations is an interesting feature. The isolation between the two orthogonal polarizations is limited however. First of all the antennas have a static limited cross-polarization discrimination. This can be better than 20 dB if required. The cross-polar discrimination is however further decreased due to the precipitation such as rain in the transmission medium.

Some of the transmitted energy in one polarization is received in the other polarization and visa versa. This effect introduces a cross-polar interference in the channel using the same frequency but the other polarization.

Before we examine the depolarization effects more closely some definitions are given according to [12] in Figure 3.29.

In this figure the transmitted and received field are defined as:

- E_{xx} is the received signal in the X-direction and transmitted in the X-direction
- E_{yy} is the received signal in the Y-direction and transmitted in the Y-direction
- E_{xy} is the received signal in the X-direction and transmitted in the Y-direction
- E_{yx} is the received signal in the Y-direction and transmitted in the X-direction

The cross-polar discrimination XPD_x in the x-direction is now defined as

$$XPD_x = -20 \log \left| \frac{E_{yx}}{E_{xx}} \right| \tag{3.61}$$

and the cross-talk discrimination in the x-direction is defined as

$$XTD_x = -20 \log \left| \frac{E_{xy}}{E_{xx}} \right| \tag{3.62}$$

For the other orientation y the same formulae holds

$$XPD_y = -20 \log \left| \frac{E_{xy}}{E_{yy}} \right| \tag{3.63}$$

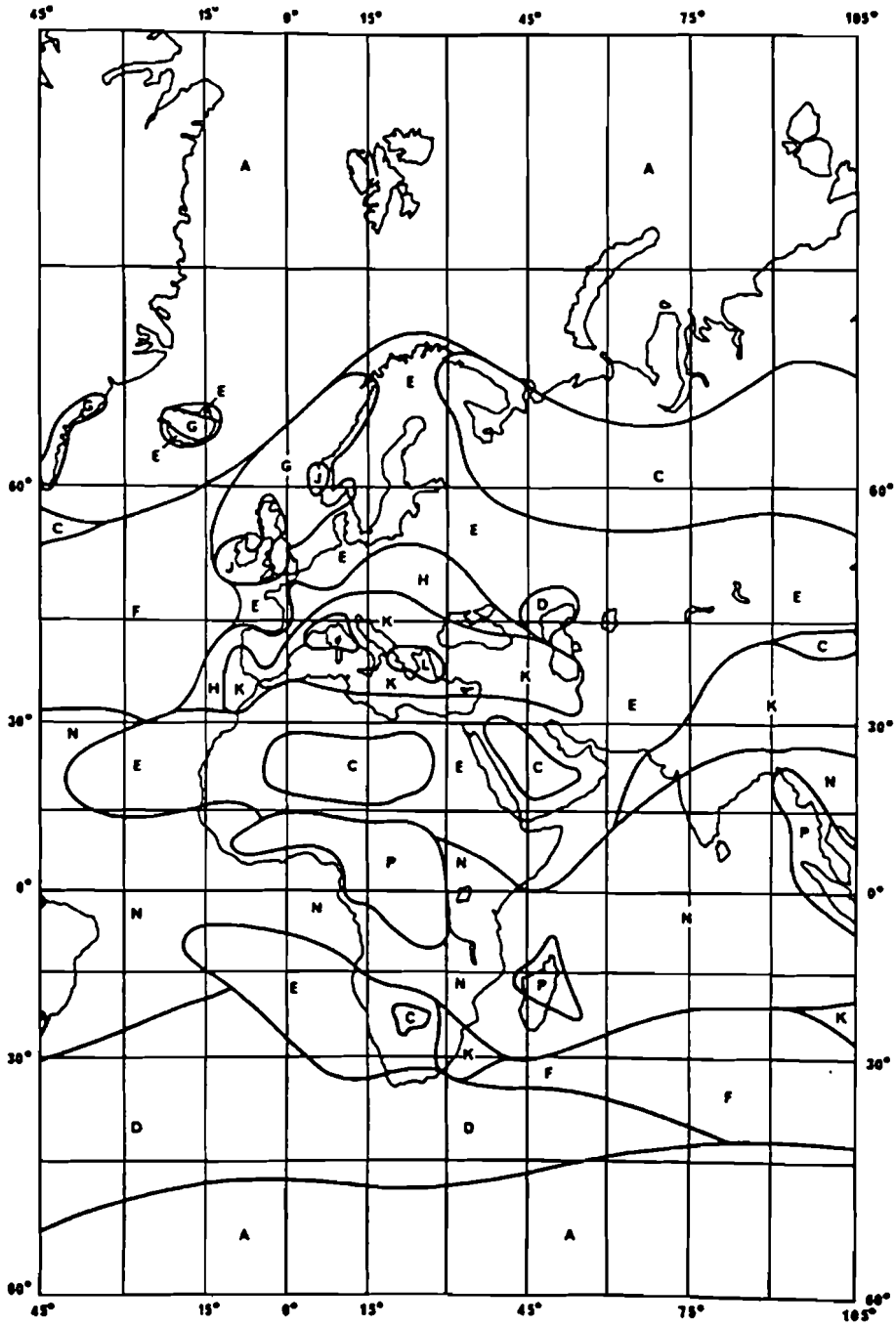

Figure 3.28: Rainfall regions for Europe and Africa [16]

and the cross-talk discrimination in the y-direction is defined as

$$XTD_y = -20 \log \left| \frac{E_{yx}}{E_{yy}} \right| \tag{3.64}$$

Raindrops falling through the atmosphere take an oblate form as a result of the air

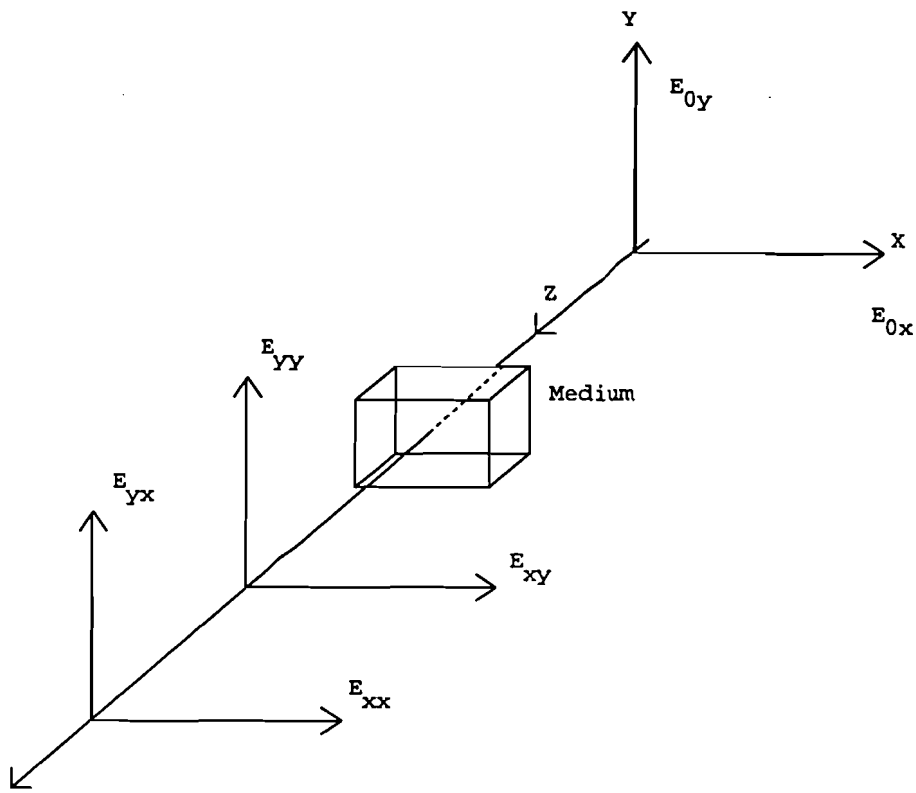

Figure 3.29: Definitions for cross-polar discrimination[12]

resistance as shown in Figure 3.25. Due to the wind gradient however the raindrop rotates as shown in Figure 3.30 [6].

A linearly polarized wave parallel to the axis of symmetry of the raindrop has its phase changed and its amplitude is attenuated. This does not introduce cross-polar interference. If there is an angle α between the linearly polarized wave and the axis of symmetry, the polarization of the wave changes because both the axis of symmetry attenuates the incident wave and changes the phase differently.

The effect can be seen as a coordinate transformation, a transmission through the rain drop and a projection on the reference axis. The same holds for the other orientation of course.

From Figure 3.30 it can be seen that

$$E_u = E_{0y} \cdot T_u \cdot \sin(\phi) \tag{3.65}$$

and

$$E_v = E_{0y} \cdot T_v \cdot \cos(\phi) \tag{3.66}$$

where the transmission coefficient T_u is defined as

$$T_u = \exp\left(-\alpha_u \cdot l - j\beta_u \cdot l\right) \tag{3.67}$$

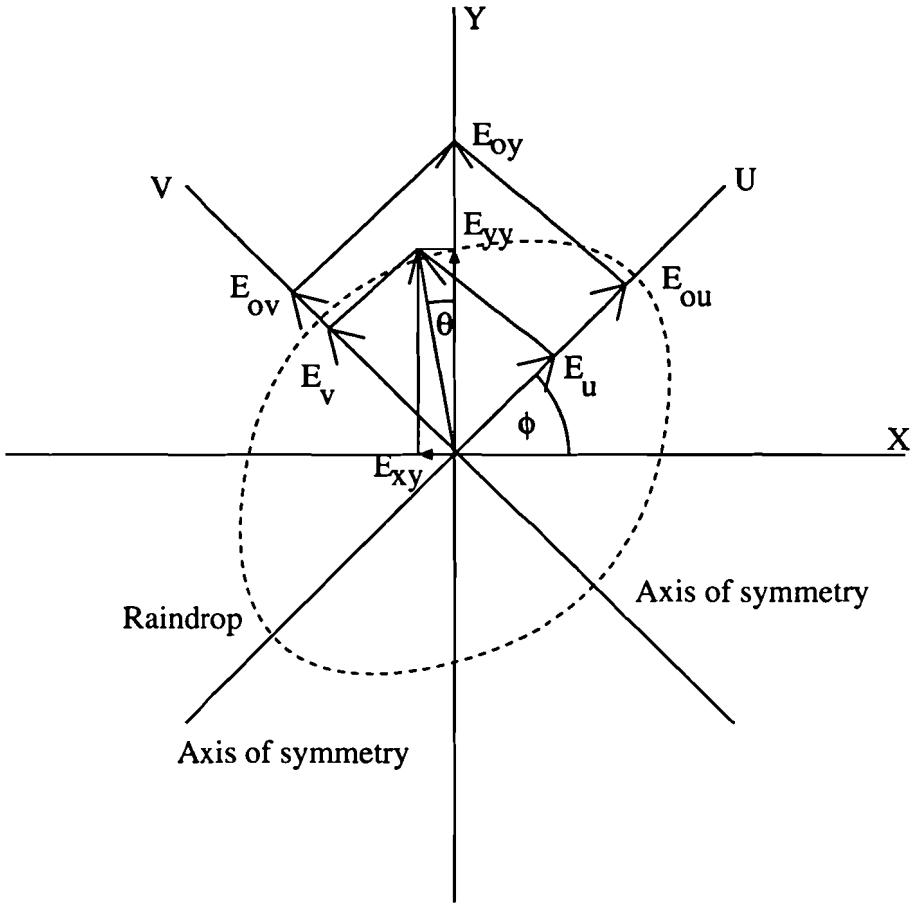

Figure 3.30: The canting raindrop

and T_v is defined as

$$T_v = \exp\left(-\alpha_v \cdot l - j\beta_v \cdot l\right) \tag{3.68}$$

where α is the attenuation per length unity, β is the phase rotation per unit of length and l is the length of the path.

Now E_{yy} can be written as

$$E_{yy} = E_{0y} \cdot T_u \cdot \sin^2(\phi) + E_{0y} \cdot T_v \cdot \cos^2(\phi) \tag{3.69}$$

and E_{xy} is defined as

$$E_{xy} = E_u \cos(\phi) - E_v \sin(\phi) \tag{3.70}$$

and thus equals

$$E_{xy} = E_{0y} \cdot \sin(\phi)\cos(\phi) \cdot (T_v - T_u) \tag{3.71}$$

After some manipulation the XPD_y can be written as

$$XPD_y = -20 \cdot \log\left|\frac{(\zeta - 1) \cdot \tan(\phi)}{1 + \zeta \cdot \tan^2(\phi)}\right| \tag{3.72}$$

where ζ is given by

$$\zeta = \exp -(\alpha_u - \alpha_v) \cdot l \cdot \exp -j(\beta_u - \beta_v) \cdot l \tag{3.73}$$

or

$$\zeta = \exp(-\Delta A) \cdot \exp(-\Delta\psi) \tag{3.74}$$

where ΔA is the differential attenuation and $\Delta\psi$ is the differential phase shift.

In Figure 3.31 and Figure 3.32 the differential attenuation and the differential phase shift can be found [18]. The differential attenuation in this figure is given in dB/km,

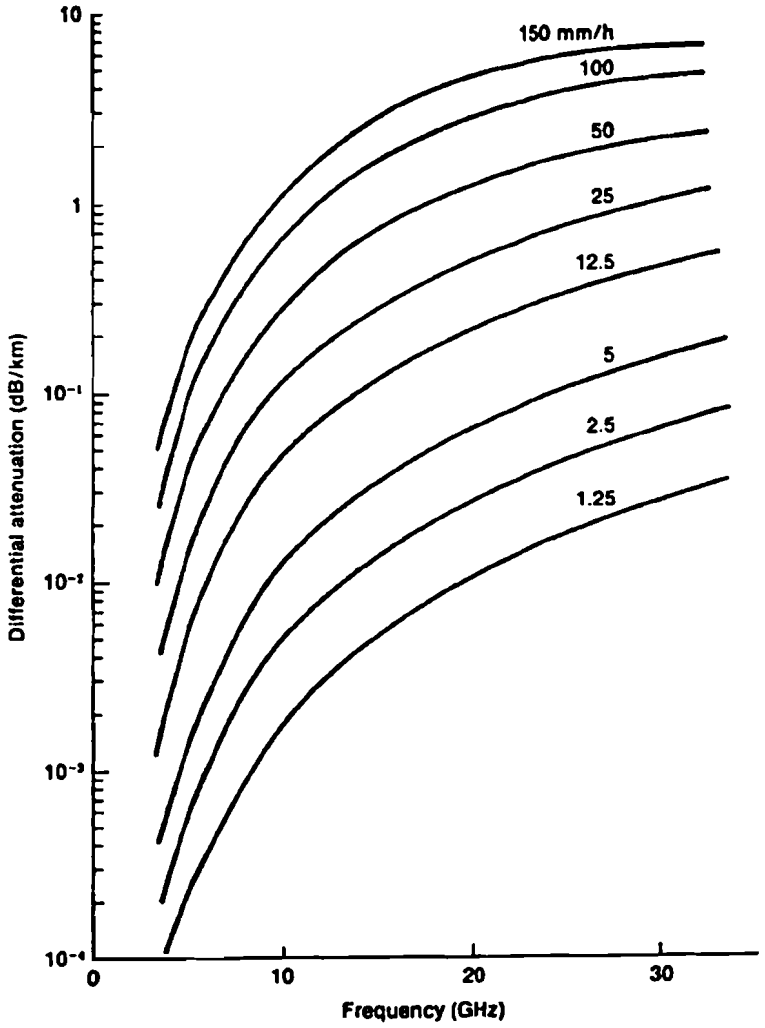

Figure 3.31: The differential attenuation[8]

this value should be converted to neper/km for use in the formulae.

For orthogonal linear polarizations it can be assumed that the mean canting angle equals a few degrees.

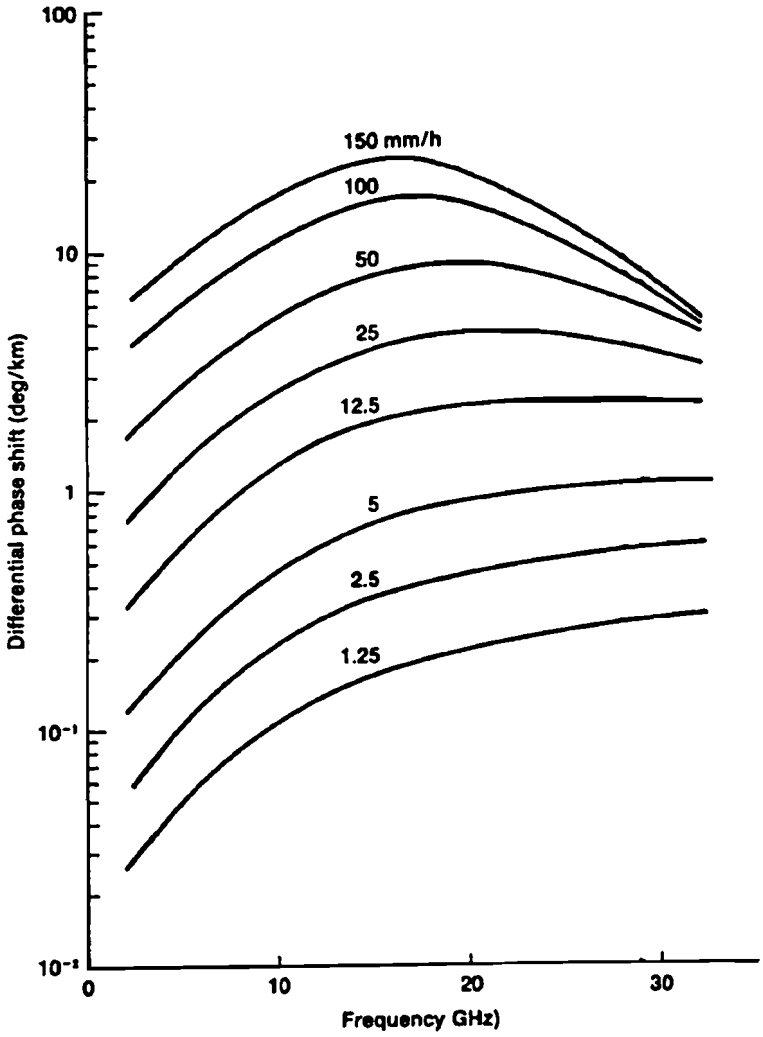

Figure 3.32: The differential phase shift[8]

The ITU-R recommends (in recommendation 530-4) [23] the following simple semi empirical formula for system planning however

$$XPD = U(f) - V(f)\log(CPA) \tag{3.75}$$

where $U(f)$ equals $9 + 30\log(f)$, $V(f)$ equals 20 and CPA is the co-polarized attenuation.

This formula will be used here because it has been proven to be accurate and is based on both the theory above and is matched on data of extensive measurements. There are however few data in the 42 GHz band, according to the ITU-R this prediction is valid up to 35 GHz. Future measurements should provide the data, with this data one can check if the model is valid for these frequencies.

In our case the CPA just equals the rain attenuation. If the rain statistics of section 3.8 are used the XPD exceeded for p % of the year can be calculated. The total

outage time does not necessarily increase because the worst cross-polar occurs most probably at the same time as the outage due to rain attenuation. Therefore it is best to add degradation in dB's instead of adding up the outage time.

As an example a path length of 5 km with rain is considered and the frequency is 42 GHz. We are now interested in the lower XPD bound which is not exceeded for 99 % of the time or 99.9 % of the time. From Section 3.8 it is found that the rain attenuation L_a not exceeded for these time percentages equals 3.38 dB and 10.76 dB respectively (horizontal polarization).

The XPD found using the formulae above, assuming a homogeneous rain rate throughout the entire path, equals 37.06 dB (99.9 %) and 47 dB (99 %). Thus the XPD is better than 37 dB for 99.9 % of the time. It is thus concluded that the XPD will not be a serious problem, the attenuation due to the rain is much more of a problem to overcome. This means that the outage time of the link is not influenced by the cross-talk between the two polarizations.

The analysis above does not mean that the total cross-polar discrimination is that good because the transmitter and receiver antennas both have a limited cross-polar discrimination. In Chapter 7 the results of a cross-polar discrimination measurement are discussed.

The total cross-polar discrimination of a link will then be determined by the cross-polar discrimination of the antennas. The total cross-polar discrimination worst case can be calculated with [18]

$$xpd_t = \frac{1}{2} \cdot \left(\frac{1}{\frac{1}{xpd_1} + \frac{1}{xpd_2}} \right) \tag{3.76}$$

where $xpd_i = 10^{XPD_i/10}$

If for instance both antennas have a XPD of 20 dB, the total resulting XPD of the link becomes 14 dB.

3.11 Sky noise temperature

The sky noise temperature T_{ant} at the antenna is also effected by rain, the antenna noise temperature can therefore depend on the rain rate. This is because the antenna noise temperature is depending on the sky noise temperature. If T_{rain} represents the rain temperature which is usually taken to be 273 K and $l = 1/g = l_a$ is the rain attenuation, then the antenna noise temperature $T_{ant,rain}$ noise temperature can be calculated with

$$T_{sky,rain} = T_{sky} \cdot \frac{1}{l_a} + (1 - \frac{1}{l_a}) \cdot T_{rain} \tag{3.77}$$

But since the elevation of the antenna is approximately 0 deg. this effect does not occur since the antenna will always look at buildings, trees and ground reflections

of which have a temperature of 290K. If the antenna is mounted very high, in relation to buildings etc., the noise temperature does change because of the sky noise temperature variations. At an elevation of 0 deg. and approximately 28 GHz the sky noise temperature varies between 220 and 290 k and for 42 GHz the sky noise temperature only varies from 270 to 290. This is depending on the water vapour concentration and surface pressure [15]. In Figure 3.33 the configuration is depicted, as we can see the antenna temperature is effected by both the sky and the ground temperature, therefore the antenna temperature can be calculated with the following formula

$$T_{ant} = \alpha \cdot T_{ground} + (1 - \alpha) \cdot T_{sky} \tag{3.78}$$

where α depends on the fraction of the antenna beam which looks at the ground.

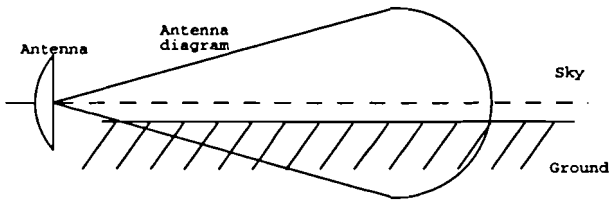

Figure 3.33: Antenna temperature depending on ground and sky temperature

At most with a high mounted antenna the sky noise temperature (42 GHz) varies due to rain from 270 to 290 K. For the system described it is realistic (though pessimistic) to assume a sky noise temperature of 290 K.

3.12 Discussion

The Fresnel zone clearance cl can be easily met if there is a LOS. The influence of the varying k-factor is negligible due to the short distances.

Diffraction around buildings can not be used on these high frequencies. Reflections however can be used, the power lost on one reflection is in the order of 10 dB. This is due to the rough surfaces of building materials.

The antenna decoupling is no problem because of the short distances used. The problem of ducting can be avoided if the angle of inclination of the LOS link is kept larger than 0.5 deg. and a minimum of energy is transmitted between -0.5 deg. and 0.5 deg. of inclination.

The cross-talk between the two polarizations is determined by the transmit and receive antennas and is of no problem.

The antenna temperature of the receiver is assumed to be 290 K.

Chapter 4

Network topology

If the system parameters are known the coverage in a given area can be calculated. If we wish to cover a large area the area must be divided in smaller cells as shown in Figure 4.1 [34]. A simple but inefficient method is to use different frequencies for the different cells.

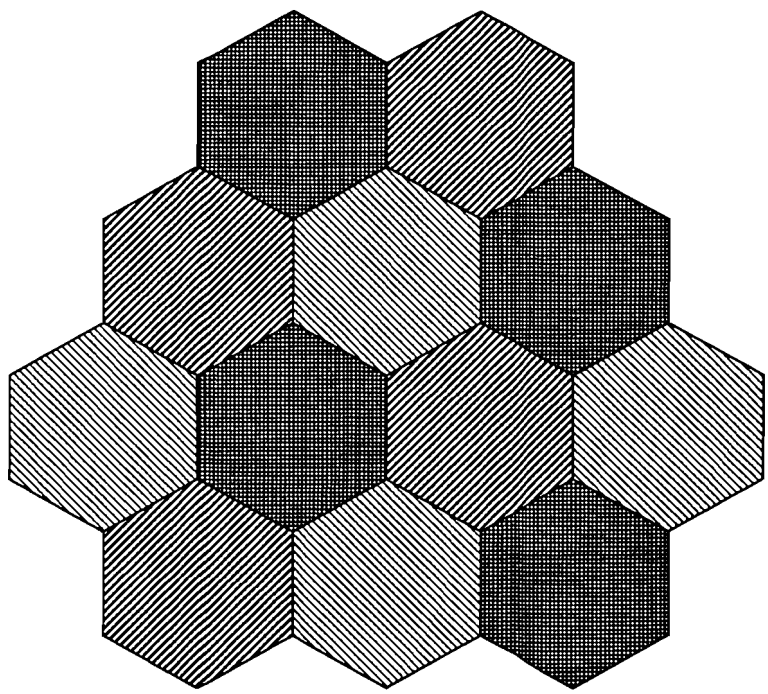

Figure 4.1: Area serviced with multiple cells

The frequency reuse distance defined as the distance where the same frequency can be reused depends on a lot of parameters [9]. For the analog test system (28 GHz) it is shown in Appendix B that the power decay corresponds to the theoretical $1/d^2$ scenario where d is the distance. In Chapter 7 measurement results are shown which shows that this is correct. It is assumed that the received power of a 42 GHz system

will also be proportional to $1/d^2$. This conclusion is based on the required LOS and Appendix B.

The ultimate situation is of course if in the adjacent cells the same frequency can be used, such a network is known as a Single Frequency Network (SFN). In the following sections the possibilities of frequency reuse in different cells are examined.

The directivity of the reception antennas used in microwave systems is very high. This is something which can be very well used in employing a frequency efficient cell structure [40].

The frequency reuse distance is determined by the amount of interference which is tolerable. In Figure 4.2 the effect of interference from other transmitters on the reuse distance is shown.

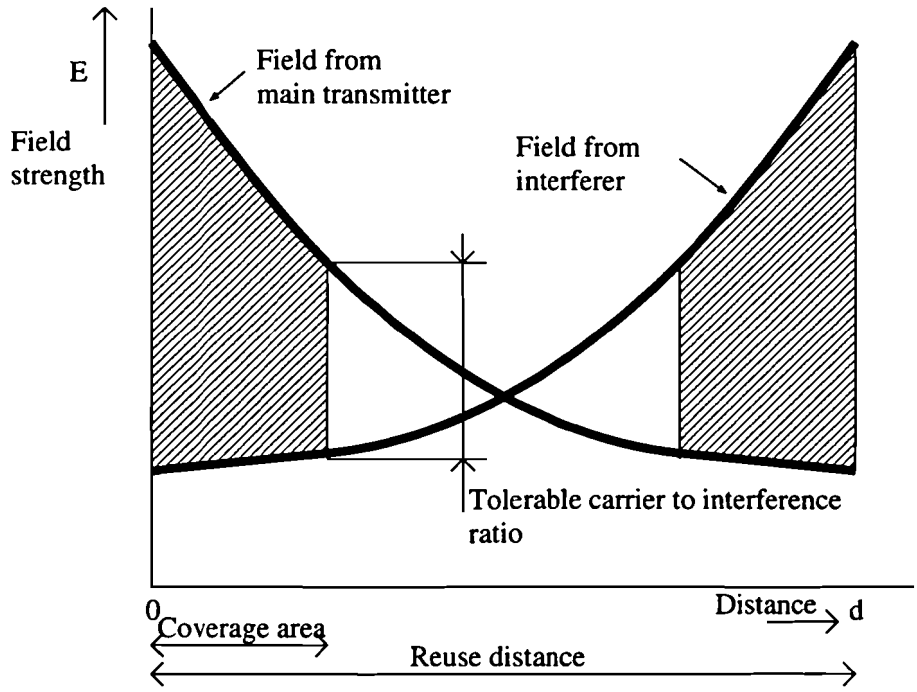

Figure 4.2: Frequency reuse distance

4.1 Cellular systems using omni directional antennas

In many cellular networks the antennas used are of the omni directional type. In our first approach we will examine the possibilities of such a network and examine the interference. In Figure 4.3 a configuration of such a network is shown which will be evaluated as an example.

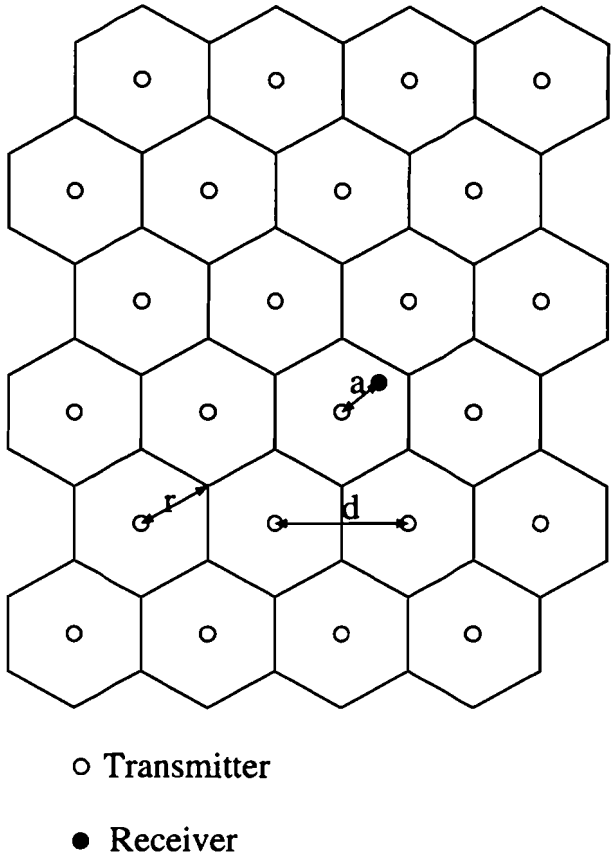

Figure 4.3: A cellular network with omni directional antennas

It is assumed that the transmitted signals are independent and thus the received interference power is the sum of the individual interferers. This is realistic because pseudo-random data are being transmitted and the signalling rate is in the order of 20-30 Mbaud. This means that if the distance between the reception point and the interferer and between the reception point and the main transmitter differ more than 15-10 m the received signals are uncorrelated. If we assume that only the 6 adjacent cells as shown in Figure 4.3 interfere the upper bound of the carrier to interference ratio (CIR) is given by [26, 27]

$$\frac{C}{I} \leq \frac{C}{\sum_{i=1}^{6} I_i} \tag{4.1}$$

where I_i is the power of the I^{th} interferer.

The power decreases simply according to the $1/r^2$ law as shown in Appendix B and the power of the main transmitter and the individual interferers are the same. The CIR is thus determined only by the distance from the receiver to the transmitter and the distance from the receiver to the interferer. Attenuation in the path such as gaseous absorption (L_m) increases the CIR because the wanted signal is attenuated less than the unwanted signal. If there is attenuation in the path due to precipitation

it is assumed that this attenuates both the wanted and the unwanted signals. Not using the medium loss L_m is thus a pessimistic approach.

A phenomena that can become a serious problem in high frequency networks is the increase in the received interference power due to ducting effects as discussed in Section 3.2. However for a ray to be captured in a duct it is necessary that the inclination of the ray is smaller than approximately 0.5 deg. This problem can thus be solved if only very little energy is radiated in the region between -0.5 deg and 0.5 deg. This puts constraints on the antenna heights and the cell sizes. For now it is assumed that no ducting problems occur.

The worst case position for the CIR is in the corner of the hexagon. A pessimistic approach is to assume that there is a line of sight with all of the 6 adjacent cells. The CIR in this position is given by

$$\frac{C}{I} = \frac{1/r^2}{1/r^2 + 1/r^2 + 1/(3r^2/2) + 1/(3r^2/2) + 1/(7r^2) + 1/(7r^2)} \leq \frac{63}{200} \tag{4.2}$$

Thus, the CIR equals -5 dB. This is of course unusable. This means that the adjacent cells can't use the same frequency in this case. To calculate the distance where the same frequency can be used it is assumed that the distance from the receiver site to the interferers all equal d and the receiver site is located on the edge of the cell. For a large ratio of r/d this is justified. The CIR can then be approximated with

$$\frac{C}{I} \approx \frac{r^{-2}}{6d^{-2}} \tag{4.3}$$

where r is the radius of the cell and d is the frequency reuse distance.

If we require a CIR of for instance 10 dB the ratio of the frequency reuse distance d and the cell radius r can be approximated by

$$\frac{d}{r} = \sqrt{n\frac{C}{I}} \tag{4.4}$$

where n equals the number of interfering cells at distance d.

If we choose n to equal 6 the calculated reuse distance d equals 7.75. This configuration is thus of no use for an efficient frequency planning.

Our goal is to reduce the interfering power, thus to reduce the number of interferers. This may be done by means of a directional antenna.

4.2 Cellular systems using directional antennas

In high frequency links it is possible to make use of very narrow-beam antennas. With such an antenna it is possible to reduce the amount of received interference [19].

Suppose we make use of a directional receiver antenna, for instance a 5 deg. opening aperture, and an omni directional transmitter antenna. This ensures that less interferers are within the opening aperture of the receiving antenna and thus less interference is expected to be received. For further computation we now define the distance between two transmitter antennas having the same orientation as d'.

In the analysis the assumption is made that only a limited number of interferers are present. This is justified because it is assumed that there is no LOS between an interferer at large distance because of buildings and vegetation etc. If this is not the case a problem arises. In Figure 4.4 a simplified figure of a network is shown. In

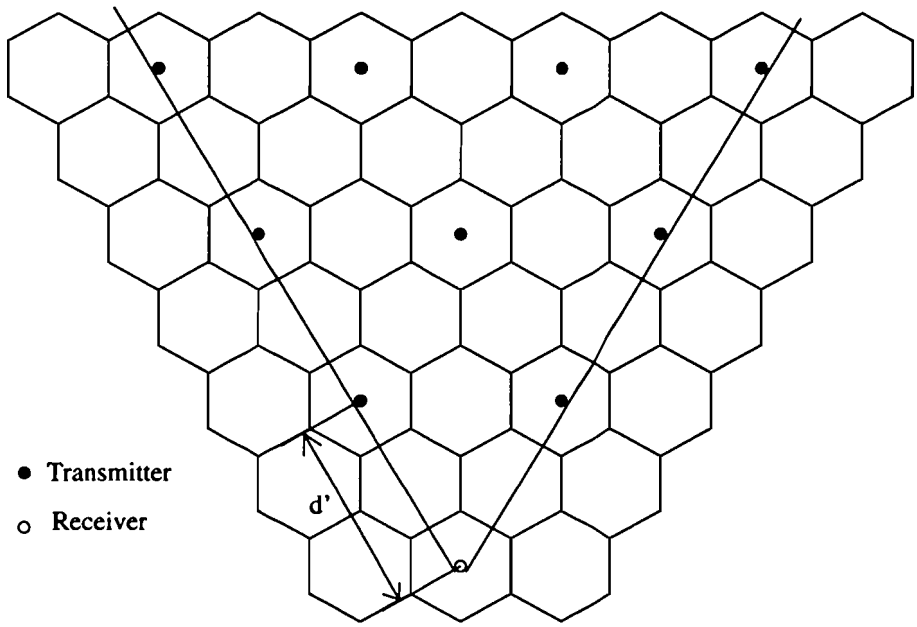

Figure 4.4: A simplified network

this figure the lines depict the opening aperture of the receiving antenna.

The total interference power I received from one interferer is given by

$$I = \frac{b}{d'^2} \tag{4.5}$$

where b is the transmitted power and d' is the distance between the interferer and the receiver. If we calculate the power ratios, we can use the normalized powers. Therefore we define the normalized power I'

$$I' = \frac{I}{b} \tag{4.6}$$

If only the interferers are taken into account which are closer than d' apart from the receiver the total interference power for this example is given by

$$I' = 2 \cdot \frac{1}{d'^2} \tag{4.7}$$

If interferers from distance 0 to $2d'$ are taken into account this results in

$$I' = 2 \cdot \frac{1}{d'^2} + 3 \cdot \frac{1}{(2d')^2} \tag{4.8}$$

Thus if interferers at an infinite distance from the receiver are taken into account the received interference power I' equals

$$I' = \sum_{i=1}^{\infty} \frac{i+1}{(id')^2} \tag{4.9}$$

and thus I' is given by

$$I' = \frac{1}{d'^2} \sum_{i=1}^{\infty} \left(\frac{1}{i} + \frac{1}{i^2} \right) \tag{4.10}$$

Now one can see that the first term in the summation $(1/i)$ does not converge. This means that if there is a LOS with all interferers that the received interference power would become infinite. This is a problem for all cellular networks which are base on a LOS (high frequencies) and thus the received power is proportional to $1/d^2$.

In a practical situation there are always other attenuation mechanisms e.g. gaseous absorption etc. These mechanisms further reduce the interference levels and help to overcome the convergence problems. Furthermore it is assumed that there is no LOS from a specific receiver with all the transmitter antennas.

All the transmitters who are within the opening aperture and have a LOS with the receiver produce interference. If the transmitter antennas are also of a directional type, the interference can be further reduced because not every transmitter antenna within the opening aperture of the receiving antenna directs its maximum of electromagnetic energy towards the receiving antenna.

4.2.1 One direction line-up of the transmitter antennas

Assume that the cells are illuminated from the edge of the cell. This can be accomplished with a sectorial horn and still preserve the circularity of the cells [39]. The most simple cellular structure with these antennas is to align all the transmitters as shown in Figure 4.5. From this figure one can see that $d = \sqrt{3}r$ and $d' = \sqrt{3}d$.

It is assumed that the transmitted signals are independent and thus the received power interference may be added up. If we take three transmitters into account, t_3 desired and t_1 and t_2 interferers, the C/I ratio CIR for worst case as in Figure 4.5 is given by

$$\frac{C}{I} = 10 \cdot \log \left(\frac{\frac{b}{a^2}}{\frac{b}{(a+d)^2} + \frac{b}{(a+2d)^2}} \right) \tag{4.11}$$

which results in

$$\frac{C}{I} = 10 \cdot \log \left(\frac{(\sqrt{3}r + a)^2 \cdot (2\sqrt{3}r + a)^2}{a^2 \cdot \left\{ (2\sqrt{3}r + a)^2 + (\sqrt{3}r + a)^2 \right\}} \right) \tag{4.12}$$

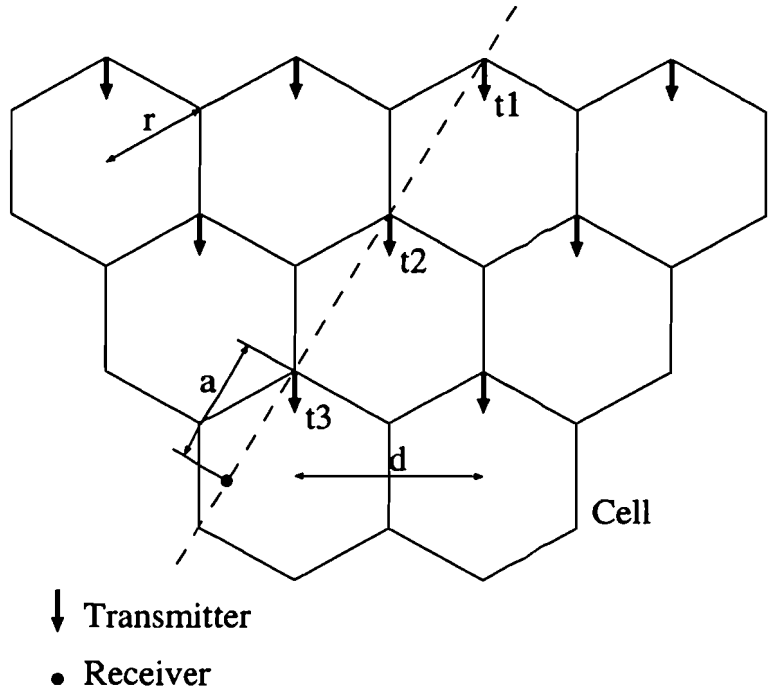

Figure 4.5: A simple aligned cell structure

where r is the radius of a cell and a is the distance between the receiver and the desired transmitter t_3.

Thus if the receiver is at the edge of the cell, $a = \sqrt{3}r$, the carrier to interference C/I = 4.4 dB. Since this is not sufficient for most transmission systems, such a simple SFN can never exist.

4.2.2 Rotated line-up of the transmitter antennas

The second approach to a single frequency network is to create a cellular system where the transmitter antennas which have the same orientation are as far apart as possible [19]. The disadvantage of such a network is shown in Figure 4.6 where in region A a receiver antenna is pointing directly to the transmitter of cell A but at an large angle α. The antenna gain in this particular direction is thus low. The transmitter antenna in cell B however is exactly pointing in the direction of the receiver. The antenna gain of the interfering transmitter is thus at its maximum. This results in a high interference level because the received power is proportional to $1/d^2$.

In an alternative setup the goal is to make sure that the problem of the configuration above does not occur. Now only three different orientations of the antennas are used. From this figure one can see that $d = \sqrt{3}r$ and $d' = 3r$.

The antennas with different orientations are positioned as far as possible apart, the

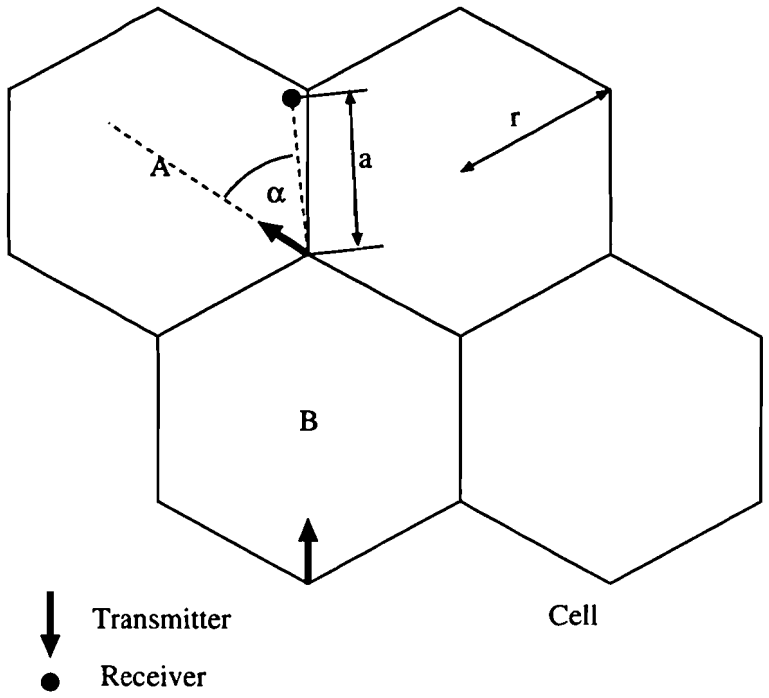

Figure 4.6: Incorrect configuration of cells

antennas with the same orientation are then much closer positioned to each other. This results in the pattern shown in Figure 4.7.

The C/I ratio then equals

$$\frac{C}{I} = 10 \cdot \log\left(\frac{\frac{1}{(2r)^2}}{\frac{1}{(5r)^2}}\right) \tag{4.13}$$

for one interferer and

$$\frac{C}{I} = 10 \cdot \log\left(\frac{\frac{1}{(2r)^2}}{\frac{1}{(5r)^2} + \frac{1}{(8r)^2}}\right) \tag{4.14}$$

if two interferers are taken into account.

The interference thus equals in the worst case 8 dB for one interferer and 6.5 dB for two interferers.

4.2.3 Rotated line-up using both polarizations

If the same configuration, as discussed in the previous section, is used but both polarizations are used, a "semi" SFN is constructed. This configuration shown in Figure 4.8. Again from this figure one can find the network parameters as, $d = \sqrt{3}r$ and $d' = 3r$.

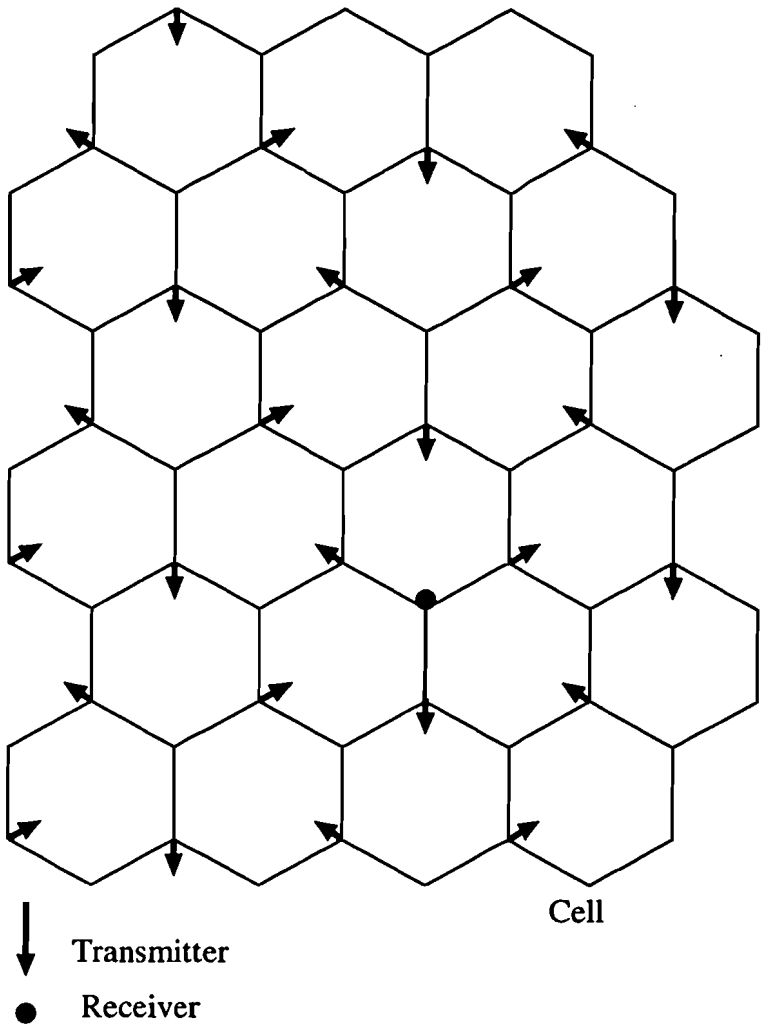

Figure 4.7: A single frequency network with 6.8 dB CIR

The worst case C/I ratio are now given by

$$\frac{C}{I} = \frac{\frac{1}{(2r)^2}}{\frac{1}{(8r)^2}} \tag{4.15}$$

and equals 12 dB assuming an infinite cross-polar discrimination. The worst case C/I ratio assuming a cross-polar discrimination of 10 dB is given by

$$\frac{C}{I} = \frac{\frac{1}{(2r)^2}}{\frac{1}{(8r)^2} + 0.1 \cdot \frac{1}{(5r)^2}} \tag{4.16}$$

and equals 11 dB.

Such a network can thus be used to create a SFN using digital QPSK modulation.

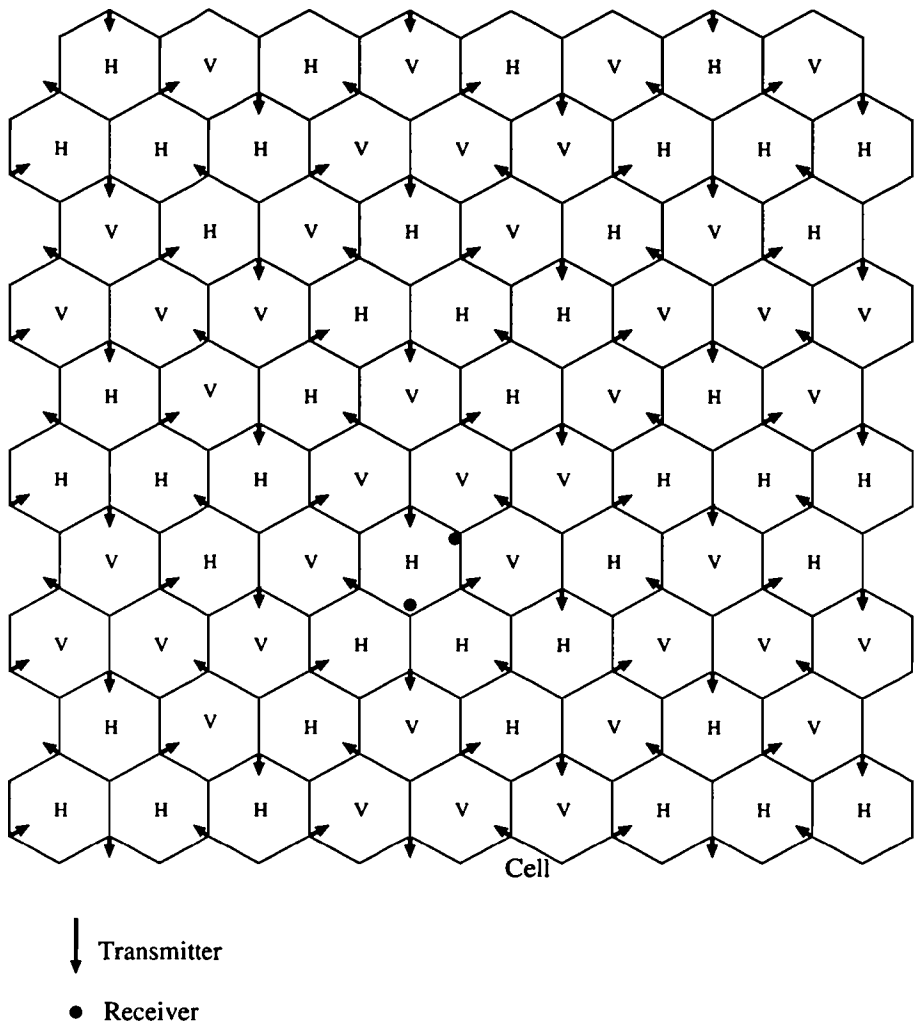

Figure 4.8: A single frequency network with 12 dB CIR

4.3 Feeding of single frequency networks

In the previous section a useful SFN network which makes use of both the polarizations has been shown. If such a network is installed a problem of feeding the transmitters with data arises. In the following section three different feed options are discussed.

4.3.1 Optical feeding of the network

One way to feed an MVDS network is by means of optical links. In such a network there has to be an optical link to every single transmitter site e. g. a ring network. The optical link can carry the bandwidth of 1 or 2 GHz at some I.F. frequency. This is of course an expensive solution because the infrastructure of a cable network is

expensive. The network could also use a coaxial cable. This is approximately as expensive as an optical link but gives a smaller bandwidth.

A nice feature of such a network is that no outage time due to rain is introduced in feeding the network.

4.3.2 Feeding the network by satellite

Another solution is to feed the network by satellite. In this scenario at every transmitter site one or more satellite receivers are required. If the full capacity of an MVDS network is used more than one satellite has to be used to feed the network. In this scenario it is possible to have some different programs transmitted in different cells which can be interesting.

4.3.3 Mutual feeding of the network

A third scheme is so-called mutual feeding by using every transmitter as a repeater. In a central cell of the network a digital signal is generated and transmitted to the adjacent cells. These cells retransmit the signal on their turn to their adjacent cells etc.

To preserve the signal quality every cell has to demodulate the signal, perform the error correction, recode the data and modulate it again. This is of course an option, if it is not used the result is error propagation through the network. The reception antenna of a repeater/transmitter can be larger in dimensions, thus have a larger antenna gain and thus less outage time. Together with the error correcting code it may be possible to protect the signal for degradation. It is simple to introduce some redundancy by having every transmitter receive the same signal from two or more repeaters. In this way it may be possible to further decrease the outage time.

In Figure 4.9 an example of the feeding of the network is shown.

In this figure three principle directions of feeding the network are shown. The arrows represent the feeding directions.

From this picture one can easily see that every transmitter can be fed from two different sources. The links between the transmitters are all shorter than the maximum path length in a cell. If more redundancy is required it is possible for a transmitter site to receive from other transmitter sites at longer distances. If the antenna gain is increased by e.g. 6 dB approximately the double path length can be achieved. The line of sight requirement will probably be met because the transmitter antennas and thus also the receive antennas at the transmitter sites are mounted at a high position.

Since the available bandwidth of a 42 GHz MVDS system is very large some local programs can be inserted in one or more channels at a transmitter site.

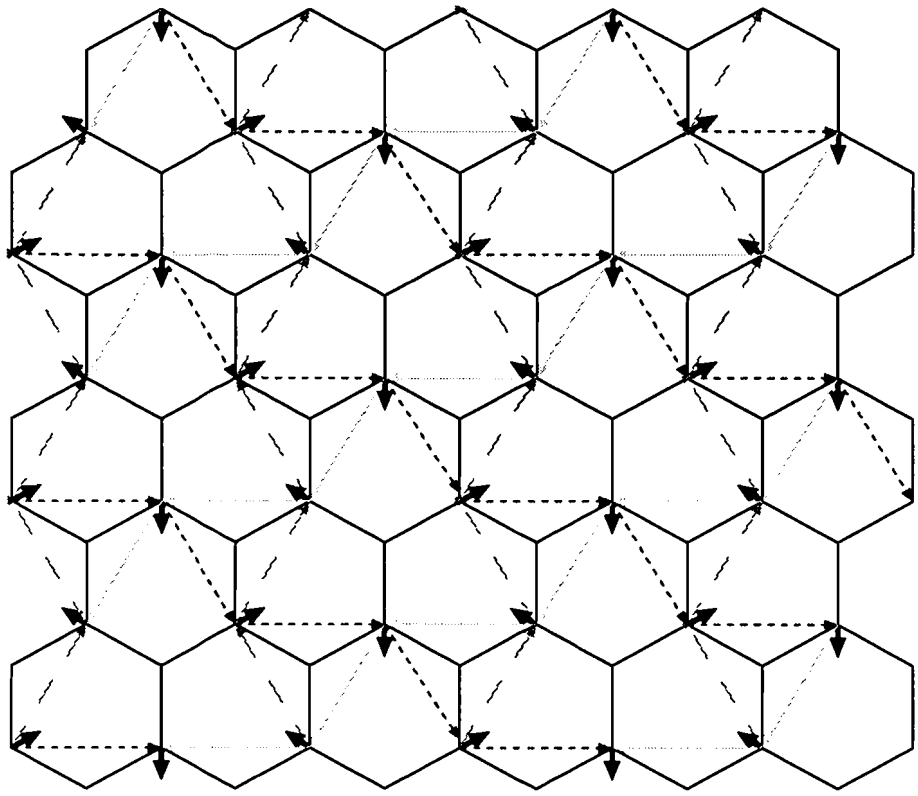

Figure 4.9: Example of feeding the network

There are probably many more solutions in feeding the network. It is therefore interesting to examine this and the costs of every solution in detail. Then the optimal solution of feeding the network can be chosen. This is however not in the scope of this report.

4.4 Discussion

Some networks have been suggested and their CIR ratios have been calculated. A semi SFN is proposed which makes use of both polarizations and narrow-beam reception antennas and has a CIR of 11 dB assuming a cross-polar discrimination of 10 dB or more.

No ducting is included, this should be avoided with a good antenna.

Three different schemes of feeding the network are discussed, feeding by cable, feeding by satellite and mutual feeding.

Chapter 5

Link budget calculations

Now we have discussed a cellular structure in the previous section we are interested in the cell sizes. Since the system aspects and the expected interference are known it is in principle possible to calculate the link budget.

To calculate the link budget we must estimate the influence of noise and interference on the QPSK link.

5.1 Tolerable noise and interference

To find the interference which can be tolerated the future system description briefly discussed in section 2.4 will be used. First the effect of noise on the digital link is discussed. Next the influence of interference and noise will be examined.

5.1.1 Influence of the Nyquist filter on the noise power

For the modulation scheme described in Section 2.4 the carrier to noise ratio C/N which is required for a quasi error free (QEF defined as a bit error rate BER of less than 10^{-11}) link will be computed. To calculate the C/N ratio in the transmission channel from the symbol energy E_s to the noise power density N_0, often used in digital modulation, it is necessary to take the bandwidths of the different signals into account. In Figure 5.1 the different bandwidths are shown.

The required E_s/N_o for a QEF QPSK operation using concatenated code are shown in table 5.1 [1].

The values E_s/N_o are equal to the C/N assuming QPSK. The values given however are the values before the demodulator as shown in Figure 5.2.

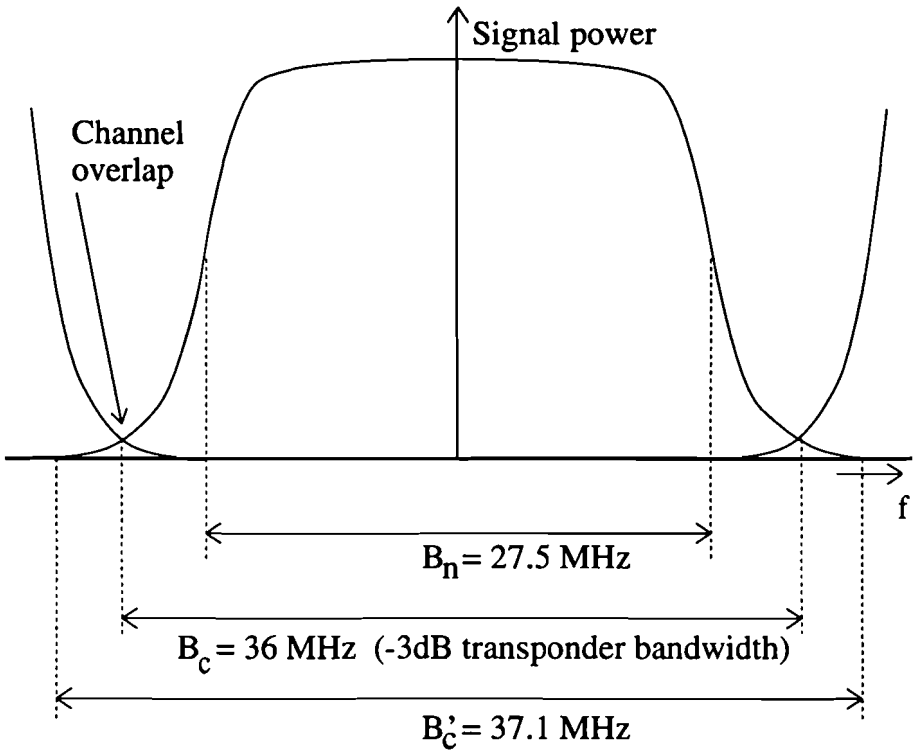

Figure 5.1: Definition of the theoretical bandwidths of a satellite channel

Inner code rate	E_s/N_0 Gaussian channel (dB)
1/2	3.1
2/3	4.9
3/4	5.9
5/6	6.9
7/8	7.7

Table 5.1: Required E_s/N_0 ratios (theoretical values)

The required channel bandwidth B_c' can found with

$$B_c' = \frac{1}{T_s} \cdot (1 + \alpha) \tag{5.1}$$

where T_s is the symbol duration and α is the roll-off factor. The roll-off factor used in satellite transmission equals 0.35. As shown in Figure 5.1 however the adjacent bands do overlap. This results in e.g. a Nyquist bandwidth B_n of e.g. 27.5 MHz and a channel bandwidth B_c of e.g. 36 MHz (B_c' = 37.1 MHz). The symbol energy E_s is defined as

$$E_s = \int_0^{T_s} s(t) \cdot s^*(t)\, dt \tag{5.2}$$

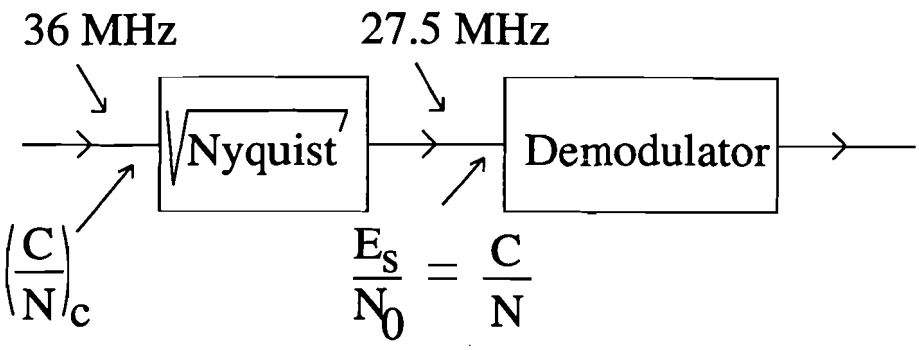

Figure 5.2: The point of observation in the link

For QPSK this results in

$$E_s = \frac{A^2 \cdot T_s}{2} \tag{5.3}$$

where A is the amplitude of the carrier.

Assuming a white Gaussian noise with spectral density N_0, E_s/N_o can written as

$$\frac{E_s}{N_0} = \frac{A^2 T_s}{2} \cdot \frac{B_n}{N} \tag{5.4}$$

where B_n is the band width of the Nyquist filter and $N = N_o \cdot B_n$ is the noise power after the Nyquist filter.

The $(C/N)_c$ is given by

$$\left(\frac{C}{N}\right)_c = \frac{A^2}{2} \cdot \frac{B_c}{N} \tag{5.5}$$

where B_c is the band width of the transponder and $N = N_o \cdot B_c$ is the noise power before the Nyquist filter.

The carrier power of the QPSK signal is given by

$$C = \frac{E_s}{T_s} = \frac{A^2}{2} \tag{5.6}$$

thus it is concluded that

$$\frac{E_s}{N_0} = \frac{C}{N} = (1 + \alpha') \cdot \left(\frac{C}{N}\right)_c \tag{5.7}$$

where $\alpha' = 0.31$ is the α corrected for the overlapping bandwidth.

$$1 + \alpha' = \frac{B_c}{B_n} \tag{5.8}$$

In table 5.2 the calculated values for the required Carrier to noise C/N ratios assuming a Gaussian channel are given for the different coding rates. These values do not include any system margin.

Inner code rate	$(C/N)_c$ (dB)
1/2	1.9
2/3	3.7
3/4	4.7
5/6	5.7
7/8	6.5

Table 5.2: Required $(C/N)_c$ ratios with $B_c = 36$ MHz and $B_n = 27.5$ MHz

The difference in dB between the $(C/N)_c$ and the E_s/N_0 thus equals 1.17 dB in this example. This depends on the different bandwidths used and thus varies with the channel spacing. In this example we use 41.6 MHz channel spacing with a 36 MHz channel bandwidth.

The MVDS system is a power restricted system. Therefore the inner code rate 1/2 is very interesting. The rate 3/4 is also very interesting because the additional required CNR is not that severe and the bit rate the channel can carry is increased by 50 %.

Since in principle the E_s/N_o is the same as the C/N ratio for QPSK systems we will use both these notations as equal. From here on E_s/N_o and C/N both denote carrier to noise levels just before the demodulator and $(C/N)_c$ denotes the carrier to noise ratio in the 36 MHz channel.

5.1.2 Influence of noise on the QPSK performance

In Figure 5.3 the constellation diagram of a QPSK signal is shown [41] and [30]. This diagram represents the constellation diagram for an ideal correlation receiver or a matched filter receiver.

The analysis performed is concerning the Symbol Error Rate SER and the Bit Error Rate BER. The probability of a symbol error P_e is given by

$$P_e = 1 - P_c \tag{5.9}$$

where P_c is the probability that a symbol is received correct. A QPSK symbol is received correct if both the in phase and the quadrature components are correct. These probabilities are denoted by P_{ci} and P_{cq} respectively. Thus

$$P_c = P_{ci} \cdot P_{cq} \tag{5.10}$$

Since the constellation diagram is symmetric it is quite obvious that P_{ci} and P_{cq} are equal. The symbol error thus reduces to

$$P_e = 1 - P_{ci}^2 \tag{5.11}$$

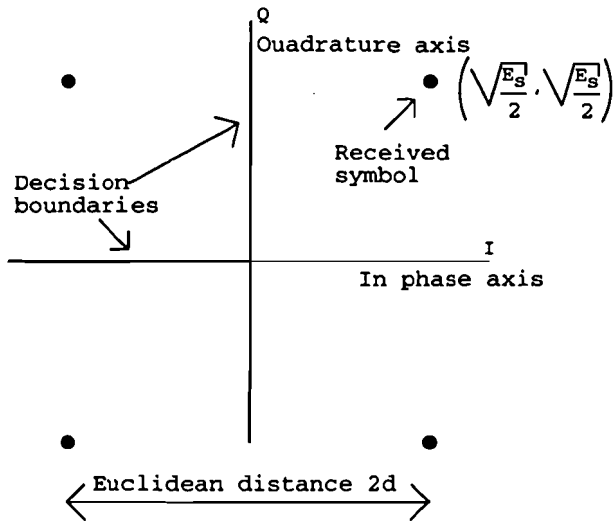

Figure 5.3: A QPSK constellation diagram

P_{ci} can be found using the probability density function of the random disturbance. The probability is depending on the distance d between the received vector in the constellation diagram and the decision boundary. If we assume that the received signal is disturbed by AWGN. The probability P_{ci} can then be found with

$$P_{ci} = P(n > -d) = \int_{-d}^{\infty} p_n(n)\, dn = 1 - \int_{d}^{\infty} p_n(n)\, dn \tag{5.12}$$

where $p_n(n)$ is the probability density function for zero mean Gaussian noise given by

$$p_n(n) = \frac{1}{\sqrt{(2\pi\sigma_n^2)}} \cdot \exp\left(-\frac{1}{2} \cdot \frac{n^2}{\sigma_n^2}\right) \tag{5.13}$$

where σ_n^2 is the variance of the noise n.

$$P_{ci} = 1 - Q\left(\frac{d}{\sigma_n}\right) \tag{5.14}$$

where the Q-function is defined as

$$Q(x) = \int_{x}^{\infty} \frac{1}{\sqrt{(2\pi)}} \cdot \exp(-\frac{x^2}{2})\, dx \tag{5.15}$$

The probability of a symbol error can now be written as

$$P_e = 1 - \left\{1 - Q\left(\frac{d}{\sigma_n}\right)\right\}^2 \tag{5.16}$$

From Figure 5.3 it can be seen that the distance d equals

$$d = \sqrt{\frac{E_s}{2}} \tag{5.17}$$

From this the probability of a symbol error is found as

$$P_e = 1 - \left\{1 - Q\left(\sqrt{\frac{E_s}{N_o}}\right)\right\}^2 \tag{5.18}$$

It is most likely that if an error occurs that the adjacent symbol is chosen. If the bits are mapped on the symbols using the Gray-mapping one symbol error introduces only one bit error and thus the BER or P_b equals

$$P_b = 1/2 - 1/2 \cdot \left\{1 - Q\left(\sqrt{\frac{E_s}{N_o}}\right)\right\}^2 \tag{5.19}$$

Assuming a small probability of error the total probability of a bit error is thus given by

$$P_b = Q\left(\sqrt{\frac{E_s}{N_o}}\right) \tag{5.20}$$

With the formula above it is very simple to calculate the bit error rate if the ratio (E_s/N_o) is known. In Table 5.1 the required (C/N) ratio before the demodulator, or the (E_s/N_o), is given. As an example we use the inner coding rate of $1/2$ and we see that (E_s/N_o) of 3.1 dB is required. Using the formula above the corresponding probability of error or BER can be calculated and equals $7 \cdot 10^{-2}$. It has been simulated [1] that this BER can be corrected to a QEF system or a bit rate of less than 10^{-11}.

5.1.3 Influence of interference on the QPSK performance

The received carrier may be impaired by other interference signals than the Additive White Gaussian Noise (AWGN). Those interfering signals may come from the adjacent cells in a cellular structure.

If we introduce an interferer our goal is to achieve a BER of $7 \cdot 10^{-2}$ so that the error correcting scheme can decrease the BER to 10^{-11}.

If it is assumed that the interfering signals and the desired signal are statistically independent and in wide sense stationary random process of zero means [18] the received power from the individual sources may be added up.

The interferers will be the transmitters in the adjacent cells and thus also transmitting a QPSK signal. The mean of the signal is thus zero. Furthermore a QPSK signal is a wide sense stationary process. Since the sources of the interfering signals are at a relatively large distance it is even in an SFN reasonable to assume that the signals are independent.

Thus the noise power plus interference power $\mathcal{N}$ equals

$$\mathcal{N} = N + \sum_{k=1}^{n} I_k \tag{5.21}$$

where N is the total received noise power and I_k is the power of the k^{th} interferer.

It is thus possible to calculate the maximum tolerable interference if the noise power and the carrier power are given. The calculations of the BER given E_s/N_0 are based on a Gaussian noise source. To use these results it is necessary that the interference is also Gaussian distributed. If the number of individual interferers is large, have the same distribution (none of them is dominant) and the individual distributions are zero mean the joint probability density function of the interferers is Gaussian distributed with a variance equal to the sum of the individual variances according to the central limit theorem.

If the received interference is dominated by one source and the probability density function is not Gaussian the calculations based on the Gaussian assumption yield a pessimistic result [18]. This results on the given noise to interference ratio N/I. In [18] it is stated that if the C/I ratio is large ($\geq$ 20 dB) and at least 3 dB larger than the C/N ratio it is allowed to treat the interference as a Gaussian source (N/I $\geq$ 3 dB).

If the N/I ratio is small the system becomes interference dominated instead of noise dominated. In the future MVDS system the interference will be dominated by one or very few interferers as is shown in the previous Chapter.

5.1.4 Worst case interference model

We will now derive a worst case model of the interference to estimate the impact of the interference.

If there is an interferer the constellation points in the constellation diagram are disturbed in a random manner. This means that some disturbances actually improve the tolerance to noise for that particular symbol as shown in Figure 5.4.

A worst case assumption is that the interferer is exactly synchronous with the received signal. This means that the sample time in the receiver samples at exact the correct time for the wanted signal as well as for the interferer. The output of the matched filter then produces the maximum output due to the interferer. Because the interferer is also a QPSK signal the filter is matched to the interferer as well.

If the modulation frequencies of the wanted signal and the interferer are exactly the same it is allowed to model the interferer as a disturbance in the constellation diagram. If the frequencies are not exactly the same the additional vector rotates during the signaling interval. It is worst case to have the interference vector in the worst case position throughout the whole signaling interval due to the integrating behaviour of the matched filter. The BER can be written as a function of the angle of the interferer γ with respect to the constellation diagram. This function can be

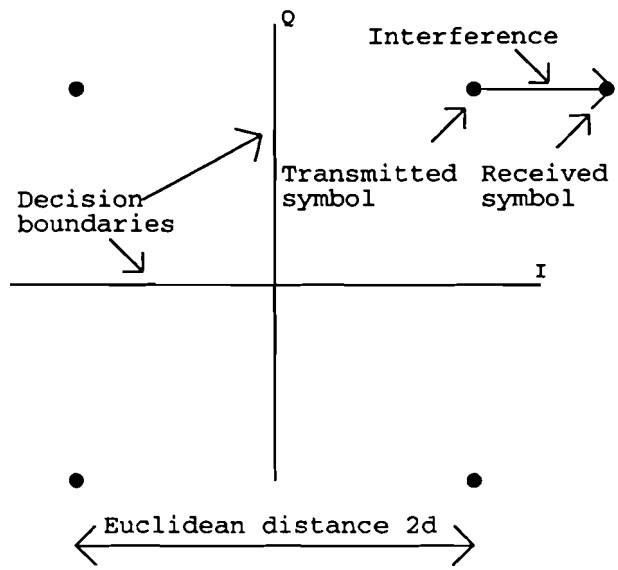

Figure 5.4: A constellation diagram with interferer

found using Formula 5.19 and is given by

$$P_b = \frac{1}{2}\left[1 - \left\{1 - Q\left(\frac{\sqrt{E_s} - \sqrt{2E_i}\cdot\cos(\gamma)}{\sqrt{N_o}}\right)\right\}\cdot\left\{1 - Q\left(\frac{\sqrt{E_s} - \sqrt{2E_i}\cdot\sin(\gamma)}{\sqrt{N_o}}\right)\right\}\right] \tag{5.22}$$

where E_i is the energy of the interfering symbol and a γ of 0 corresponds to the interferer given in Figure 5.4.

This function is plotted in Figure 5.5 for a C/N ratio of 15 dB and a varying N/I ratio. From this plot one can see that the worst case angle γ is π or $3/2\pi$. In the constellation diagram this corresponds to the situation where the interferer points towards a decision boundary.

For our worst case assumption we assume that the interfering signal is always at a worst case position, e.g. γ equals π, as shown in Figure 5.6.

All the above assumptions made thus far lead to a pessimistic upper bound for the BER. This analysis assumes however that the receivers carrier recovery and clock recovery circuits work perfectly. For very low SNR or a high CIR this might not be the case. This depends on the algorithms used and is beyond the scope of this report.

Another point is that the different carriers may run on nearly the same frequency. This results in slow rotating of the interferer in the constellation diagram. In this case the interference can be at a worst case position for a relative long time. This effect can be interpreted as slow fading.

The probability of a bit error P_b can now be found using the formulae above (Figure

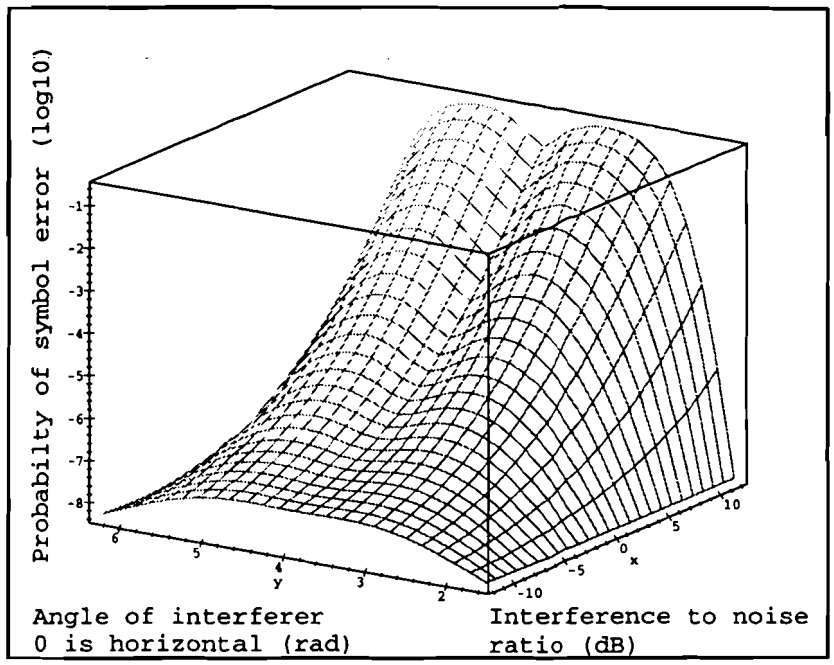

Figure 5.5: BER as a function of the interferer angle

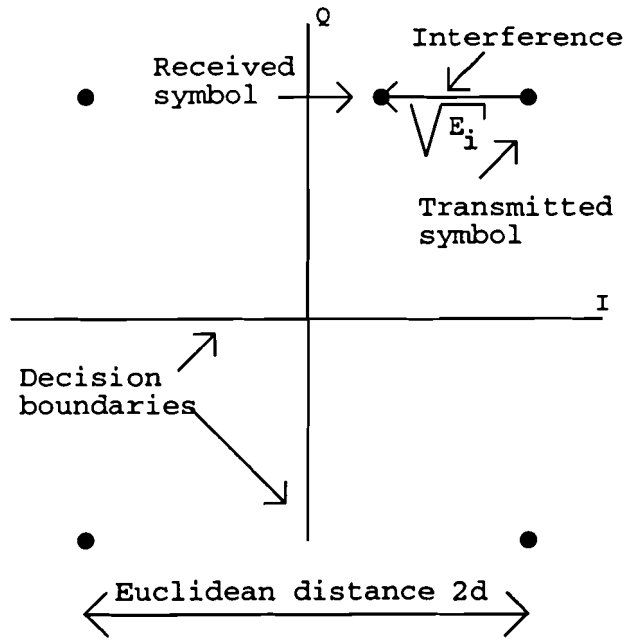

Figure 5.6: The worst case interferer

5.6) and equals

$$P_b = \frac{1}{2}\left[1 - \left\{1 - Q\left(\frac{\sqrt{E_s} - \sqrt{2E_i}}{\sqrt{N_o}}\right)\right\} \cdot \left\{1 - Q\left(\sqrt{\frac{E_s}{N_o}}\right)\right\}\right] \qquad (5.23)$$

It is interesting to have the probability of a bit error P_b as a function of the carrier to noise plus interference ratio $C/\mathcal{N}$ and the interference to noise ratio N/I. The formula above can be rewritten as

$$P_b = \frac{1}{2}\left[1 - \left\{1 - Q\left(\sqrt{\frac{C}{\mathcal{N}}(1+\frac{I}{N})} - \sqrt{2\frac{I}{N}}\right)\right\} \cdot \left\{1 - Q\left(\sqrt{\frac{C}{\mathcal{N}}(1+\frac{C}{N})}\right)\right\}\right] \tag{5.24}$$

With this formula the effect of interchanging noise for interference can be studied. In Figure 5.7 the BER as a function of the $C/\mathcal{N}$ is given for some Noise to Interference Ratios (N/I).

From Figure 5.7 one can see that for large $C/\mathcal{N}$ ratios the treatment of non Gaussian interferers as Gaussian interferers results in a pessimistic result. For a very low $C/\mathcal{N}$ ratio the result is optimistic.

This analysis can be very well used for estimating the influence of an interferer. Much more sophisticated analyses are performed by [35, 33, 29]. These result in a more tight upper bound as shown in Figure 5.8 [35]. The difference in the calculated bound above and the work of [35] is less than 1 dB. The P_e in Figure 5.8 denotes the probability of a symbol error. The factor k denotes the interference to noise ratio.

Some simulations have been performed to verify the analysis. In these simulations again a perfect carrier and clock recovery is assumed. In Figure 5.9 an eye pattern is shown when there is no interference. In this figure one can see that the eye pattern is maximal opened at the sample moment.

In Figure 5.10 an eye pattern is shown with a carrier to interference ratio of 12 dB.

In Figure 5.11 a plot is shown with the simulation results of the BER together with the bounds given by the theoretical analysis. In this plot the BER is a function of the CNR with different CIR ratios.

This plot is presented this way because of the time required to simulate the BER for one interference level. It is thus difficult to give the BER as a function of the $C/\mathcal{N}$. Formula 5.23 can be rewritten as

$$P_b = \frac{1}{2} \cdot \left[1 - \left\{1 - Q\left(\sqrt{\frac{C}{N}} \cdot (1 - \sqrt{2\frac{I}{C}})\right)\right\} \cdot \left\{1 - Q\left(\sqrt{\frac{C}{N}}\right)\right\}\right] \tag{5.25}$$

and thus used to give a plot of the BER as a function of the CNR.

From this figure one can see that the simple theoretical analysis is a good upper bound for the BER with an interfering signal.

The conclusions of this analysis is that it can be very well used and it is computational very simple as well. Since we know what un coded BER requirement we have to meet we can now calculate the maximum amount of noise which can be tolerated given the level of interference. These relations are then of much use in planning the network.

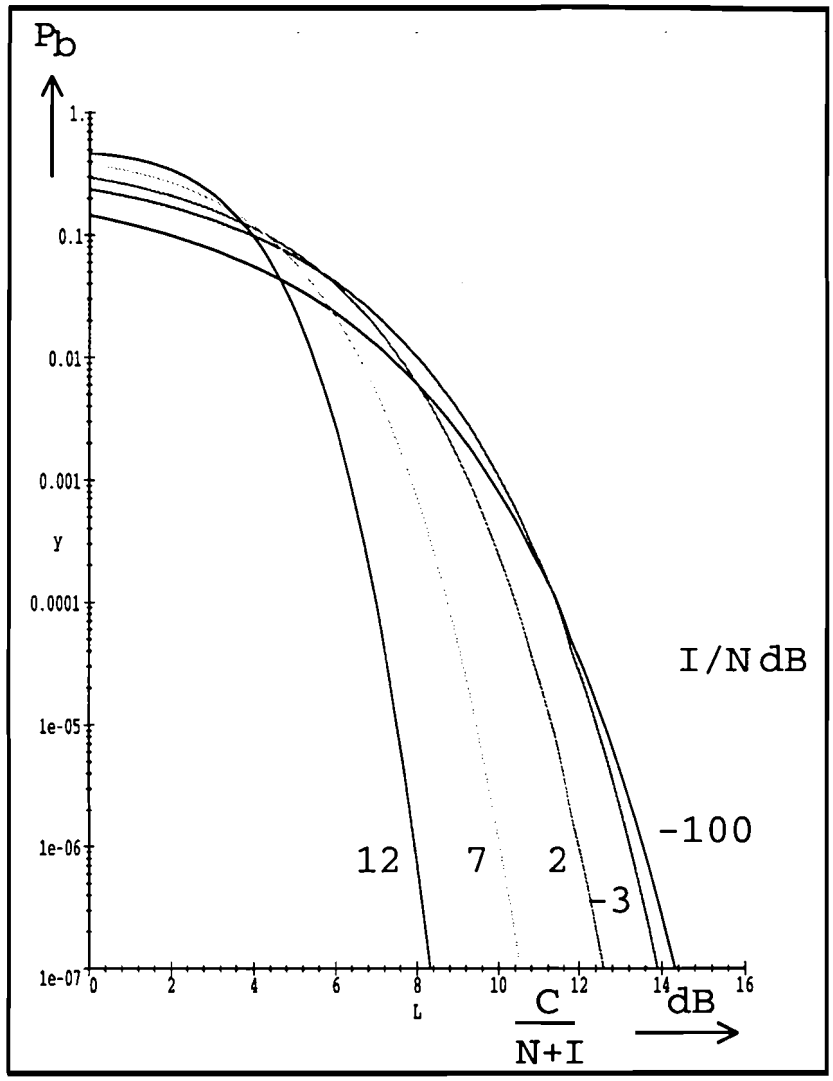

Figure 5.7: The upper bound of the BER as a function of noise and interference

5.2 Link budget with noise

The link budget calculations are based on the provided service by the MVDS operator. We assume here that a service of a quasi error free performance is to be provided for more than 99.9 % of the time. From this very low BER of $1 \cdot 10^{-11}$ the BER before Viterbi decoding can be found if the coding rate is known. In this report two convolutional coding rates will be given as an example to calculate the link budget; $R = 1/2$ and $R = 3/4$. From this un-coded BER the required E_s/N_o just before the demodulator will be calculated. Further a implementation margin of

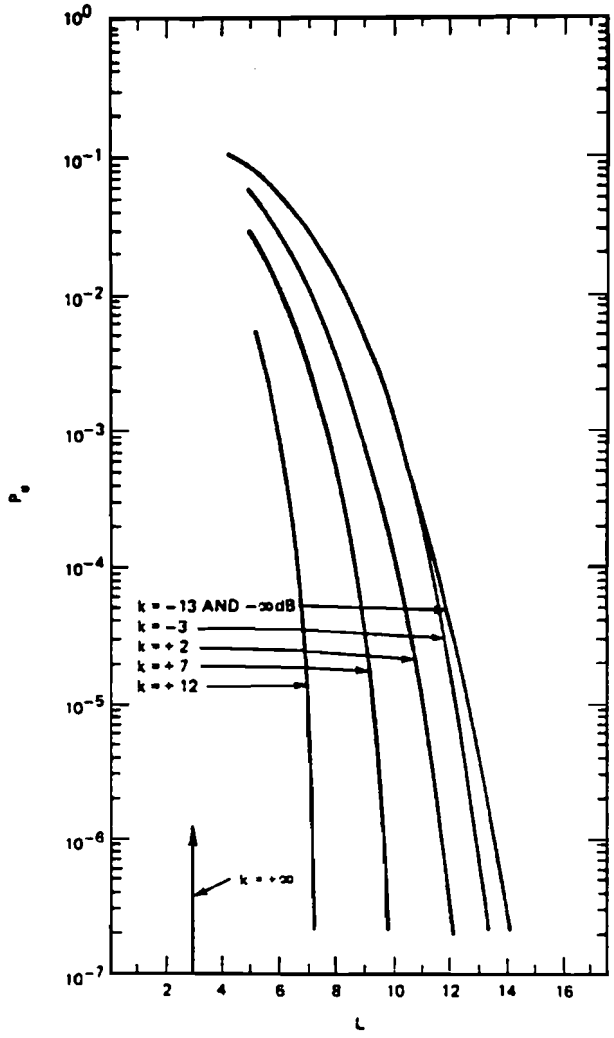

Figure 5.8: The upper bound of the BER as found by [35]

1 dB is taken into account. This value will then be converted to the required CNR in the channel. From this point on the transmission aspects as discussed in Section 3 will be taken into account to calculate the maximum path length based on the system components characteristics and the maximum outage time. In this section the results from the previous sections as well as from the Appendices are used.

We will first calculate the link budget based on one cell. Such a link budget is thus a noise limited budget since no interference is involved. In the following section interference from adjacent cells is taken into account. This will change the link budget and thus the cell sizes.

From Table 5.1 in Section 5.1 the required E_s/N_o ratios are found for a QEF operation and equal 3.1 dB for a coding rate of 1/2 and 5.9 dB for a coding rate of 3/4. Taking the effect of the root Nyquist filter into account we obtain the required C/N in the 36 MHz channel of 1.9 dB for $R = 1/2$ and 4.7 dB for $R = 3/4$. Now

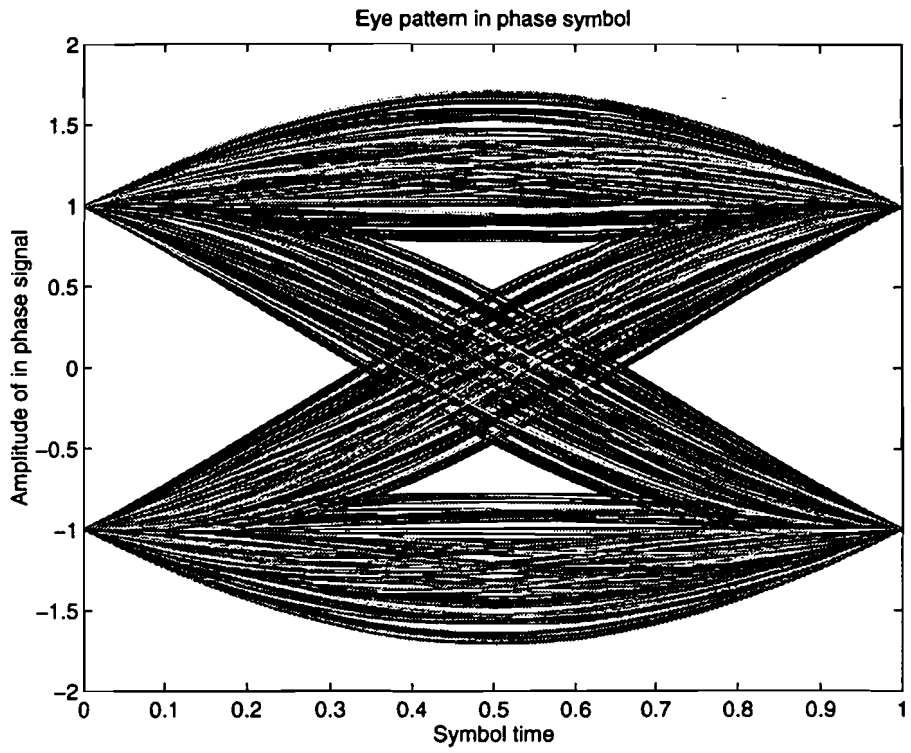

Figure 5.9: Eye pattern without interference, without noise

we know the required CNR in the 36 MHz channel, from this the link budget will be calculated.

As shown before in Chapter 3 and Appendix A

free space loss	$= l_{bf} = (\frac{4\pi d}{\lambda})^2$
transmitter isotropic antenna gain	$= g_t$
receiver isotropic antenna gain	$= g_r$.

The Effective Isotropic Radiated Power $eirp$ is defined as $p_t \cdot g_t$. We also introduce a general system loss l_{sys} which consists of several factors and will be defined below. The carrier power is now given by

$$c = \frac{eirp}{l} \cdot \left(\frac{\lambda}{4\pi d}\right)^2 \cdot g_r \tag{5.26}$$

The received noise power is n given by

$$n = kTB \tag{5.27}$$

where

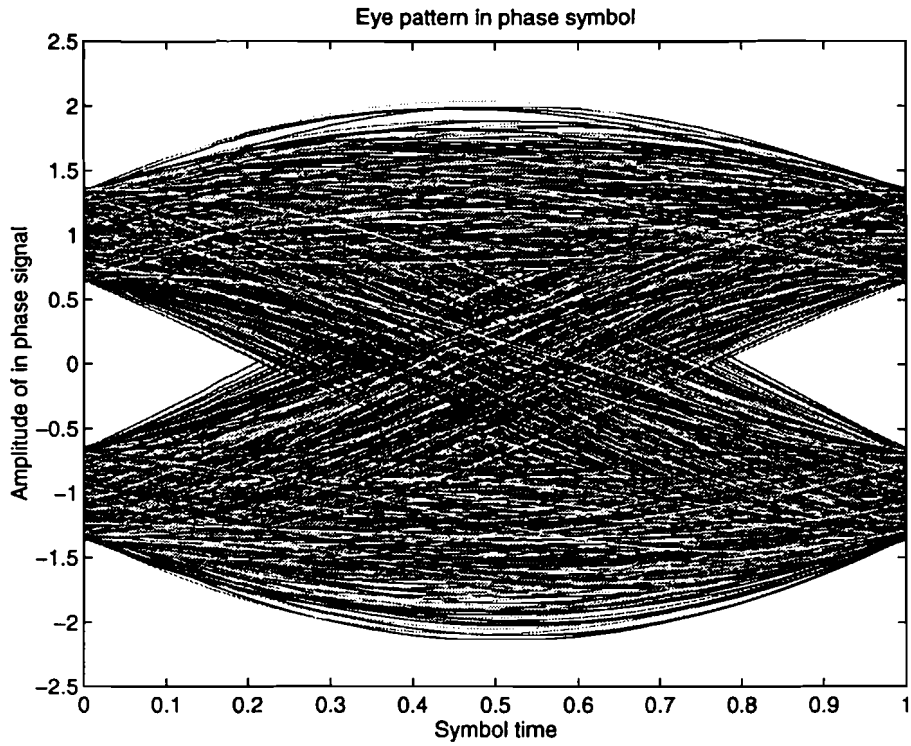

Figure 5.10: Eye pattern with a CIR of 12 dB, without noise

k = Boltzmann's constant (J/K)
T = the temperature (K)
B = the receiving bandwidth (Hz).

This simple analysis result in the well known formula [18]:

$$(\frac{c}{n}) = (\frac{eirp}{l}) \cdot (\frac{\lambda}{4\pi d})^2 \cdot (\frac{g_r}{T}) \cdot (\frac{1}{kB}) \tag{5.28}$$

where

c = carrier power
n = noise power
$eirp$ = Effective Isotropic Radiated Power
l = system loss
d = distance
λ = wavelength
k = Boltzmann constant
B= receiving bandwidth
g_r = the receiver antenna gain
T = the temperature.

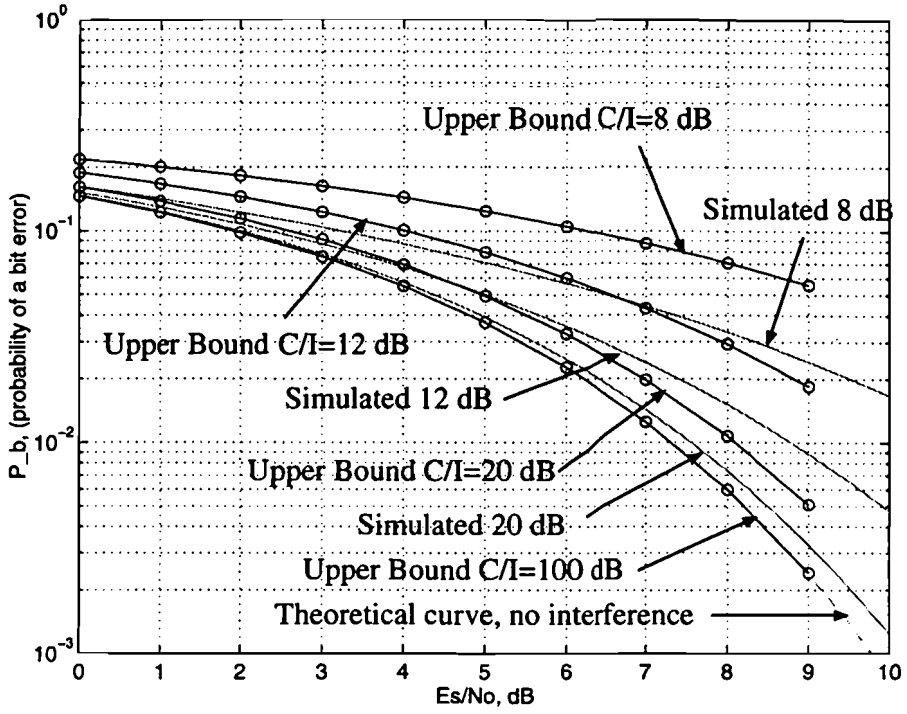

Figure 5.11: The BER function, C/I =∞, 20, 12, 8 dB

In this formula the system loss $L = 10 \cdot \log(l) = L_m + L_a + L_p + L_f$.

where

L_m = medium loss (dB)
L_a = loss due to rain attenuation (dB)
L_p = pointing loss (dB)
L_f = loss due to fading (dB).
L_{feed} = antenna feeding loss (dB).

The medium loss, which is the loss due to gaseous absorption in the troposphere, L_m is taken to be 0.16 dB/km for 42 GHz. This is derived from Figure 5.12 [15] and the CCIR report 719-3 [22].

In this loss the absorption and attenuation due to fog is lumped together.

The loss due to rain can be calculated with the formulas in section 3.9. According to the CCIR rain model the attenuation at 42 GHz can be found with

$$L_{a,\mathrm{dB}}(d) = 2.58 \cdot \frac{d}{1 + \frac{d}{25.16}} \tag{5.29}$$

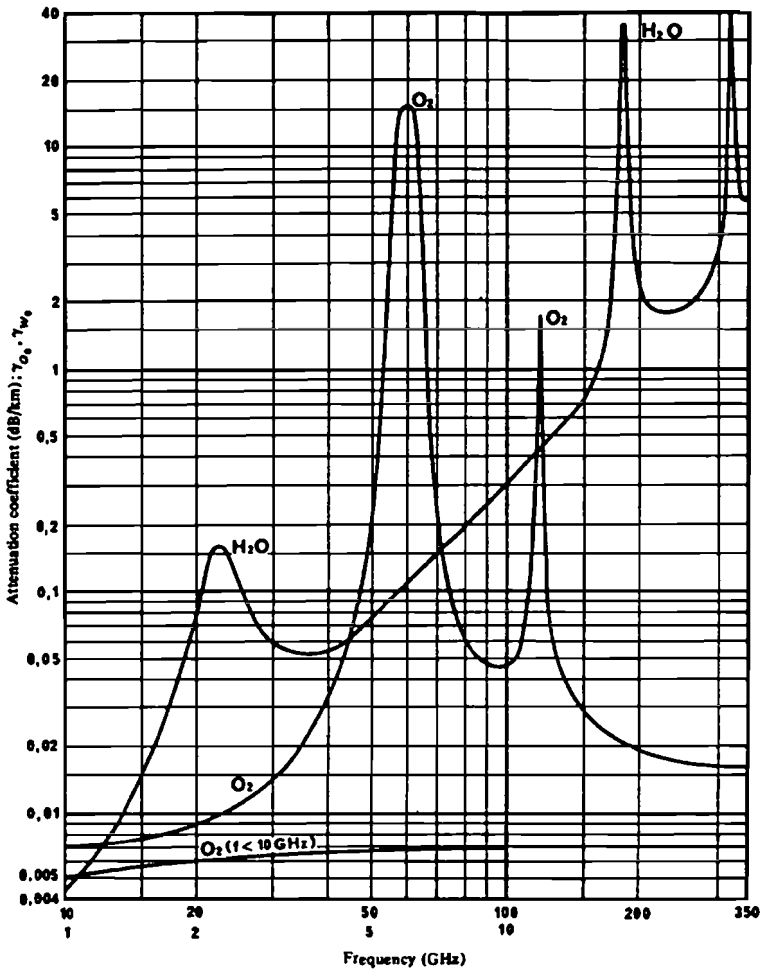

Figure 5.12: Atmospheric attenuation by oxygen and water vapour[15]

for horizontal polarization and

$$L_{a,\mathrm{dB}}(d) = 2.23 \cdot \frac{d}{1 + \frac{d}{25.16}} \tag{5.30}$$

for vertical polarization, where d = path length in km between the transmitter and the receiver.

The pointing loss originates from a finite pointing accuracy. This can be a result from installation and wind effects on the antenna pole. It is supposed that the antenna deflection due to the wind shall not exceed 0.5 degree in any direction when subjected to a 3 second wind gust of 45 m/s as stated in the British Telecommunications specifications SS6003 [37].

The antenna gain pattern of a dish antenna can be approximated with a parabolic

function for small angles θ, referring to the main beam, with

$$G(\theta)_{\text{dB}} = \left(G(0) - 3 \left(\frac{\theta}{\frac{1}{2} \cdot \theta_{3\text{dB}}} \right)^2 \right)_{\text{dB}} \tag{5.31}$$

where θ_{3dB} is the 3 dB beamwidth which can be calculated with [11] (parabolic).

$$\theta_{3\text{dB}} = \frac{72.7 \cdot \lambda}{D} \tag{5.32}$$

where D = antenna diameter (m) and λ = the wavelength (m).

This results in a pointing loss of approximately 0.45 dB.

The loss due to fading can be found in Table 3.4 of Section 3.7.

The loss due to fading L_f is simply added to the other losses, this might not be correct. It may be more realistic to add the outage times instead of the attenuations since they will probably not occur at the same time. Here we take the pessimistic approach and add the different attenuations.

The *eirp* (Effective Isotropic Radiated Power) is given by $eirp = p_t \cdot g_t$. The transmit antenna is assumed to be a sectorial horn with a horizontal 3 dB beam width of 64 deg. and a vertical 3 dB beam width of 10 deg. This antenna illuminates the cell from the edge of the cell. This choice is discussed in Section A.3 of Appendix A and in Section 4.2. The gain of such an antenna equals 15 dBi as can be seen in the Appendix A.

The transmitted power P_t in the future 42 GHz system is assumed to be 21 dBm per channel (saturated). The required back-off depends on the characteristics of the amplifier. Here a required back-off of 3 dB is assumed using the QPSK modulation. The transmitter antenna gain equals 15 dBi. This will result in a EIRP of 33 dBm per channel. There is however some loss in the antenna feed and the wave guides L_{feed} which is assumed to be 0.5 dB. The EIRP then becomes 32.5 dBm (1.78 W). This will be the value we will be using for further calculations.

To calculate the signal-to-noise ratio we have to calculate the in band noise in the receiver. The receiver is modeled as shown in figure 5.13.

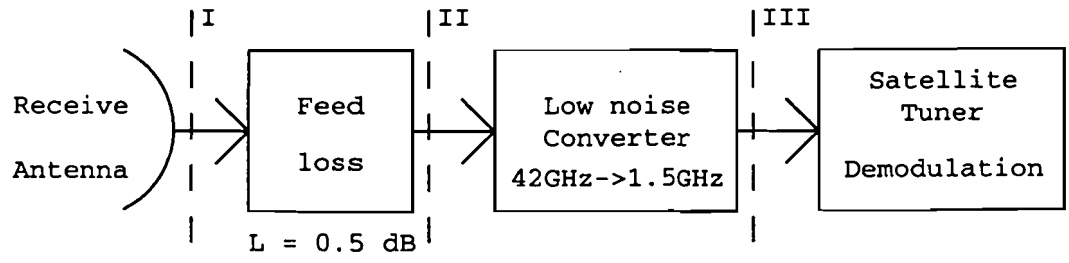

Figure 5.13: Receiver model

It is assumed here that the down conversion is performed in 2 steps. In this concept the standard satellite down converter can be used and only the mixer (42 GHz to 12 GHz) and the reception antenna has to be added. The noise figure of a satellite down converter equals 1 dB. The first mixer has a conversion loss of 6 dB. For noise calculations this mixer is modelled as a loss and thus it has a noise figure of 6 dB. Using Friis formula this results in a noise figure of 7 dB at reference plane II. It is possible to add a 30 dB low noise MMIC amplifier just before the first mixer stage, the total noise figure at the antenna wave guide output can then be reduced to about 5 dB. For further calculations the total noise figure of the receiver is taken 7 dB for the production models.

The effective temperature of the receiver at reference plane II thus equals 1163 K. The total system temperature equals

$$T_{sys} = T_{ant,II} + T_e \tag{5.33}$$

where $T_{ant,II}$ = the antenna noise temperature at the output of the wave guide and T_e = the effective receiver noise temperature.

The antenna temperature at plane II can be calculated with

$$T_{ant,II} = T_{ant,I} \cdot g_a + (1 - g_a) \cdot T_o \tag{5.34}$$

where g_a is the available gain of the wave guide.

The loss of the wave guide L_{feed} up to the converter is estimated at 0.5 dB. T_A is taken 290 K as shown in Chapter 3. From this we conclude that for this system the antenna noise temperature $T_{ant,II}$ equals 290 K. The total system temperature at plane II thus equals 1453 K.

The gain of the receiver antenna (20 cm dish) equals 36 dB (efficiency from 0.5 to 0.6). The figure of merit G/T then becomes 3.9 dB and is of course independent from the reference plane.

With the information summarized above the maximum path length is calculated and equals 5.74 km for vertical polarization and 5.33 km for the horizontal polarization. The cell radius determined by the horizontal polarization thus equals 2.87 km and its area equals 22.3 km^2.

In Table 5.3 the numerical results of the link budget are presented in tabular form.

5.3 Link budget with noise and interference

In the previous section the link budget was calculated. This resulted in a maximum cell diameter. Now we will introduce the interference as expected from Section 4 and calculate again the cell diameter. One can see directly the influence of the interference.

The CIR is assumed to be 11 dB, this is with a cross-polar discrimination of 10 dB or better. It is thus assumed that no ducting as discussed in 4 and 3.2 occurs.

Using the results of Section 5.1.3 the influence of the interference can be estimated and the equivalent extra noise is found. To achieve a QEF operation with a CIR of 11 dB the required CNR before the demodulator equals 5.7 dB. The CNR in the 36 MHz channel thus equals 4.53 dB. From this point the same procedure as in the previous section is used to find the maximum distance. The maximum cell diameter equals 5.04 km for the vertical polarization and 4.69 km for the horizontal polarization. The radius of the cell size then equals 2.35 km and its area equals 17.3 km^2.

In Table 5.4 the numerical results of the link budget are presented in tabular form.

It was assumed that no ducting occurs because of the inclination of the transmitted rays. If we take for instance the coding rate R is 1/2 then the maximum diameter size with interference was 4.69 km. Further it is also assumed that the receiver antennas are mounted at the rooftops (10 m). Then one can calculate the minimum transmitter height, this equals 51 m. It is however better to increase the antenna height to increase the inclination angle and thus make the system more robust to ducting. In Chapter 6 it will be shown that the percentage of area illuminated within the cell increases also if the height of the transmitter antenna increases.

5.4 Link budget for the feeding network

The link budget of the feeding network is calculated exactly the same as in the previous section except that an extra receiver antenna gain is used. Since the distance between two transmitters is always shorter than the maximum cell radius the extra power results in a shorter outage time due to propagation aspects.

5.5 Discussion

The CNR in the channel is 1.17 dB lower than the CNR just before the demodulator. The two interesting coding rates are 1/2 and 3/4. The minimum theoretically required CNR , to have a QEF performance, before the demodulator using a coding rate R is 1/2 equals 1.9 dB.

The interference decreases the performance of the link. An upper bound of the performance degradation due to the interference is calculated. The BER can be calculated as a function of the noise level and the interference level.

The maximum cell diameter is calculated and equals 5.33 km ($R = 1/2$) and 4.66 km ($R = 3/4$). Using the proposed semi SFN the maximum cell radius equals 4.69 km ($R = 1/2$) and 3.97 km ($R = 3/4$). Using the proposed network the area of the

cells then becomes 17.3 km^2 ($R = 1/2$) and 12.3 km^2 ($R = 3/4$). The minimum transmitter height equals 51 m ($R = 1/2$) and 44.6 m ($R = 3/4$).

Using the narrow-beam reception antennas the pointing loss is not negligible. The system noise temperature T_{sys} equals 1453 K, the figure of merit (G/T) equals 3.9 dB.

The outage time chosen here equals 0.1 % and is based on the outage time in direct broadcasting satellites. In broadcasting it is very common to have an outage time of 0.01 % or 0.03 % of the time. It is believed that for a commercial usage of an MVDS system 0.1 % outage time is acceptable.

The outage time influences the link budget dramatically of course. The link budget calculated however is just an indication and an example. Many more parameters in the link can be varied which decrease or increase the area covered.

		Rate $R = 1/2$	Rate $R = 3/4$
	Requirements		
1	Coded BER	$1 \cdot 10^{-11}$	$1 \cdot 10^{-11}$
2	Un-coded BER	$7.4 \cdot 10^{-2}$	$2.4 \cdot 10^{-2}$
3	Link availability	99.9 %	99.9 %
4	Implementation margin (M)	1 dB	1 dB
	Required CNR ratios		
5	CNR before demodulator	3.1 dB	5.9 dB
6	CNR in channel	1.9 dB	4.7 dB
	Transmitter		
7	Saturated power (P_s)	-9 dBW	-9 dBW
8	Output back-off (BO)	3 dB	3 dB
9	Radiated power (P_t)	-12 dBW	-12 dBW
10	Transmit antenna gain (G_t)	15 dBi	15 dBi
11	Transmit feed loss (L_{feed})	0.5 dB	0.5 dB
12	EIRP $= P_s - BO + G_t - L_{feed}$	2.5 dBW	2.5 dBW
	Channel		
13	Free space loss (L_{bf})	139.4 dB	138.3 dB
14	Medium loss (L_m)	0.852 dB	0.746 dB
15	Rain attenuation (L_a)	11.34 dB	10.14 dB
16	Multipath fade margin (L_f)	3.90 dB	3.59 dB
17	System loss $L_{sys} = L_{bf} + L_m + L_a + L_f$	155.5 dB	152.7 dB
	Receiver		
18	Receive antenna gain (G_r)	36 dBi	36 dBi
19	Pointing loss (L_p)	0.45 dB	0.45 dB
20	Receiver feed loss (L_{feed})	0.5 dB	0.5 dB
21	Total receiver gain $G = G_r - L_p - L_{feed}$	35.05 dB	35.05 dB
	Noise		
22	Receiver noise figure (F)	7 dB	7 dB
23	Receiver noise temperature (T_r)	1175 K	1175 K
24	Antenna noise temperature (T_a)	290 K	290 K
25	System noise temperature $T_s = T_a + T_r$	1465 K	1465 K
26	Channel noise Bandwidth (B)	75.6 dB Hz	75.6 dB Hz
27	Noise due to interference (N_i)	0 dB	0 dB
28	Boltzmann's constant ($k' = 10\log(k)$)	-228.6 dBW/K/Hz	-228.6 dBW/K/Hz
29	Noise Power $N = k' + 10\log(T_s) + B + N_i$	-121.3 dBW	-121.3 dBW
	Receive levels		
30	Faded iso. rec. level $= EIRP - M - L_{sys}$	-154 dBW	-151.2 dBW
31	Faded rec. level $= EIRP - M - L_{sys} + G$	-119 dBW	-116.2 dBW
	Coverage		
32	Path length	5.33 km	4.66 km
33	coverage area	22.3 km^2	17 km^2

Table 5.3: Link budget with noise (no interference)

		Rate $R = 1/2$	Rate $R = 3/4$
	Requirements		
1	Coded BER	$1 \cdot 10^{-11}$	$1 \cdot 10^{-11}$
2	Un-coded BER	$7.4 \cdot 10^{-2}$	$2.4 \cdot 10^{-2}$
3	Link availability	99.9 %	99.9 %
4	Implementation margin (M)	1 dB	1 dB
	Required CNR ratios		
5	CNR before demodulator	3.1 dB	5.9 dB
6	CNR in channel	1.9 dB	4.7 dB
	Transmitter		
7	Saturated power (P_s)	-9 dBW	-9 dBW
8	Output back-off (BO)	3 dB	3 dB
9	Radiated power (P_t)	-12 dBW	-12 dBW
10	Transmit antenna gain (G_t)	15 dBi	15 dBi
11	Transmit feed loss (L_{feed})	0.5 dB	0.5 dB
12	EIRP $= P_s - BO + G_t - L_{feed}$	2.5 dBW	2.5 dBW
	Channel		
13	Free space loss (L_{bf})	138.3 dB	136.9 dB
14	Medium loss (L_m)	0.75 dB	0.635 dB
15	Rain attenuation (L_a)	10.19 dB	8.85 dB
16	Multipath fade margin (L_f)	3.60 dB	3.26 dB
17	System loss $L_{sys} = L_{bf} + L_m + L_a + L_f$	152.9 dB	149.6 dB
	Receiver		
18	Receive antenna gain (G_r)	36 dBi	36 dBi
19	Pointing loss (L_p)	0.45 dB	0.45 dB
20	Receiver feed loss (L_{feed})	0.5 dB	0.5 dB
21	Total receiver gain $G = G_r - L_p - L_{feed}$	35.05 dB	35.05 dB
	Noise		
22	Receiver noise figure (F)	7 dB	7 dB
23	Receiver noise temperature (T_r)	1175 K	1175 K
24	Antenna noise temperature (T_a)	290 K	290 K
25	System noise temperature $T_s = T_a + T_r$	1465 K	1465 K
26	Channel noise Bandwidth (B)	75.6 dB Hz	75.6 dB Hz
27	Noise due to interference (N_i)	2.63 dB	3.13 dB
28	Boltzmann's constant ($k' = 10\log(k)$)	-228.6 dBW/K/Hz	-228.6 dBW/K/Hz
29	Noise Power $N = k' + 10\log(T_s) + B + N_i$	-118.7 dBW	-118.2 dBW
	Receive levels		
30	Faded iso. rec. level $= EIRP - M - L_{sys}$	-151.4 dBW	-148.1 dBW
31	Faded rec. level $= EIRP - M - L_{sys} + G$	-116.3 dBW	-113.1 dBW
	Coverage		
32	Path length	4.69 km	3.97 km
33	coverage area	17.3 km^2	12.3 km^2

Table 5.4: Link budget with noise and interference

Chapter 6

Expected coverage in a city

Now it is possible to calculate the cell size from the previous Chapter, one is very interested in the coverage within a cell (the number of homes seen). In Section 3.4 it is shown that diffraction at high frequencies is not very useful. The diffraction loss increases very rapidly if the diffraction angle increases. This means that for reception of MVDS signals there has to be a direct LOS between the transmitter and the receiver or a "semi" LOS, i.e. a LOS if one reflection on a good reflecting surface is allowed. Since one reflection attenuates the signal approximately 10 dB, it is only in a small part of the coverage area possible to make use of a reflection. The maximum path length with one reflection can be calculated with the link-budget in Chapter 5 if one takes into account an extra loss of 10 dB.

The total coverage area served for 99.9% of the time is 17.3 km^2 (maximum range is 4.69 km). If an extra attenuation of 10 dB is included (one reflection) the maximum path length reduces to 2.7 km. The reception sites who can actually make use of a reflection must have a maximum path length (reflection) of 2.7 km and furthermore there must be a good reflecting surface at the correct position and at the correct angle. This further reduces the possibilities of reception by means of a reflection. It is thus concluded that the increase in the percentage of coverage due to a reflection will be very small if not negligible.

If an MVDS operator wishes to exploit an MVDS system in a given area he wishes to predict the number of homes seen in that area. This is very interesting if not essential for MVDS operators. Using such an estimation the value of a future MVDS network can be calculated on fore-hand.

To estimate the percentage of coverage in a cell or the number of homes seen, a program has been written which predicts the possibilities of reception within a given city. The input of this program is either a deterministic presentation of the city (coordinates of buildings, heights, rotation angles, sizes) or a statistical distribution of the sizes and heights of the buildings within a city. If the statistical approach is used the program generates random but typical cities and calculates the percentage of coverage within the generated cities.

The program is in principle a 3-D ray tracing program. It tries to find from every location within the cell either a LOS or a semi LOS to the transmitter antenna. The extra percentage in coverage due to reflections can thus be very well studied with this program.

With this program it is also possible to calculate the most interesting antenna height and position of the transmit antenna, the costs of the antenna mast construction can then be compared with the value of the future MVDS network with that specific antenna height.

In Figure 6.1 the graphical presentation of part of the city of Eindhoven is shown. The circle depicts the cell with a radius of 2.5 km and the squares are the high buildings within this part of Eindhoven.

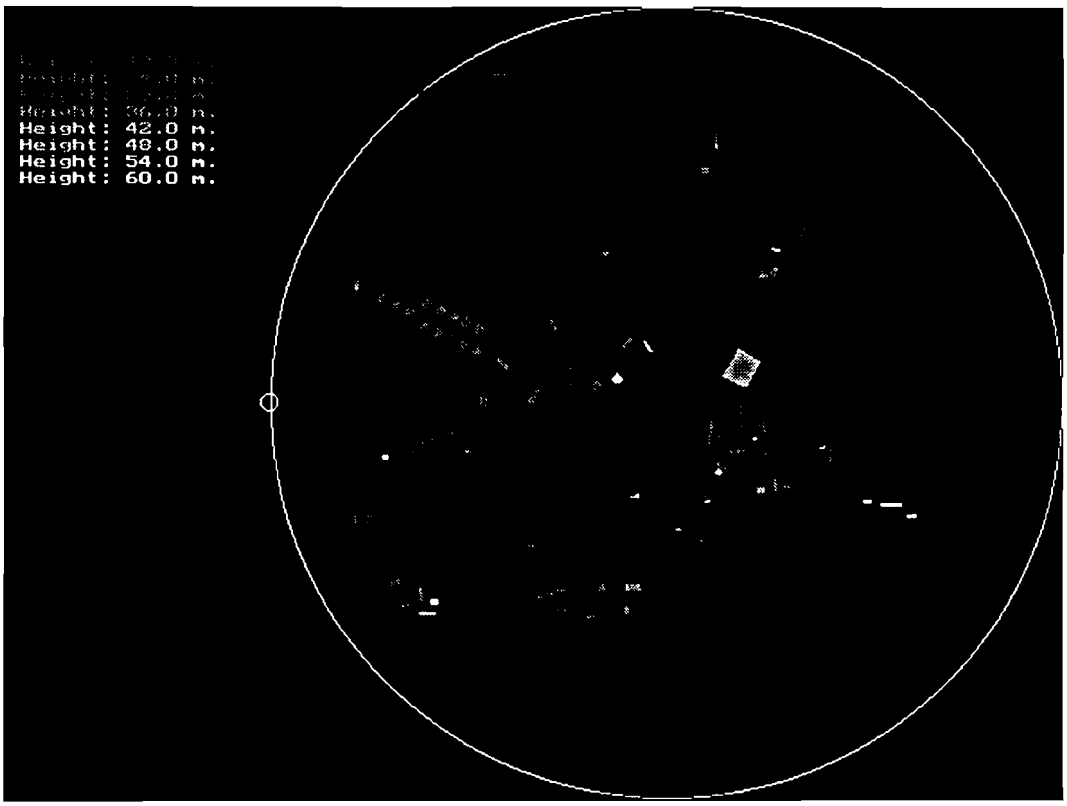

Figure 6.1: The graphical presentation of Eindhoven

The different colors of the buildings denote the height of the buildings. The transmit antenna at the NatLab building WY with a height of 65 m is positioned at the leftmost position of the cell (small circle).

We will now predict the coverage within the city of Eindhoven as an example. First we will only use the LOS and secondly also reflections will be included.

6.1 Line of sight coverage

As an example we calculate the percentage of LOS in Eindhoven. In this simulations a cell diameter of 5 km is chosen.

Figure 6.2: The output of the simulation program (Eindhoven)

In Figure 6.2 the graphical output of a simulation of the city Eindhoven without reflections is shown. In this simulation a transmitter antenna height of 65 m and a receiver antenna height of 10 m is used. The areas illuminated with the electromagnetic signal is represented by the white color and the shaded area is represented by the black color.

In Figure 6.3 the percentage LOS is shown if the transmitter antenna height would be varied.

From this figure one can see that increasing the transmit antenna height is interesting. If for instance a percentage of coverage of 80 % is required for an MVDS system to be commercially interesting a minimum height of 95 m is required.

Since the coverage area of one transmitter is small, several of these high antennas have to be placed in a city like Eindhoven. It is disputable if this is aesthetical acceptable.

To overcome this problem one could increase the transmitted power or the size of

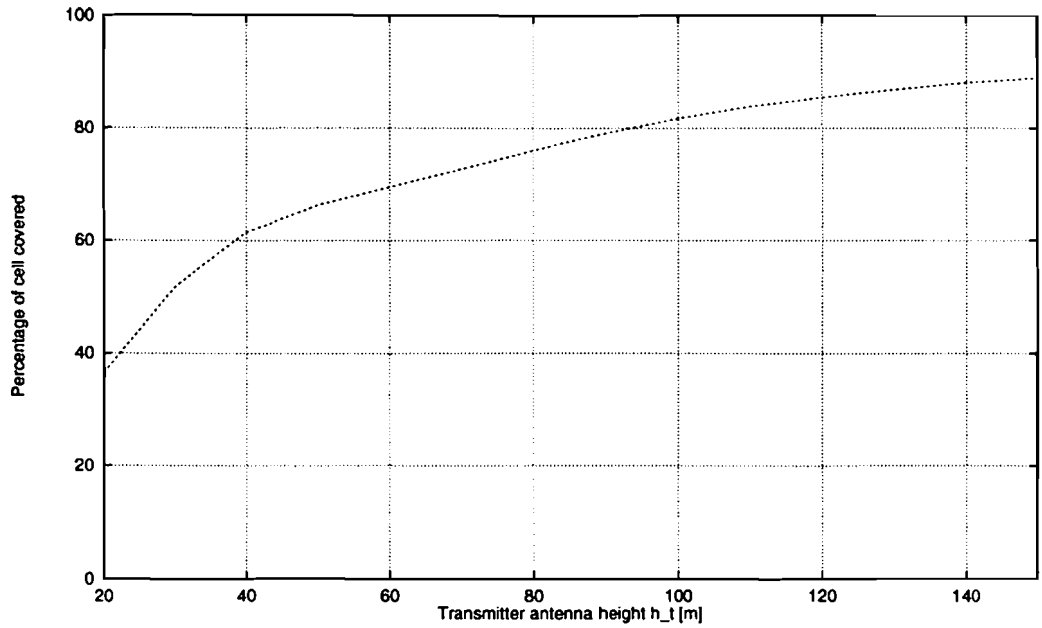

Figure 6.3: LOS as a function of the transmitter antenna height

the receiver antennas and thus increase the area covered. This reduces the number of high positioned transmit antennas in a given area. An other option is to raise the reception antennas (currently 10 m) such that the transmitter antenna can be lowered to achieve the same percentage of coverage. In Figure 6.4 the increase in coverage due to increasing the receiver antenna height is shown with a transmitter antenna height of 65 m. Both options are again aesthetical not desirable. A tradeoff of the problems mentioned above has to be made. The outcome depends very much on the environment and can be predicted with this program.

In Figure 6.5 an example is shown of a statistical approach of the simulations. In this simulation the transmitter height was 65 m and the receiver height was 10 m. The width and length of the buildings was uniformly distributed from 10 to 60 m, the height of the buildings was uniformly distributed from 20 to 65 m and a total of 90 buildings were generated. The cell diameter again equals 5 km. A number of runs have been performed and the result was an average cell coverage of 71.6 %. This statistical model is thus a usable model for the city of Eindhoven.

6.2 Coverage using reflections

Now reflections are included in the prediction program, such that the increase in the percentage of coverage can be found. In Figure 6.6 the graphical output with perfect reflections is shown. This means that the extra path length and the reflection loss is not taken into account.

The gray color in this diagram represents the area covered by means of a reflection.

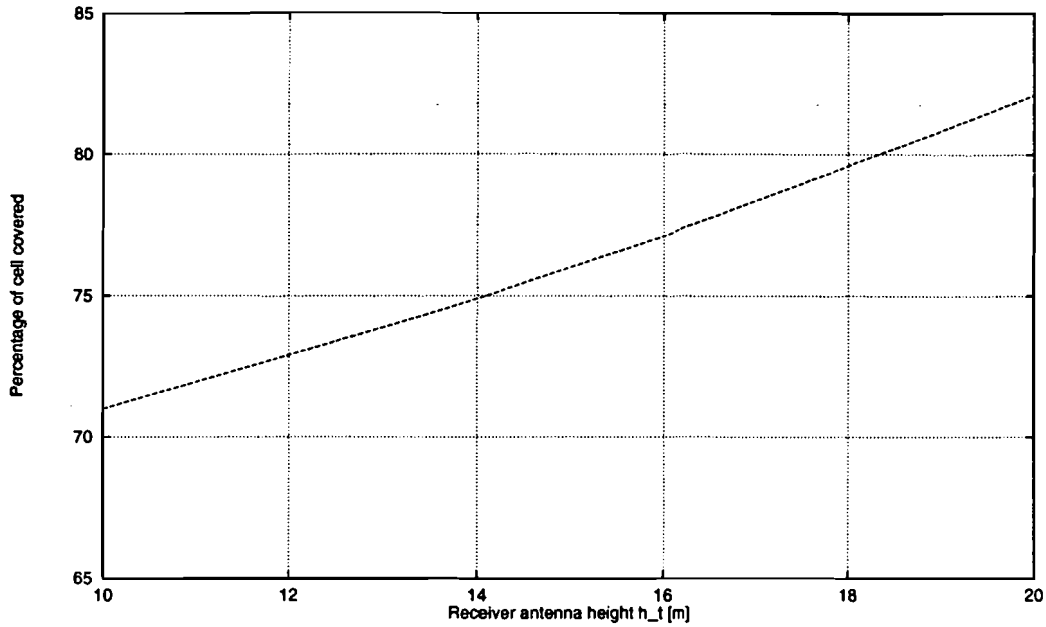

Figure 6.4: The coverage with increasing receiver antenna height

In Figure 6.7 the percentage LOS and semi LOS is shown again as a function of the transmitter antenna height. In this figure the LOS without reflections and using one reflection is shown. This is however assuming a perfect reflection. One can see that the increase in percentage of coverage, even with perfect reflections, in the city of Eindhoven is very small.

If the reflection loss is taken into account the maximum path length with one reflection becomes 2.92 km. The coverage gain due to reflections is then even smaller. This is because the relative large distance between the transmitter and the high buildings in the center of the city. In Figure 6.8 the graphical simulation result is shown and in Figure 6.9 the numerical simulation result is shown.

From this simulation it is concluded that planning service coverage relying on reflections makes no sense in the city of Eindhoven.

6.3 Discussion

It has been shown that the coverage within a city can be predicted. The difficult part is however to obtain the data of the buildings in the city. If these data are available, or alternatively the distributions of the dimensions of the buildings, it is possible to predict the coverage in a city.

The increase in coverage in a cell due to accepting one reflection can be very well studied with this program and it is concluded that it is negligible in an environment as the city of Eindhoven.

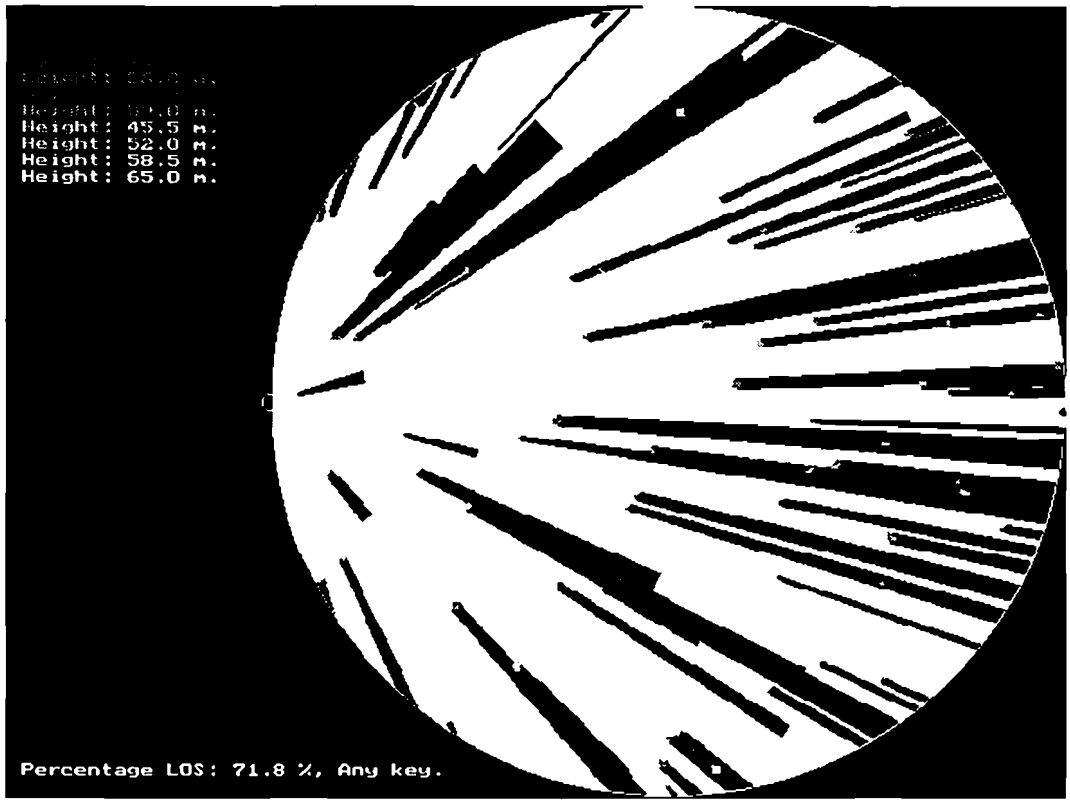

Figure 6.5: A statistical simulation

The required height of the transmitter antenna to have a cell coverage of 80 % or more equals 95 m with the reception antennas at 10 m. The coverage depends also on the height of the receive antenna. It may be more interesting to increase the receive antenna height in some areas instead of the transmit antenna.

One can see from Figure 6.2 that the transmit antenna is not positioned at the best location. It is believed that the coverage could increase if the antenna is positioned either at the north or south of the city. This is due to the orientation and location of the large buildings in the center of the city. The position chosen in the simulation is where the antenna of the test equipment was positioned (Natlab building WY).

The program can be used to estimate an acceptable antenna height based on the percentage of coverage to be expected in a specific cell. A transmitter site selection can also be supported by the output of this program.

If the dimensions of the buildings within a city are known the shaded areas can be predicted. From this and the type of buildings in a shaded area the number of homes seen can be predicted and thus the value of the network can be predicted.

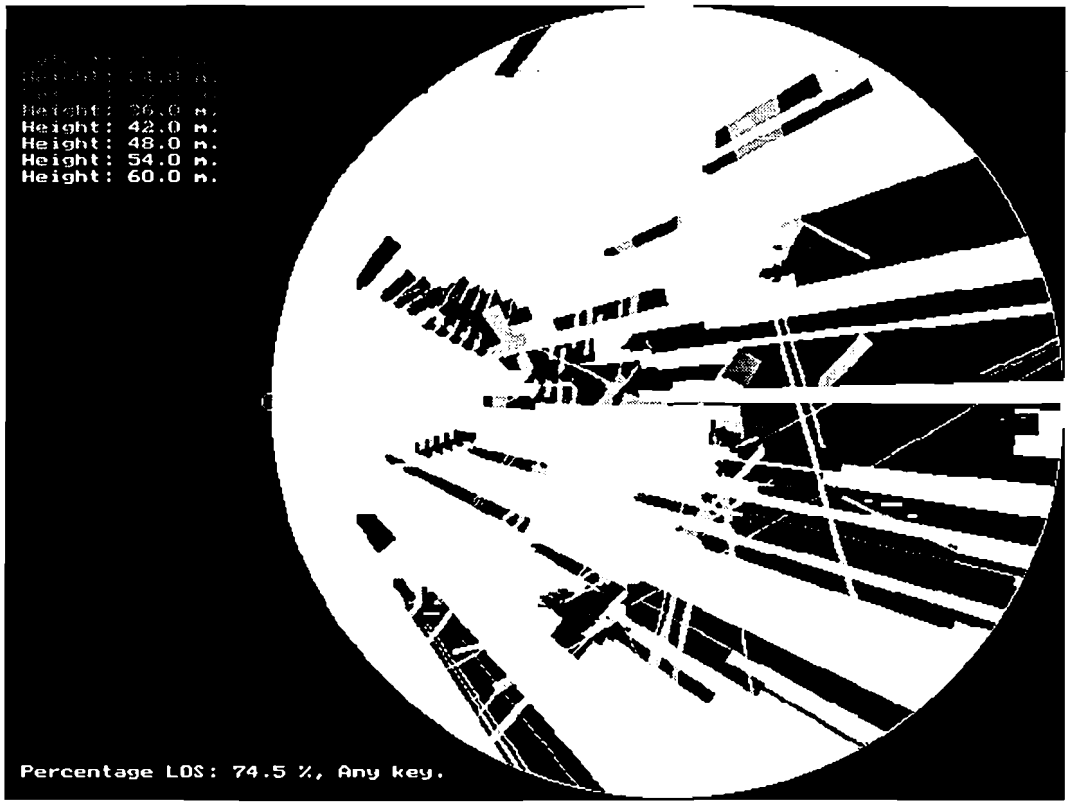

Figure 6.6: The output with perfect reflections(Eindhoven)

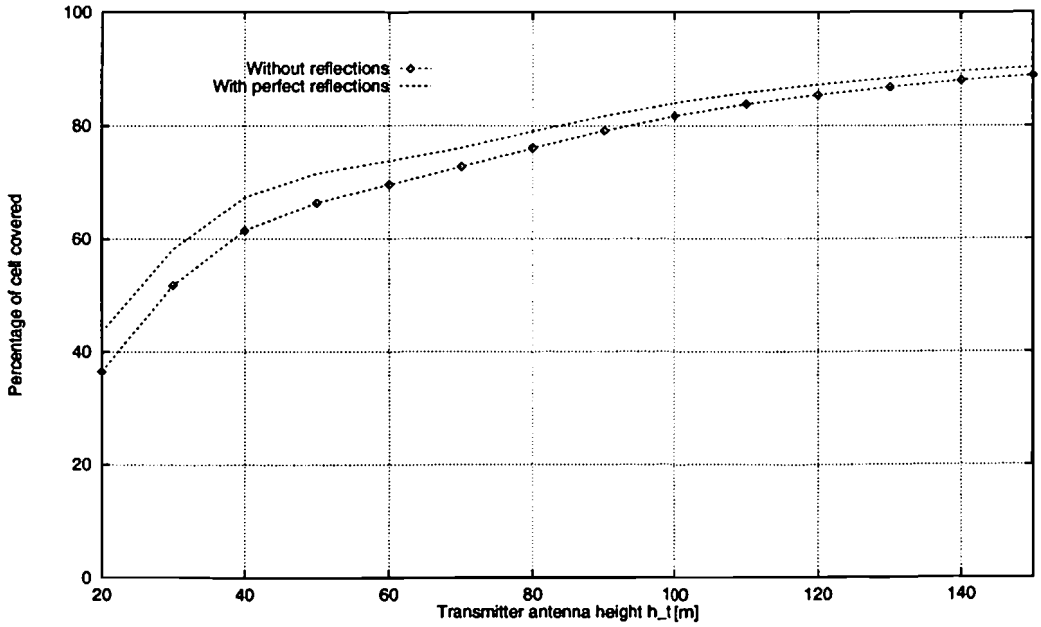

Figure 6.7: LOS as a function of the transmitter antenna height

Figure 6.8: The coverage with reflections in Eindhoven

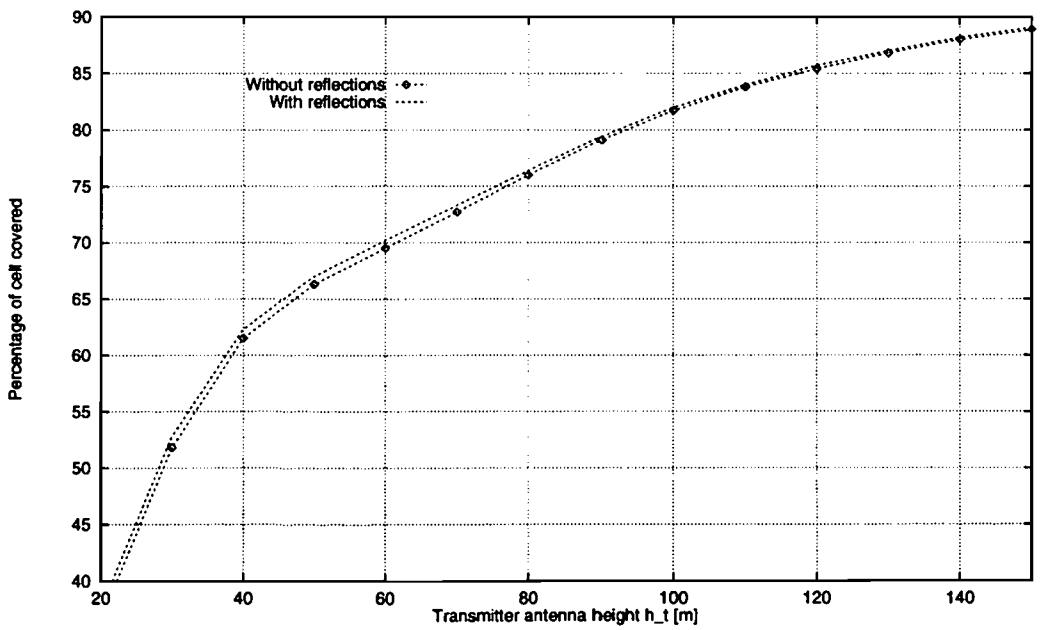

Figure 6.9: LOS with reflection as a function of the antenna height

Chapter 7

Measurements

In this Chapter, measurements are described which were performed in January 1995. The measurements were performed with the 28 GHz link as described in Appendix A. The measurements are very time consuming, therefore only a limited number of 63 measurements were performed at 37 locations. The object of the measurements therefore is to observe some phenomena rather than produce a model. The produced data are however still very interesting to confirm the theoretical models. The measurements also yield insight to the propagation aspects.

In Figure 7.1 a diagram of the measurement setup is shown.

This block diagram shows the transmitter setup as well as the receiver setup. Along the blocks the expected power level at that point in the link is given. The factor L in this diagram represent all the losses in the propagation path. The specific losses can be found in the Appendix A or report [39].

The measurements were performed to get an impression of the propagation aspects at 28GHz. The aspects of interest were:

- the possibilities of a LOS within a city.
- the attenuation if the LOS is obstructed.
- loss due to foliage.
- reflection of buildings within the city.
- reflection coefficients of building materials.
- robustness with respect to unwanted reflections.
- usefulness of diffraction around obstacles.
- depolarization of the electromagnetic waves.

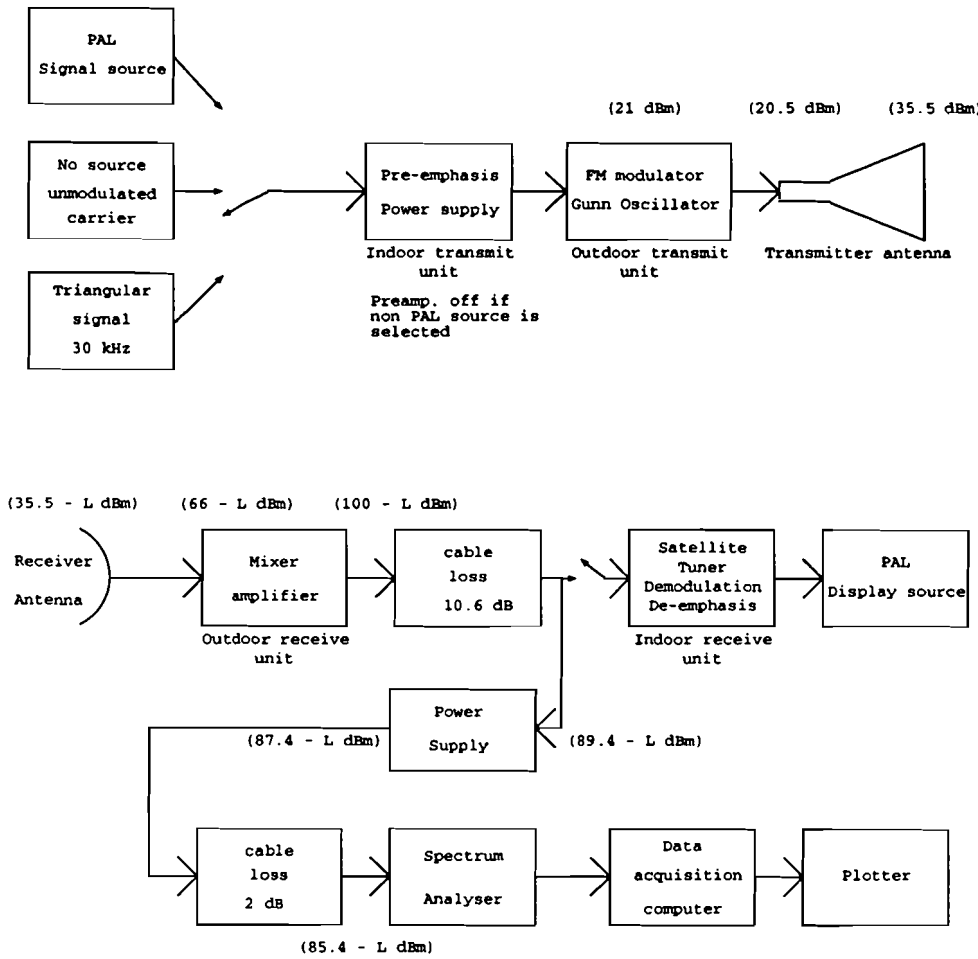

Figure 7.1: The measurement setup

In Figure 7.2 the results of the field trial are shown. The continuous line represents the expected power if the only propagation loss is the free space loss L_{bf}. The + marks represent the measured values if the link was a LOS link. The rectangles represent values measured with a known obstruction. At three places there was no reception possible these measurements are denoted with the crosses.

7.1 Link budget verification

The measurements matched the calculated link budget in report [39] very well. Therefore it is concluded that the power decreases simply according $1/r^2$. In Appendix B it was shown that indeed that it is expected that the power should decrease with $1/r^2$ instead of the $1/r^4$ often used in urban areas.

During these measurements it is shown that, as expected, a LOS is required between the transmitter and the receiver. Some obstruction can be tolerated e.g. a small

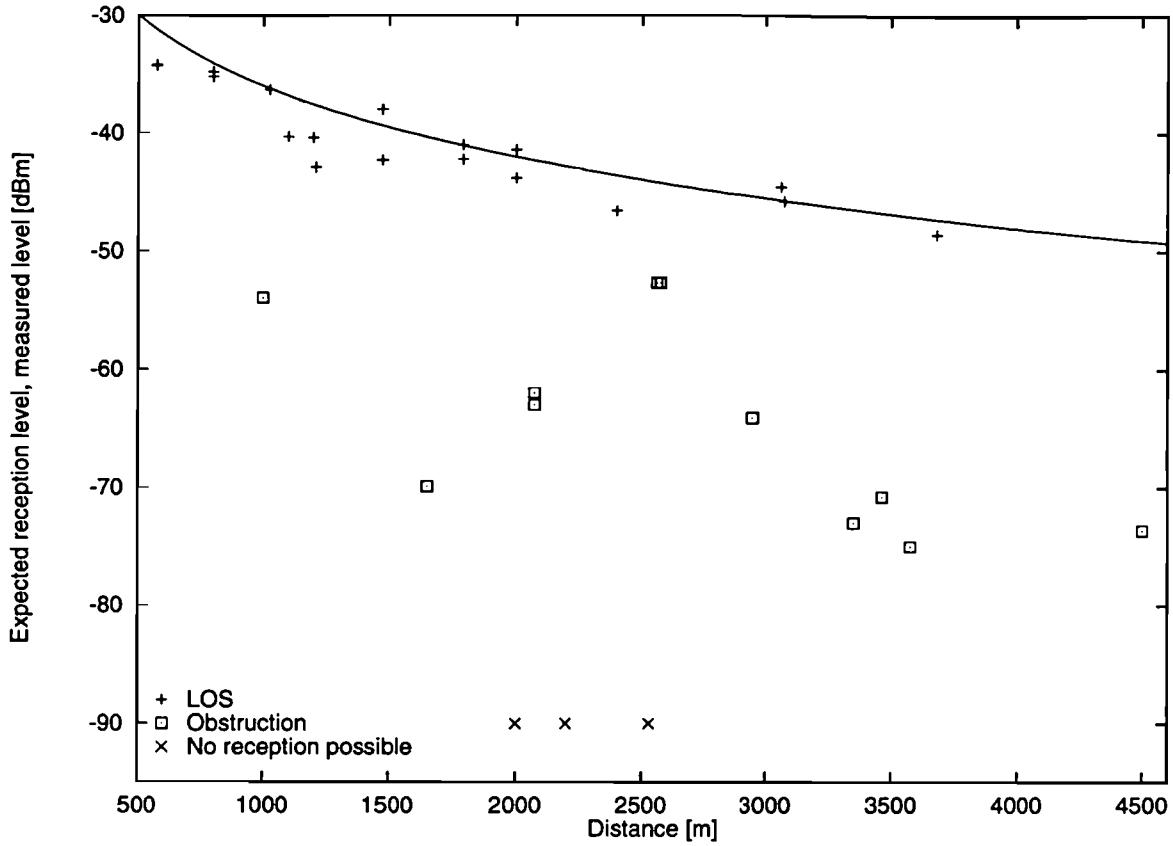

Figure 7.2: Measurement results

tree. The power decreases however very rapidly if the first Fresnel zone is not free of obstruction all over the radio path. For instance it has been found that a single tree can attenuate the received power in the order of 20 to 30 dB.

The measurements have also shown that the height of the receiver antenna should be at the rooftops of the houses. If the antenna height is reduced the percentage of sites which can receive the signal rapidly decreases.

No ducting was found, this is there were no measurements of receiving significantly more power than expected using the calculations of free space loss L_{bf}.

7.2 Reflection

The possibility of reception via a reflection has been confirmed. The measurements showed that reflection coefficients as calculated in Section 3.5 can be used.

The absolute values of the orthogonal reflection coefficients measured in a practical situation at 28 GHz are in the order of 0.2 for brick at an angle of 10 deg. and 0.3 for concrete at an angle of 20 deg. If we compare this with the Fresnel reflection coefficients it is concluded that the variance σ in the model of Beckmann would be

1.1 mm for brick and 0.92 mm for concrete. The actual values were not available.

It is concluded from measurements that in a practical environmental situation the losses from one reflection are in the order of 10 dB or more for concrete or brick.

From this information it is easy to predict at what distance effective use can be made of the a reflection under a specified angle. Within a coverage area it is possible to draw lines to which it is possible to make use of reflections. Whether the reflections can be of any use will highly depend on the layout of the coverage area. In the Netherlands for instance there are very few high buildings in comparison to ordinary houses in a city. In such a case it is believed that the extra percentages of coverage due to effectively making use of a reflection is very low. If in an other situation the city is build up of almost all tall buildings the reception by means of reflection might be the only way to have some coverage in such an area. In Chapter 6 this is simulated.

Echoes can be a severe problem in a digital link. The impulse response is therefore very important. It is obvious that the impulse response is very dependent on the environment, type of buildings etc.

In the measurements done in January some reflections have been found. In Figure 7.3 a received spectrum is shown which suffers severely from frequency selectivity due to reflections. The distance between the notches in the frequency response Δf

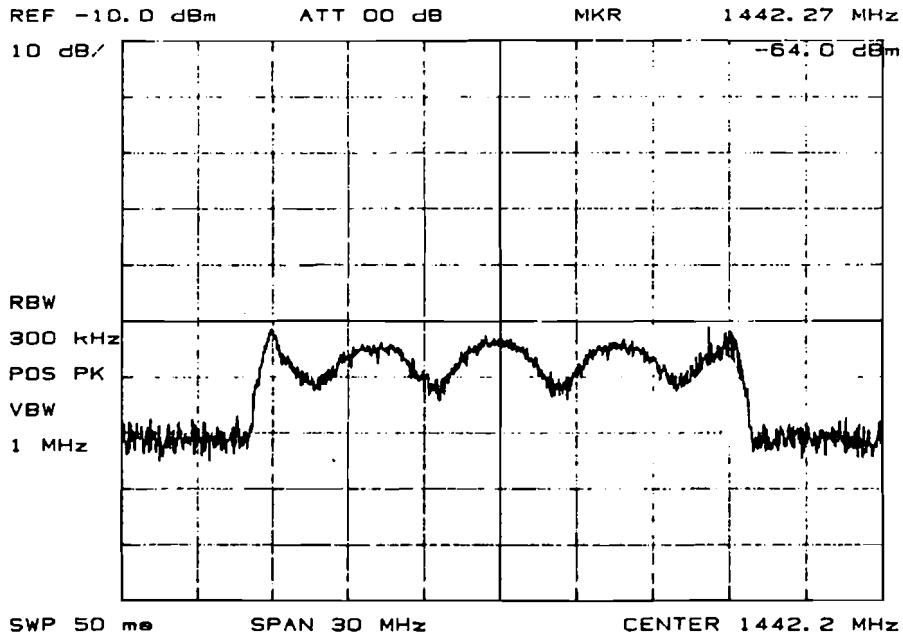

Figure 7.3: The received spectrum with multipath reception

equals 4.8 MHz. The time difference Δt between the two received signals thus equals 208 ns and the path length difference Δs equals 62.5 m. With the signalling rate of 27.5 M symbols per second this means the delay equals 5.7 symbols. From Figure 7.3 one can also estimate the CIR, this is approximately 6.4 dB. In Chapter 4 we

have seen that this level of interference is unacceptable. Since the two signals are correlated this could be solved with an equalizer however.

Figure 7.3 was found after mispointing the receive antenna on purpose. It has also been shown however that at every location measured the received spectrum was completely free of frequency selectivity if the antenna was correctly positioned. In Figure 7.4 the spectrum is shown measured at the same location as in Figure 7.3 but with the antenna aligned correctly. It is therefore concluded that in an environment

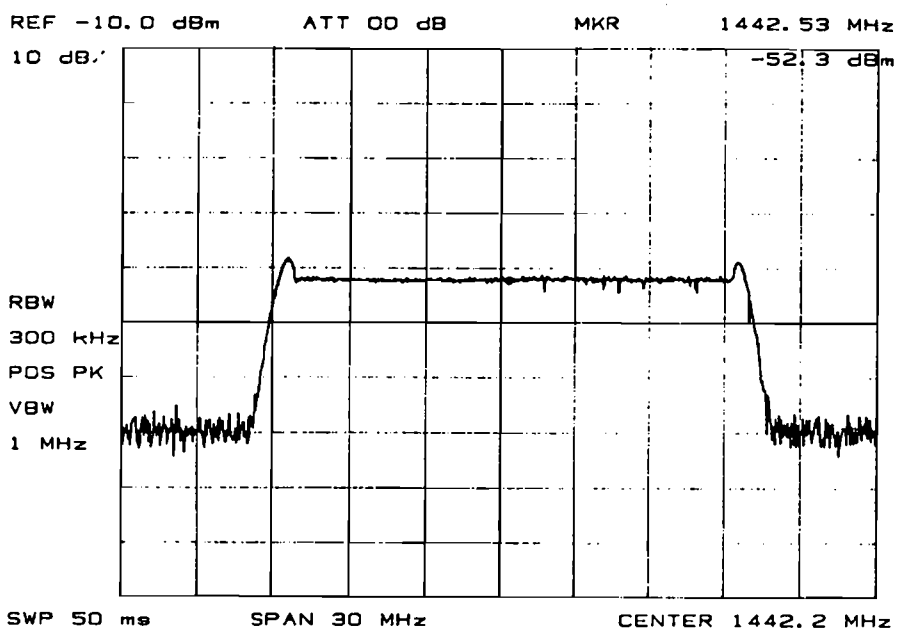

Figure 7.4: The received spectrum without multipath reception

as the Netherlands, a very small number of tall buildings and no mountains, the problem of reflection can be solved if the antenna has a high directivity (±5 degrees or less). In such a case the impulse response of the link should be no problem.

The reflection losses found were in the range of 7.5dB to 13.5 dB which yield a reflectivity R of approximately 0.04 to 0.18.

where the reflectivity R is defined as

$$R = |\rho|^2 \tag{7.1}$$

In this relation ρ is the reflection coefficient if the incident angle θ_i is 0 (orthogonal).

If one excepts the difficulties in aligning the antenna it is very interesting to increase the antenna directivity to increase the gain, reduce the amount interference received and acquire a flat spectrum.

7.3 Diffraction

Some experiments have been performed trying to measure if reception via diffraction is possible. In Appendix D it is shown that it is expected that the received power drops rapidly if there is any form of obstruction. Reception by means of a diffraction link should be possible with very low diffraction angles. It hasn't been possible to have an acceptable reception based on diffraction. This was due to the very instable signal which is due to movement of the antenna in the test setup.

7.4 Depolarization

In Section 3.10 it is predicted that the cross-polar discrimination should be of no problem. However only the depolarization of the medium is taken into account. One measurement has been performed on a LOS link of 3.68 km to check the cross-polar discrimination. The value found was 15 dB. This is much less as the predicted value. This low cross-polar discrimination is due to the cross-polar of both the receiver and the transmitter antennas. If for instance both antennas have a cross-polar discrimination of 21 dB the total cross-polar discrimination ends up 15 dB. A high quality antenna however can achieve for instance 30 dB or more. This results in a total cross-polar discrimination of better than 24 dB. Since in Chapter 4 a cross-polar discrimination of 10 dB is assumed it is concluded that the cross-polar discrimination of the antennas is no problem.

7.5 Discussion

The 28 GHz link budget calculated has been checked and found to be accurate. The received power is proportional to $1/d^2$ in an urban area using these high frequencies.

The loss due to foliage is very high, a single tree attenuates the signal in the order of 20 to 30 dB.

Rooftop reception is required to have a LOS. Reflections can be used, the loss from one reflection is in the order of 10 dB.

Due to the directivity of the reception antenna it was always possible to acquire a flat spectrum, no multipath reception.

Making effective use of diffraction was not possible with the used frequency.

The cross-polar discrimination is no problem if the proposed network is used.

No ducting has been measured.

Chapter 8

Conclusions and recommendations

In this Chapter some conclusions and recommendations are given with respect to the work carried out and the future MVDS system.

8.1 Conclusions

The future MVDS system will be a digital system based on the Digital Video Broadcasting (DVB) satellite standard. This results in a relatively inexpensive solution for digital MVDS. The modulation used is non differential QPSK-modulation with forward error correction (FEC) consisting of concatenated coding of Reed-Solomon outer coding and convolutional inner coding. Raised cosine filtering is used with a roll-off factor of 0.35.

The Fresnel zone clearance cl can be easily met if there is a LOS. The influence of the varying k-factor is negligible due to the short distances. Diffraction around buildings can't be used on these high frequencies. Reflections however can be used, the power lost on one reflection is in the order of 10 dB. This is due to the rough surfaces of building materials.

The antenna decoupling is no problem because of the short distances used. The problem of ducting can be avoided if the angle of inclination of the LOS link is kept larger than 0.5 deg. and a minimum of power is transmitted between -0.5 deg. and 0.5 deg. inclination.

The cross-polar discrimination is determined by the transmit and receive antennas and is thus of no problem since we only require a total cross-polar discrimination XPD of more than 10 dB.

The antenna temperature of the receiver is assumed to be 290 K and not depending on weather conditions due to the low elevation of the antenna.

Using the narrow-beam reception antennas the pointing loss is not negligible. The system noise temperature T_{sys} equals 1453 K, the figure of merit (G/T) equals 3.9

dB.

Because of the transmit power limitations (linear amplification) and the large propagation losses it is necessary to use multiple cells to cover a larger area. This results in interference between the different cells if a Single Frequency Network is used.

Some networks have been suggested and their CIR ratios have been calculated. A semi SFN is proposed which makes use of both polarizations and has a CIR of 11 dB assuming a cross-polar discrimination of 10 dB or more.

The interference decreases the performance of the link. An upper bound of the performance degradation due to the interference is calculated. The BER can be calculated as a function of the noise level and the interference level.

Three different schemes of feeding the network are discussed, feeding by cable, feeding by satellite and mutual feeding.

The CNR in the channel is 1.17 dB lower than the CNR just before the demodulator. The two interesting coding rates are 1/2 and 3/4. The minimum theoretically required CNR , to have a QEF performance, before the demodulator using a coding rate $R = 1/2$ equals 1.9 dB.

The maximum cell diameter is calculated and equals 5.33 km ($R = 1/2$) and 4.66 km ($R = 3/4$). Using the proposed semi SFN the maximum cell radius equals 4.69 km ($R = 1/2$) and 3.97 km ($R = 3/4$). Using the proposed network the area of the cells then becomes 17.3 km^2 ($R = 1/2$) and 12.3 km^2 ($R = 3/4$). The minimum transmitter height equals 51 m ($R = 1/2$) and 44.6 m ($R = 3/4$).

It has been shown that the coverage within a city can be predicted. The difficult part is however to obtain the data of the buildings in the city. If these data are available, or alternatively the distributions of the dimensions of the buildings, it is possible to predict the coverage in a city.

The increase in coverage in a cell due to accepting one reflection can be very well studied with the simulation program and it is concluded that it is negligible in an environment as the city of Eindhoven.

The required height of the transmit antenna to have a cell coverage of 80 % or more equals 95 m with the reception antennas at 10 m. The coverage depends also on the height of the receive antenna. It may be more interesting to increase the receive antenna height in some areas instead of the transmit antenna.

The simulation program can be used to estimate an acceptable antenna height based on the percentage of coverage to be expected in a specific cell. A transmitter site selection can also be supported by the the simulation program.

The 28 GHz link budget calculated has been checked and found to be accurate. It is found that the power decreases proportional to $1/d^2$ in an urban area using these high frequencies.

The loss due to foliage is tremendous, a single tree attenuates the signal in the order

of 20 to 30 dB.

Rooftop reception is required to have a LOS. Reflections can be used, the loss from one reflection is in the order of 10 dB.

Due to the selectivity of the reception antenna it was always possible to acquire a flat spectrum, no multipath reception.

To measure the effective use of diffraction was not possible with the used frequency due to the unstable antenna construction.

The cross-polar discrimination is no problem if the proposed network is used.

A future digital MVDS system proposed can approximately carry 48 channels (a channel spacing of 41.6 MHz is assumed) in the 40.5-42.5 GHz band. In one channel 25 Mb/s (R is 1/2) or 38 Mb/s (R is 3/4) can be transmitted. This means that the MVDS system can provide 240 programs (R is 1/2) or 336 programs (R is 3/4).

8.2 Recommendations

To acquire a good model for terrestrial propagation of 42 GHz spherical electromagnetic waves over an urban area, measurements must be performed. These channel measurements should lead to a model for instance for fading. Since the nature of the reflections determine the channel, Rayleigh or Ricean, the reflection on building materials needs to be further examined. The statistics of multipath fading and ducting at 42 GHz has to be thoroughly examined. For instance it is interesting if stratified conditions occur which can cause ducting together with precipitation. With good models, the attenuation etc. can be predicted on fore-hand given the type of area to be covered.

In this report an analytical estimation was performed of the influence of the interference on the BER using QPSK modulation. This analysis must be improved to acquire a more tight upper bound as done by [35, 33, 29]. The authors mentioned, however have only found a good upper bound for high CNR. For this application a bound is required for low CNR and thus high BER before decoding. The nature of the errors using such a low CNR might change because the carrier recovery and the clock recovery circuits become a problem at very low CNRs. This means that research has to be done to examine the performance of the different recovery algorithms using the low CNR.

If one takes a look at the area to be covered, and the transmit height and the receive height one can see that a symmetrical gain pattern in the vertical direction is not the best solution. In Figure 8.1 a more efficient antenna diagram is depicted. This pattern could be approximated with a cosecant-squared antenna [36]. Most of the electromagnetic energy is directed to the edge of the cell. A null in the gain pattern at an elevation of 0 deg. reduces the interference for the adjacent cell and can reduce the probability of ducting.

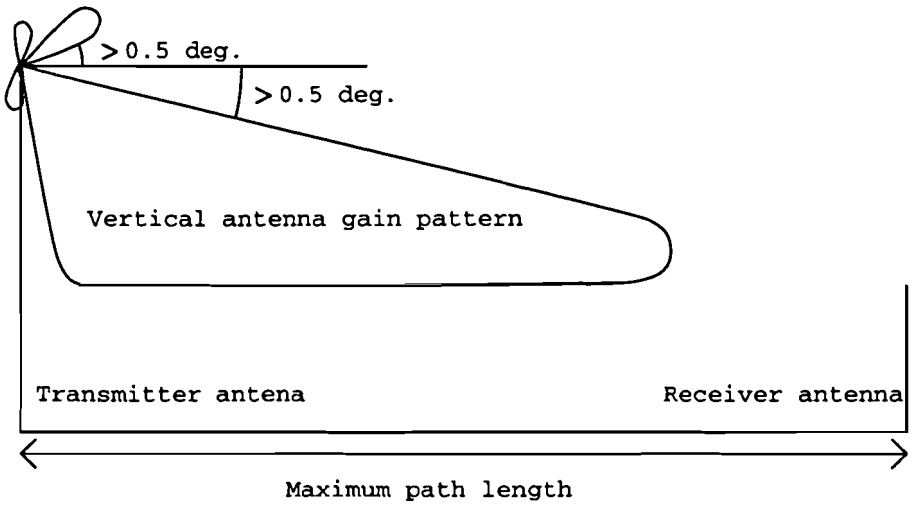

Figure 8.1: A more efficient antenna diagram

It is interesting to increase the antenna directivity since firstly it increases the antenna gain and secondly the system becomes more robust to multipath reception. The installation of the receive antenna however becomes more complicated, the antenna becomes larger and antenna decoupling can become a problem. Another issue is that the receive antenna should be as small as possible for aesthetical reasons. A good trade-off has to be made between the phenomena discussed above.

Chapter 9

Acknowledgements

The author would like to thank all the people who have helped carrying out this research work and writing this report. Thanks especially to Ir. P.G.M. de Bot for coaching and giving technical assistance. Thanks also to Prof. Dr. Ir. G. Brussaard and Ir. J. Dijk from the Eindhoven University of Technology for their assistance in and coaching of this graduation project. The author would like to thank W.J. van Houtum and ir. H. L. Vermeer for their extensive support in the field trials carried out for this research project.

Further the author likes to thank Mr. I. Clarke from Philips Microwave for providing technical information and support.

Bibliography

[1] Strawman specification for digital terrestrial television, March 1995. Draft.

[2] J.C. Arnbak, J. Dijk, M.H.A.J. Herben, and J.T.A. Neessen. *Radio en radar.* Eindhoven University of Technology, Eindhoven, The Netherlands, 1993. Lecture Notes Nr.: 5653.

[3] J.C. Arnbak and W. van Blitterswijk. Capacity of slotted ALOHA in rayleigh-fading channels. *IEEE Journal on Selected Areas in Communications*, SAC-5(2):261–269, February 1987.

[4] P. Beckmann. *Scattering of electromagnetic waves from rough surfaces.* Artech House, Inc., Norwood, 1987.

[5] J. Borish. Self contained Crosscorrelation Program for Maximum-length Sequences. *J. Audio Eng. Soc.*, 33(11):888–891, 1985.

[6] G. Brussaard. A meteorological model for rain-induced cross-polarization. *IEEE Trans. Antennas and Propagation*, AP-24:5–11, January 1976.

[7] J.B. Cain, G.C. Clark, and J.M. Geist. Punctured convolutional codes of rate $(n-1)/n$ and simplified maximum likelihood decoding. *IEEE Trans. Information Theory*, IT-25(1):97–100, January 1979.

[8] T.S. Chu. Rain induced cross-polarization at centimeter and millimeter wavelengths. *Bell Systems Technical Journal*, 53(8):1557–1579, October 1974.

[9] Commission of the European Communities. *Influence of the atmosphere on interference between radio communication systems at frequencies above 1 GHz.* Commission of the European Communities, Luxembourg, 1990.

[10] L. M. Correia and P. O. Françês. Estimation of materials characteristics from power measurements at 60 GHz. In *Proc. PIMRC 94 Wireless Networks*, The Hague, September 1994.

[11] Robert K. Crane. Prediction of attenuation by rain. *IEEE Communications Magazine*, 28(9):1717–1732, September 1980.

[12] J. Dijk, M.H.A.J. Herben, and E.J. Maanders. *Antennes en propagatie.* Eindhoven University of Technology, Eindhoven, The Netherlands, 1987. Lecture Notes Nr.::

[13] Digital Video Broadcasting DVB. Background documents on digital video broadcasting. April 1994.

[14] EBU/ETSI. Digital broadcasting systems for television, sound and data services; Framing structure, channel coding and modulation for 11/12 GHz satellite services. *European Telecommunication Standard*, August 1994. Draft prETS 300 421.

[15] Roger L. Freeman. *Radio system design for telecommunications (1-100GHz).* Wiley, New York NY, 1987.

[16] Roger L. Freeman. *Reference manual for telecommunications engineering.* Wiley, New York NY, 1994.

[17] T. h. Scharten. *Elektromagnetisme.* Eindhoven University of Technology, Eindhoven, The Netherlands, 1992. Lecture Notes Nr.: 5757.

[18] T.T. Ha. *Digital Satellite Communications.* McGraw-Hill, New York NY, 1986.

[19] S. Heeralall and C.J. Hughes. High capacity cellular patterns for land mobile radio systems using directional antennas. *Proc. IEE, Part I*, 136(1):75–80, February 1989.

[20] ITU-R. *Propagation in non-ionized media*, volume V. ITU-R, 1978.

[21] ITU-R. *Propagation in non-ionized media*, volume V. ITU-R, 1986.

[22] ITU-R. *Propagation in non-ionized media*, volume V. ITU-R, 1990.

[23] ITU-R. *CCIR RECOMMENDATIONS New and revised as of 8 October 1992*, volume V. ITU-R, 1992.

[24] B. Langen, G. Lober, and W. Herzig. Reflection and transmission behaviour of building materials at 60 GHz. In *Proc. PIMRC 94 Wireless Networks*, The Hague, September 1994.

[25] E.A. Lee and D.G. Messerschmitt. *Digital communication.* Kluwer Acadamic Publishers, Boston, 1994.

[26] W.C.Y. Lee. Spectrum efficiency in cellular. *IEEE Transactions on Vehicular Technology*, 38(2):69–75, 1989.

[27] W.C.Y. Lee. *Mobile communications design fundamentals.* Wiley, NY, 1993.

[28] S. H. Lin. Emperical rain attenuation model for earth-satellite paths. *IEEE Communications Magazine*, 27(5):812–817, May 1979.

[29] V.K. Prabhu. Error Rate Considerations for Coherent Phase-Shift Keyed Systems with Co-Channel Interference. *Bell Systems Technical Journal*, 48:743–767, March 1969.

[30] J.G. Proakis. *Digital Communications.* McGraw-Hill, Singapore, second edition, 1989.

[31] Qualcomm. Q1650 K=7 multi code rate Viterbi decoder, December 1991. Technical data sheet of the Qalcomm Q1650.

[32] P. L. Rice and N. R. Holmberg. Cumulative time statistics of surface point-rainfall rates. *IEEE Communications Magazine*, 21(10):1131–1136, October 1973.

[33] A.S. Rosenbaum and F.E. Glave. An Error-Probability Upper Bound for Coherent Phase-Shift Keying with Peak-Limited Interference. *IEEE Trans. Communications*, 22:6–16, January 1974.

[34] J. Sarnecki and C. Vinodrai et. al. Microcellular design principles. *IEEE Communications Magazine*, 31(4):76–82, April 1993.

[35] O. Shimbo and R. Fang. Effects of cochannel interference and gaussian noise in m-ary psk systems. *IEEE Trans. Communications*, COM-21(10):1108–1115, October 1973.

[36] M.I. Skolnik. *Introduction to radar systems.* McGraw-Hill, New York NY, 1980.

[37] British Telecommunications. 29 GHz terrestrial microwave systems for satellite services. ss6003.

[38] W. v. Houtum. Digital transmission scheme for terrestrial tv, based on the european transmission standard for digital cable tv. Technical report, Philips Research Laboratories Eindhoven, Eindhoven, The Netherlands, January 1995.

[39] J. Vugts. Multipoint video distribution system test setup at philips research eindhoven. Technical Report 326, Philips Research Laboratories Eindhoven, Eindhoven, The Netherlands, November 1994.

[40] S. Wang and S.S. Rappaport. Signal to interference calculations for corner-excited cellular communications systems. *IEEE Trans. Communications*, 39(12):1886–1895, December 1991.

[41] J.M. Wozencraft and I.M. Jacobs. *Principles of Communication Engineering.* Wiley, New York NY, 1965.

Appendix A

Analog system description

A.1 Indoor transmit unit

The indoor transmit unit consists mainly of three parts, power supply unit, cable equalization circuitry and the pre-emphasis.

The power supply supplies several dc voltages for the transmitter outdoor unit and monitors the dc voltages at the outdoor unit. The different supplies are for the varactor offset, the video amplifiers and the gun oscillator in the outdoor unit.

The cable equalization circuitry provides high frequency tilt to compensate for the attenuation within coax cable from the indoor unit to the outdoor unit. This is externally adjustable to adapt to the cable length used.

Since the modulation currently used is FM it is common to use pre-emphasis. This will yield a higher signal-to-noise ratio at the receiver. The actual curve used is found in the recommendation report CCIR 405-1 curve B (625 lines) and shown in Figure A.1.

Figure A.1: Base band pre-emphasis

A.2 Outdoor transmit unit

The outdoor transmit unit consists of a voltage controlled gun oscillator with active internal temperature control, a video amplifier and a power supply unit. The FM-sweep (peak-peak) can be adjusted between 10 MHz and 25 MHz. The free running gun oscillator is directly modulated (varactor-tuned).

Because of the inherent instability of the gun oscillator, a channel spacing of 38.4 MHz is required.

The output power of the unit is typical 125 mW (21 dBm). This however depends on the temperature. The output power guaranteed within the range of 19 dBm to 26 dBm [37].

A.3 Transmitter antenna

Traditionally omni-directional antennas are used for broadcasting services. However sectorial antennas seem to be more suitable for this application. Omni-directional antennas are very difficult to implement in the millimeter wave region. Sectorhorn antennas can have a near circular coverage area as well. An omni-directional antenna has to be positioned near the center of the cell whereas the sectorial antenna can be placed on the fringe off the cell as shown in Figure A.2.

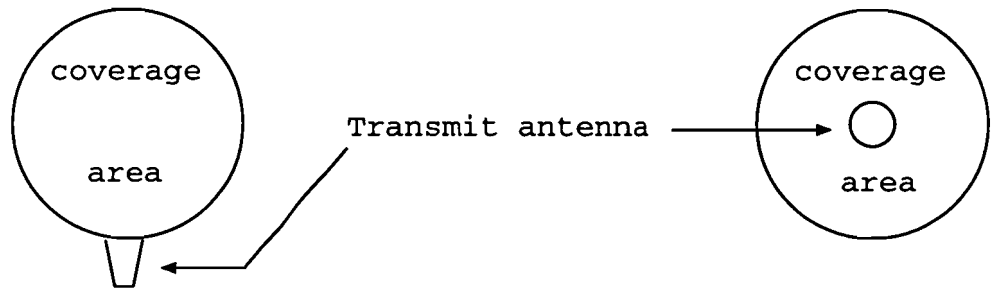

Figure A.2: Antennas related to there coverage area

Another major advantage is that the gain difference between the front and the back of the antenna is already more than 30 dB. This can be very well exploited in single frequency networks where discrimination between different transmitted signals is very important. With such an antenna the opening angle is much smaller and thus less power from unwanted signals will be received.

The sector horn antennas are cheap, so more antennas at the transmit site can be used. It is then possible to use more than one transmitter on one site for the different channels. In this way the transmitter back off can be increased and thus intermodulation problems are reduced. The problem of the output power restrictions then becomes less severe.

The used sector horn has a nearly circular coverage. This is the case if loss due to rain and absorption is included and the coverage area is defined as the area which can be served for 99.9% of the time. In figure A.3 the circularity of the coverage area due to attenuation by rain is shown.

The antenna has a 3 dB horizontal beam width $\Delta_1 = 64$ deg. and a 3 dB vertical beam width $\Delta_2 = 10$ deg. as can be seen in Figure A.5 and Figure A.6. In Figure A.4 a drawing of the sectorhorn is shown.

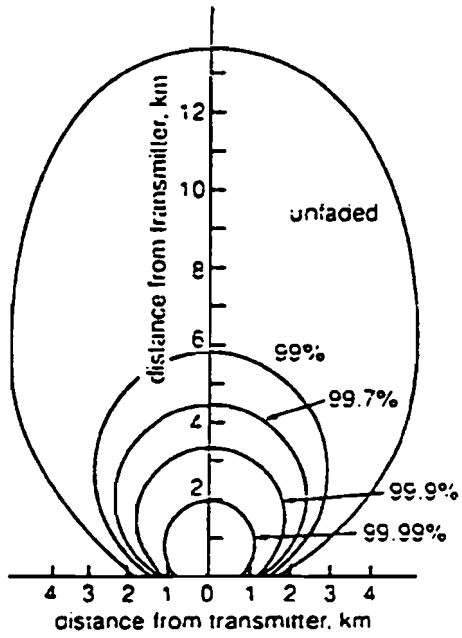

Figure A.3: Variation of coverage area with availability for a specific situation

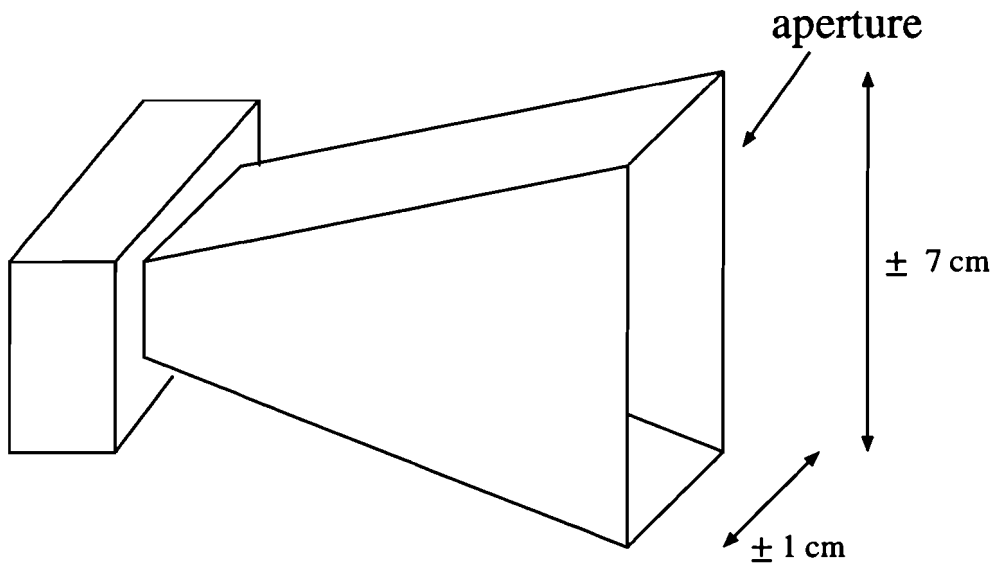

Figure A.4: The sectorhorn transmitter antenna

The isotropic transmitter antenna gain G in dB can be estimated by [2]

$$G_{\mathrm{dB_i}} = 10 \log \left(\frac{27000}{\Delta_1 \cdot \Delta_2} \right) \approx 16_{\mathrm{dB_i}} \tag{A.1}$$

The specified antenna gain is however 15 dBi.

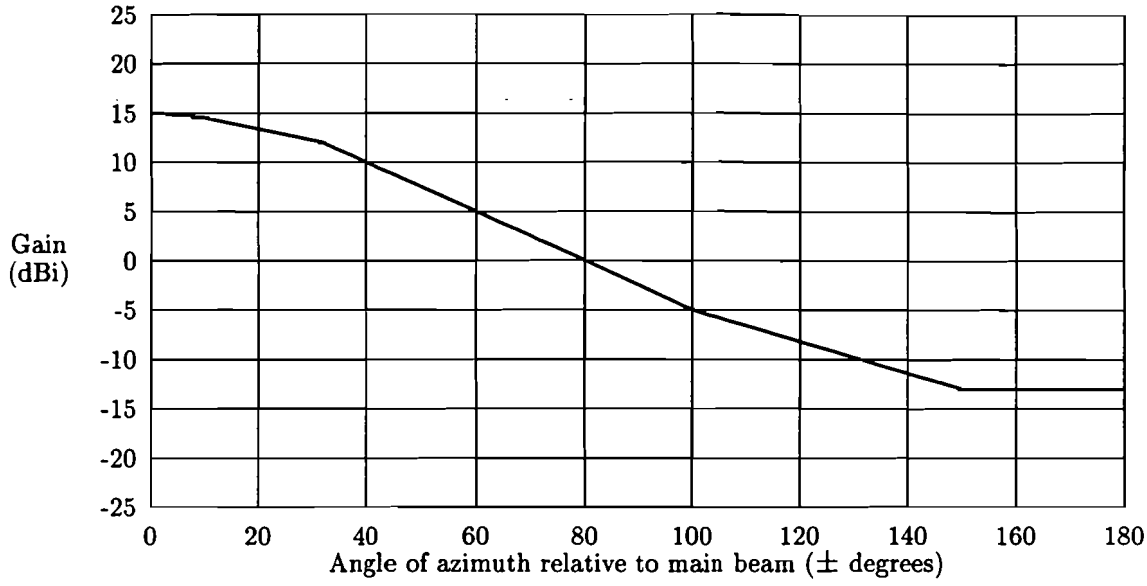

Figure A.5: Transmitter antenna gain (64/10 deg. horn) azimuth

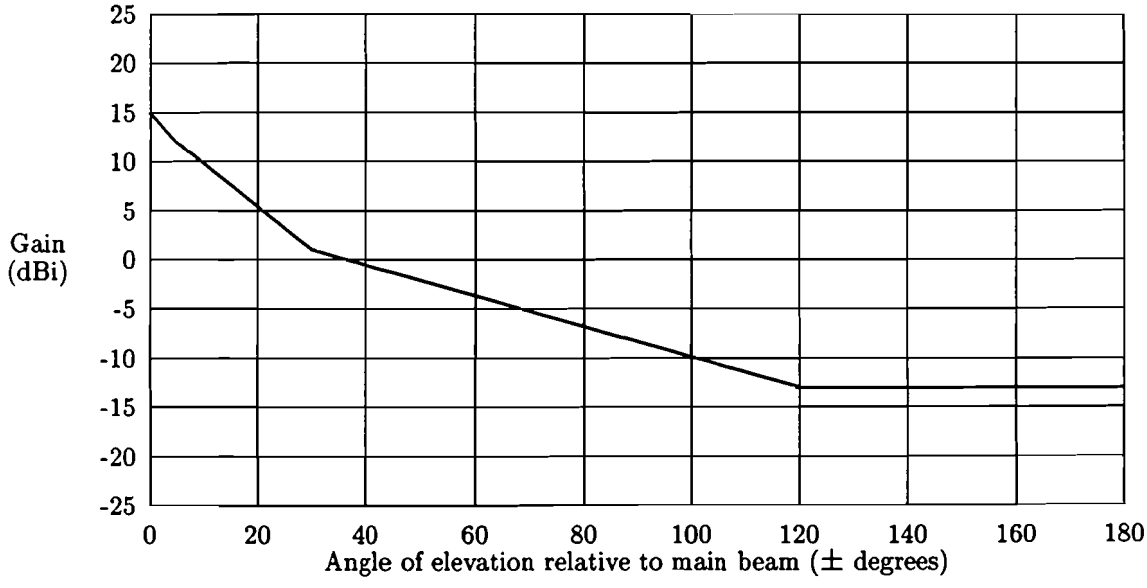

Figure A.6: Transmitter antenna gain (64/10 deg. horn) elevation

A.4 Receiver antenna

The receiver antenna plays an important role in the link. First of all its gain directly contributes to the link budget. Secondly, its directivity prevents interference from co-channel transmitters in adjacent cells. If the receiver antenna has a narrow beam width and is pointed to the transmitter there is already much discrimination between

the signals of the different transmitters.

A larger antenna increases the antenna gain, however the loss due to incorrect positioning of the antenna also increases. This means that wind gusts may play a role or the supporting construction becomes complicated, neither of these issues being very attractive. Another issue is that the antenna should be as small as possible for aesthetical reasons. A smaller antenna however makes a receiving set more expensive because the coverage area becomes smaller, and thus the number of receivers per transmitter becomes smaller or the noise figure has to be decreased. The smaller the antenna, the cheaper the mechanical support construction is. Thus the installation of the antenna becomes less complicated.

The antenna size must be based on some kind of trade off of the factors discussed above.

The antenna gain g_r can be calculated with

$$g_r = \eta \left(\frac{\pi D}{\lambda}\right)^2 \tag{A.2}$$

where η is the efficiency, D is the antenna diameter (m) and λ is the wavelength (m).

The antenna efficiency is taken to be approximately 0.65. This number is estimated on common antenna parameters [11]. This yields in an antenna gain of 31 dBi at 28 GHz ($\lambda = 10.7$ mm) and a diameter $D = 0.15$ m.

For small angles θ, referring to the main beam, the antenna gain pattern can be approximated with a parabolic function. An antenna gain pattern $G(\theta)$ for a parabolic dish can then be approximated by

$$G(\theta)_{\mathrm{dB}} = \left(G(0) - 3\left(\frac{\theta}{\frac{1}{2}\cdot\theta_{3\mathrm{dB}}}\right)^2\right)_{\mathrm{dB}} \tag{A.3}$$

where θ_{3dB} is the 3 dB beamwidth which can be calculated with [11] (parabolic).

$$\theta_{3\mathrm{dB}} = \frac{72.7\cdot\lambda}{D} \tag{A.4}$$

where

D = antenna diameter (m)
λ = the wavelength (m).

If the antenna is misaligned by installation or due to the wind, the main lobe will not be pointed exactly to the transmitter. This results in a pointing loss. With $d = 0.15$ m and $\lambda = 10.7$ mm, we get a beam width θ_{3dB} of approximately 5 deg. With formula A.3 the pointing loss can be determined. For small pointing deviations of the antenna the loss will be very low or negligible.

A.5 Outdoor receive unit

The outdoor receive unit consists of 5 parts, the RF band pass filter, local oscillator, the mixer, IF amplifier and a power supply. In Figure A.7 the block diagram is shown.

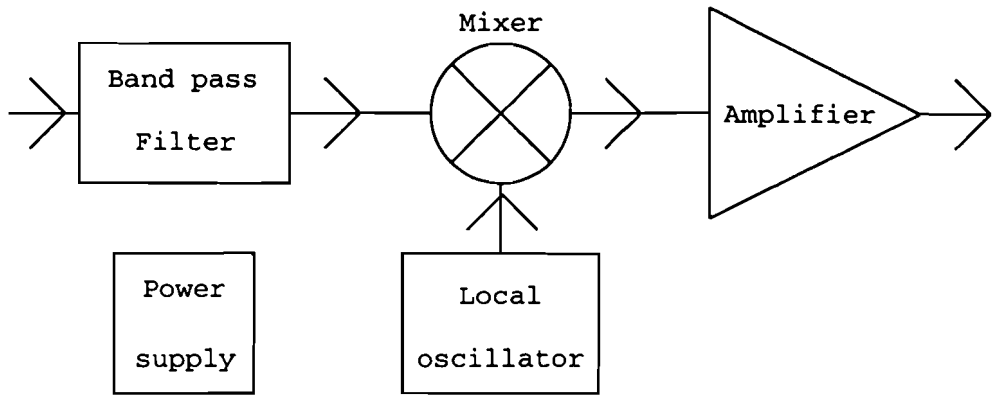

Figure A.7: The block diagram of the outdoor unit

The RF filter has a pass band of 800 MHz centered at 28.5 GHz. This filter gives an image rejection of not less than 35 dB. The local oscillator runs at a frequency of 27.375 GHz (± 1 MHz) which mixes the RF signal to the L-band. The IF amplifier amplifies the signal to an acceptable value for the indoor receive unit (-60 to -20 dBm) depending on the receive level. The system noise figure up to the low noise block equals 10 dB.

A.6 Indoor receive unit

The indoor receive unit is currently a standard satellite tuner. It uses a bandwidth of 27 MHz and is tunable over the L-band from 950 MHz to 1750 MHz. The tuner uses a PLL to demodulate the FM signal yielding an FM threshold of 8 dB. In Figure A.8 the threshold effect is shown. In this figure the signal-to-noise ratio is plotted versus the carrier-to noise ratio. The noise generated by this module is included in the noise figure of the outdoor receiver.

Figure A.8: signal-to-noise ratio versus carrier-to-noise ratio

Appendix B

Power decay rate

For "low" frequencies (1 GHz) the power decay rate in urban areas is of the order of 4 instead of 2. In this section we will show that this is not the case for frequencies used in the MVDS system.

If it is assumed that the ray beams obey the rules of optical reflection, no refraction, the received field strength with one reflection is given by the following formula as shown in Section 3.5.

$$\frac{E}{E_o} = |2 \cdot \sin(\frac{2\pi h_r h_t}{\lambda \cdot d})| \tag{B.1}$$

where h_t is the transmitter height, h_r is the receiver height, λ is the wave length and d is the path length.

This is under the assumption that the distance d is much larger than the heights of the antennas and thus the reflection coefficient ρ = -1. Further we assume a totally flat earth ($k = \infty$).

Now for very large wave lengths λ the product $\lambda \cdot d$ is much larger than $2 \cdot \pi \cdot h_t h_r$. Then we approximate the sin(x) with the first term of the taylor series x. This yields

$$\frac{E}{E_o} = |\frac{4\pi h_r h_t}{\lambda \cdot d})| \tag{B.2}$$

Since the field strength E_o is inversely proportional to the distance d, an electromagnetic wave is a spheric wave, the received field strength E is inversely proportional to d^2. Since the power is direct proportional to the square of the received field E the received power is then proportional to $1/d^4$.

For the frequency of 42 GHz however this is not true because $\lambda \cdot d$ is at most in the order of $7.14 \cdot 10^{-3} \cdot 10 \cdot 10^3 = 71.4$. If we assume a transmitter height of more than 50 m and a receiver antenna height of approximately 10 m one can see that the series approximation for the sine function is not valid. The received field strength will then maintain its sinusoidal behaviour as a function of the distance d. Thus the power decay rate of 4 due to a reflection will not be the case.

If the first Fresnel zone is not completely free from obstruction the received field strength reduces as we have seen in Chapter 3.3. This partially obstructing of the Fresnel zones introduces extra attenuation which depends on the type of obstructing structures. In an urban area the first Fresnel zone can easily be obstructed with buildings etc. This results in a statistical average power decay rate which is larger than 2 in an urban area.

The radius of the Fresnel zone is given by

$$R_n = 547 \cdot 10^3 \sqrt{\frac{n}{f} \cdot \left(\frac{d_1 d_2}{d_1 + d_2} \right)} \tag{B.3}$$

where

R_n = the radius of the n^{th} Fresnel zone (m)
d_1 and d_2 are the distances from a point in the radio path to the antennas (km)
f = the used frequency (Hz).

One can see that for decreasing frequency the radius of the Fresnel zone increases and also increases if the path length is increased. This means that for links using lower frequencies and larger path lengths the first Fresnel zone becomes easily obstructed.

In the short 42 GHz links the Fresnel zones become very small, thus it is much easier to keep the first Fresnel zone free from obstruction. As an example the maximum radius of the first Fresnel zone at a 42 GHz link of 5 km equals 2.98 m and with a 1 GHz path of 50 km this equals 61.16 m (19.34 m for a path of 5 km). A 42 GHz link is entirely based on a LOS, it is thus assumed that at least half of the first Fresnel zone is free of obstruction throughout the entire path. . Since the electromagnetic waves are spheric the free space loss is due to the spheric expansion and thus proportional to $1/d^2$.

Appendix C

Snellius law for a round earth

From the definition of the refractivity index and the fact that it decreases with altitude it follows that the travelling speed of the waves increases with increasing altitude [2]. This results in a curved ray path. Measurements have shown that the refractivity index doesn't change too much in the horizontal direction. It is therefore allowed to look at the problem as if the atmosphere is divided into spherical layers.

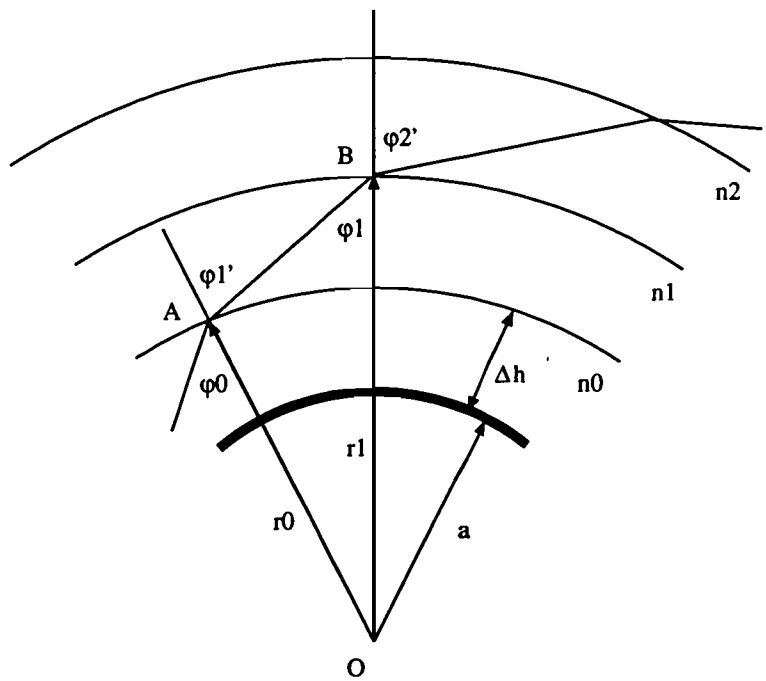

Figure C.1: Ray path through a spherical atmosphere[2]

In figure [2] C.1 we see the earth with part of its atmosphere. From this figure we can see that

$$n_0 \sin \psi_0 = n_1 \sin \psi_1' \tag{C.1}$$

$$n_1 \sin \psi_1 = n_2 \sin \psi_2' \tag{C.2}$$

If we multiply these with the different radii we get

$$n_0 \cdot r_0 \sin \psi_0 = n_1 \cdot r_0 \sin \psi_1' \tag{C.3}$$

$$n_1 \cdot r_1 \sin \psi_1 = n_2 \cdot r_1 \sin \psi_2' \tag{C.4}$$

Since

$$\frac{\sin(\pi - \psi_1')}{r_1} = \frac{\sin \psi_1}{r_0} \tag{C.5}$$

we get

$$n_0 \cdot r_0 \sin \psi_0 = n_1 \cdot r_1 \sin \psi_1 = n_2 \cdot r_2 \sin \psi_2 = ... \tag{C.6}$$

As a result we have

$$n \cdot r \sin \psi = n_0 \cdot r_0 \sin \psi_0 = constant. \tag{C.7}$$

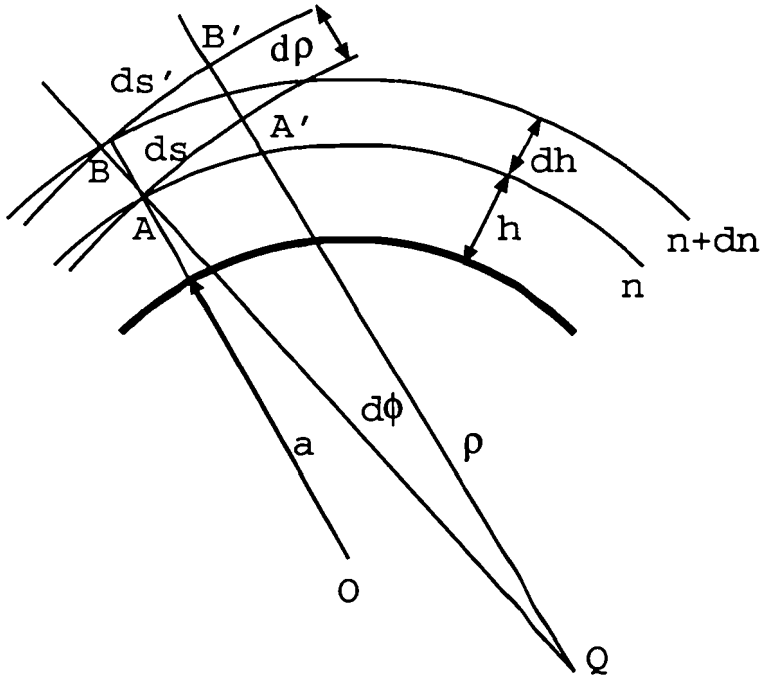

Figure C.2: Model to calculate the curvature ρ[2]

To calculate the actual curvature of a radio beam we proceed as follows. We take two spherical layers very near to each other (Figure C.2) [2]. From AB there is travelling a wave front of the beam. The phase speed at point B ds' is higher than

the phase speed ds at point A. Suppose $ds = v$ and $ds' = v + dv$. This yields the following equations:

$$ds = \rho \cdot d\psi = v \cdot dt \rightarrow \frac{d\psi}{dt} = \frac{v}{\rho} \tag{C.8}$$

$$ds' = (\rho + d\rho) \cdot d\psi = (v + dv) \cdot dt \rightarrow \frac{d\psi}{dt} = \frac{v + dv}{\rho + d\rho} \tag{C.9}$$

This leads to

$$\frac{dv}{v} = \frac{d\rho}{\rho} \tag{C.10}$$

where $\rho = ds/d\phi$ is the radius of curvature of the curve AA'.

According to the definition of the refractivity index n the velocity v of the traveling wave through the medium is defined as

$$v = \frac{c}{n} \tag{C.11}$$

where c is the velocity of an electromagnetic wave in a vacuum.

The derivative of the speed related to the refractivity yields

$$\frac{dv}{dn} = -\frac{c}{n^2} = -\frac{v}{n} \tag{C.12}$$

$$\frac{dv}{v} = -\frac{dn}{n} \tag{C.13}$$

Using (C.10) we get

$$\frac{1}{\rho} = -\frac{1}{n}\frac{dn}{d\rho} \tag{C.14}$$

From Figure C.2 we can see that

$$dh \approx d\rho \cos(\psi) \tag{C.15}$$

With terrestrial transmission the angle ψ almost equals 0. Assuming the refractivity almost 1 results in the following equation

$$\frac{1}{\rho} \approx \frac{dn(h)}{dh} \tag{C.16}$$

where $n(h)$ is the refractivity as a function of height.

The curvature of the ray beam can now be calculated if the function $n(h)$ is known.

There are two common models to describe the curvature of the ray beam. The model described here is the k-factor model. In this model it is assumed that the ray beam follows a straight path. The curvature $1/\rho$ is then accounted for in the effective earth radius a_e as shown in Figure C.3.

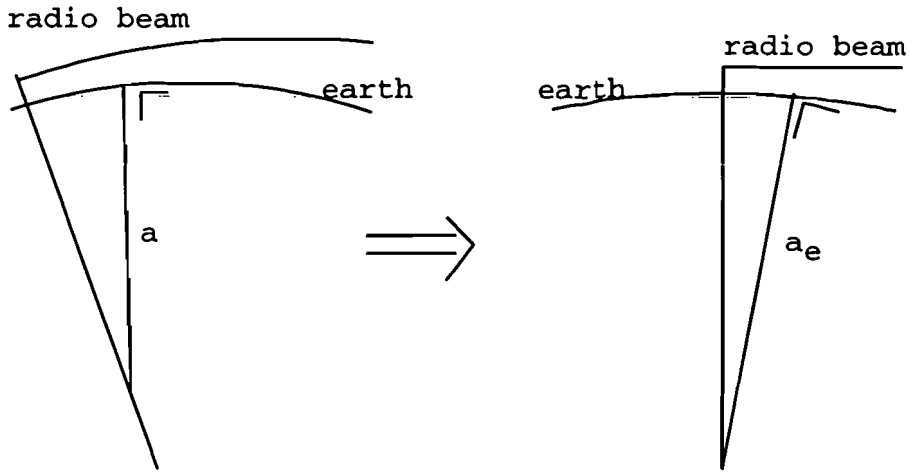

Figure C.3: Earth radius a and effective earth radius a_e in the k-factor model

From this figure the next equation can be derived[2]

$$\frac{1}{a} - \frac{1}{\rho} = \frac{1}{a_e} \tag{C.17}$$

where $1/a$ is the curvature of the earth, $1/\rho$ is the curvature of the radio beam and $1/a_e$ is the effective earth curvature.

The relative curvature between the earth and the radio beam in Figure C.3 is kept constant. The k-factor is now defined as

$$k = \frac{a_e}{a} \tag{C.18}$$

Now it can be concluded that

$$k = \frac{1}{1 - \frac{1}{\rho}} \approx \frac{1}{1 + a\frac{dn}{dh}} \tag{C.19}$$

and using the refractivity this yields in

$$k = \frac{1}{1 + a\frac{dn}{dh} \cdot 10^{-6}} \tag{C.20}$$

With this formula the k-factor can be calculated and thus the effective earth radius can be calculated.

Appendix D

Diffraction

In this chapter a simple model of the diffraction theory is shown. With this theory it is then possible to model a tall building. With this model the attenuation due to diffraction can be estimated.

This analysis is based on the Huygens principle. The Huygens principle states that every wave front is build up of an infinite number of infinite small sources which all interfere. This interference results in a new wave front. In Figure D.1 this idea is shown.

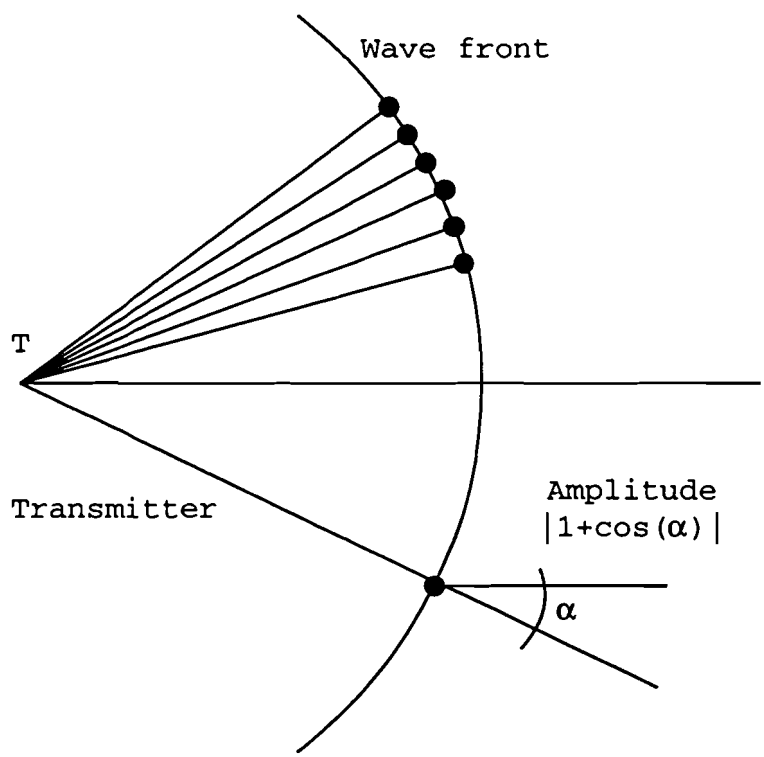

Figure D.1: The Huygens principle

In Figure D.2 the setup of the transmitter and receiver is shown. For very small angles β the setup is simplified as shown.

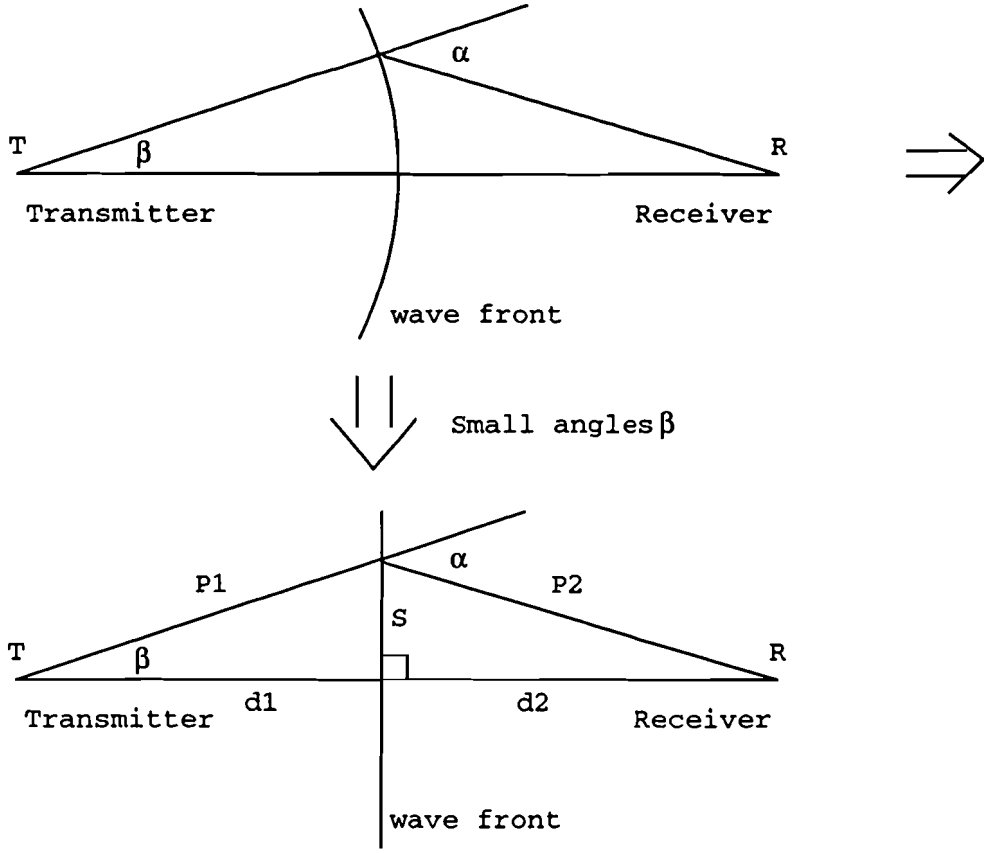

Figure D.2: Transmitter and receiver configuration

According to Kirchoff the electric field E on the surface S is proportional to the reciprocal of the distance P_1 from the source T to the surface S.

$$E \sim \frac{A}{P_1} \tag{D.1}$$

For small angles β the received field in R can be approximated with Kirchoffs law

$$E \sim \int_s \frac{A}{P_1}\frac{1}{P_2} \cdot e^{-jk(P_1+P_2)}\, ds \tag{D.2}$$

where A is an arbitrary constant.

If the distance between the receiver and the transmitter is large, β very small, the electric field can be approximated by

$$E \sim \int_s A' \cdot e^{-jk(P_1+P_2)}\, ds \tag{D.3}$$

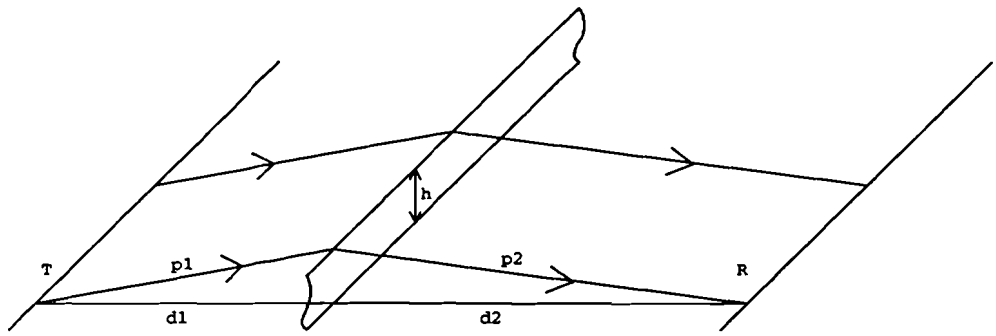

Figure D.3: A two-dimensional model

A two-dimensional model is presented in Figure D.3. In this model an infinite long line source is assumed. An obstacle is now idealized as an infinite long surface with a sharp edge to simplify calculations. This model yields usable results [2].

The phase ϕ of the received electric field is given by

$$\phi = \frac{2\pi}{\lambda}(P_1 + P_2) \tag{D.4}$$

The distance P_1 can be approximated with

$$P_1 = \sqrt{d_1^2 + S^2} = d_1\sqrt{1 + \frac{S^2}{d_1^2}} \approx d_1 + \frac{S^2}{2d_1} \tag{D.5}$$

This results in a phase relation like

$$\phi = \frac{2\pi}{\lambda} \cdot \left(d_1 + d_2 + \frac{s^2}{2} \cdot \left(\frac{1}{d_1} + \frac{1}{d_2}\right)\right) \tag{D.6}$$

Now we are only interested in the phase difference so

$$\phi = \frac{2\pi}{\lambda} \cdot \frac{S^2}{2} \cdot \left(\frac{1}{d_1} + \frac{1}{d_2}\right) \tag{D.7}$$

and thus

$$E \sim A' \int_S \exp\left(j \cdot \frac{\pi}{\lambda} \cdot S^2 \left(\frac{1}{d_1} + \frac{1}{d_2}\right)\right) dS \tag{D.8}$$

Introducing a new variable ν

$$\nu^2 = S^2 \cdot 2 \cdot \frac{d_1 + d_2}{\lambda d_1 d_2} \tag{D.9}$$

the electric field can be written as

$$E \sim A'' \int_S \exp\left(j\frac{\pi}{2} \cdot \nu^2\right) d\nu \tag{D.10}$$

If the electromagnetic field is obstructed as depicted in Figure D.3 it is necessary to set the integration limits from the obstacle hight h to infinity. The limit infinity comes in very handy and is allowed because the contributions to the received electric field in R for large diffraction angles becomes zero. If we set Δ to

$$\Delta = h \cdot \sqrt{\frac{2}{\lambda}(\frac{1}{d_1} + \frac{1}{d_2}} \tag{D.11}$$

the received field can be written as

$$E \sim A'' \int_{\Delta}^{\infty} \exp(j\frac{\pi}{2}\nu^2)\, d\nu \tag{D.12}$$

This equation can be expanded as

$$E \sim A'' \left\{ -\int_0^{\Delta} \cos(\frac{\pi}{2} \cdot \nu^2)\, d\nu - j\int_0^{\Delta} \sin(\frac{\pi}{2} \cdot \nu^2)\, d\nu + \right. \tag{D.13}$$
$$\left. \int_0^{\infty} \cos(\frac{\pi}{2} \cdot \nu^2)\, d\nu + j\int_0^{\infty} \sin(\frac{\pi}{2} \cdot \nu^2)\, d\nu \right\}$$

Since

$$\int_0^{\infty} \cos(ax^2)\, dx = \int_0^{\infty} \sin(ax^2)\, dx = \frac{1}{4} \cdot \frac{\pi}{a} \tag{D.14}$$

the electrical field becomes

$$E \sim A'' \cdot \left(\frac{1}{2}(1+j) - [C(\Delta) + j \cdot S(\Delta)]\right) \tag{D.15}$$

where $C(\Delta)$ and $S(\Delta)$ are the cosine and sine Fresnel integrals defined as

$$C(\Delta) = \int_0^{\Delta} \cos(\frac{\pi}{2} \cdot \nu^2)\, d\nu \tag{D.16}$$

and

$$S(\Delta) = \int_0^{\Delta} \sin(\frac{\pi}{2} \cdot \nu^2)\, d\nu \tag{D.17}$$

The free space electrical field strength is given by

$$E_0 = A'' \int_{-\infty}^{\infty} \exp(j\frac{\pi}{2} \cdot \nu^2)\, d\nu = A'' \cdot (1+j) = A''\sqrt{2} \cdot e^{j \cdot \frac{\pi}{4}} \tag{D.18}$$

therefore the attenuation due to shielding can be estimated with

$$\frac{E}{E_0} = \frac{e^{j\frac{\pi}{4}}}{\sqrt{2}} \cdot \left(\frac{1}{2}(1+j) - (C(\Delta) + j \cdot S(\Delta))\right) \tag{D.19}$$

and the loss L_{df} due to diffraction is thus given by

$$L_{df} = 20 * \log\left(\left|\frac{1}{2}\sqrt{2} \cdot \left[\frac{1}{2}(1+j) - (C(\Delta) + j \cdot S(\Delta))\right]\right|\right) \tag{D.20}$$

with

$$\Delta = h \cdot \sqrt{\frac{2}{\lambda} \cdot (\frac{1}{d_1} + \frac{1}{d_2})} \tag{D.21}$$